FLUID STRUCTURE INTERACTION IN TRANSIENT CAVITATING FLOW IN PIPES

Submitted in fulfilment of the requirements

of the degree of

DOCTOR OF PHILOSOPHY

by

MIJI CHERIAN R.

Supervisors: **Dr. N. Sajikumar & Dr. Sumam K.S.**

Department of Civil Engineering

GOVERNMENT ENGINEERING COLLEGE THRISSUR

UNIVERSITY OF CALICUT

(September 2020)

UNIVERSITY OF CALICUT

BONAFIDE CERTIFICATE

Certified that this thesis titled **"FLUID STRUCTURE INTERACTION IN TRANSIENT CAVITATING FLOW IN PIPES",** is the bonafide work of Mrs. MIJI CHERIAN R. who carried out the research under our supervision. Certified further that to the best of my knowledge the work reported herein does not form part of any other thesis or dissertation on the basis of which a degree or award was conferred on an earlier occasion of this or any other candidate.

Dr. N. SAJIKUMAR
(Supervisor)
Professor
Department of Civil Engineering
Government Engineering College, Thrissur

Dr. SUMAM K.S.
(Supervisor)
Associate Professor
Department of Civil Engineering
Government Engineering College, Thrissur

Place: Thrissur
Date: 09.09.2020

Certified that the corrections/suggestions, recommended by the adjudicators as per Ref. no. 149180/RESEARCH-C-ASST-1/2020/Admn, dated 25.03.2021 from the Director of Research, University of Calicut, have been incorporated in the thesis and that the contents in the thesis and the soft copy are one and the same.

Dr. N. SAJIKUMAR
(Supervisor)
Professor
Department of Civil Engineering
Government Engineering College, Thrissur

Dr. SUMAM K.S.
(Supervisor)
Associate Professor
Department of Civil Engineering
Government Engineering College, Thrissur

Place: Thrissur
Date: 15.04.2021

DECLARATION

I hereby declare that this submission is my own work and that, to the best of my knowledge and belief, it contains no material previously published or written by another person nor material which has been accepted for the award of any other degree or diploma of the university or other institute of higher learning, except where due acknowledgement has been made in the text.

Place: Thrissur

Date: 09.09.2020

Signature:

Name: MIJI CHERIAN R.

Registration No. 8979/RESEARCH-B-SO/2014/CU Dated 19.02.2014

ACKNOWLEDGEMENT

First of all, I thank God Almighty for giving me the strength throughout the period of my research work and completion of this task.

I wish to express my sincere gratitude to my research supervisors Dr. N. Sajikumar and Dr. Sumam K.S., for motivating, guiding and supporting me during the course of my research work. Both of them have taken a lot of pain for me, and have become a beacon of guidance during the course of my work.

I would like to express my gratitude to my doctoral committee members Dr. Santosh G. Thampi, Professor, NIT Calicut and Dr. Manesh K.K., Associate Professor in Mechanical Engineering, GEC Thrissur for their valuable suggestions during my research work. I am also grateful to the Head of Civil Engineering Department Dr. C.V. Lal and former heads of department Dr. P. Vijayan, Prof. K.S. Dinesh Kumar and Dr. P. Vinod for their support during my research.

I am also thankful to Dr. K. P. Indiradevi and Dr. K. Vijayakumar, former Directors of Technical Education, Kerala for their whole hearted support during the entire length of this research. I am grateful to Dr. V. S. Sheeba Principal, Government Engineering College Thrissur, for providing all the facilities of this college for the conduct of this research work. At this moment I also acknowledge former principals Dr. B. Jayanand and Dr. K. P. Indiradevi, for providing all the facilities of this college for the conduct of this research work during those periods.

I take this opportunity to gratefully acknowledge the project grant by the Kerala State Council for Science, Technology and Environment under Engineering and Technology Programme (Project No.ETP/8/2015/ KSCSTE Dated Thiruvananthapuram 21.11.2016) Kerala, India. I express my sincere gratitude to Dr. K. P. Sudheer (Professor, IIT Madras and Mentor of the project). I also thank all the officials of the Kerala State Council for Science, Technology and Environment for their timely supports during the research.

I would like to express my gratitude to the Fluid Control Research Institute, India, for providing all necessary facilities to conduct the experiments in their Water Flow Laboratory. I also convey my heartfelt gratitude to Mr. P.K. Suresh, Mr. K. Suresh and Mr. Jayesh of the FCRI Palakkad for all the help extended during the experimental investigation.

I also thank project fellows Mr. Roopesh Kaimal and Ms. Bhagyasree P.P. and project assistants Ms. Samily C Vijayan and Neethu P.K. for their help during this research work. I am also grateful to my colleagues Dr. P. T. Nowshaja, Dr. E. A. Subaida, Dr. S. Arun, Prof. Smitha Mohan K. and Dr. Abdul Samad P.A. for their help and constant mental support given during this research period. I also thank my fellow research scholars and my colleagues of Civil Engineering Department for their timely help extended always.

Above all I would like to thank my spouse Mr. Paulachan Iype, my children Alan Paul and Milan Paul and my parents for their compassionate consolations, timely mental support and encouragement given, to make this research a reality.

MIJI CHERIAN R.

CONTENTS

LIST OF FIGURES

LIST OF TABLES

NOTATIONS

A	Area of cross section
A_f	Area of fluid, Area of face f
A_t	Area of pipe
a_p, a_{nb}	Momentum equation coefficients
$[B]$	Strain displacement matrix
B_x, B_y, B_z	Body forces in x, y, z directions including inertia force per unit volume
b	Net flow rate to the cell
$[C]$	Structural damping matrix
$C_{1\varepsilon}, C_{2\varepsilon}, C_{3\varepsilon}$	Constants
c	Pressure wave velocity
$[D]$	Constitutive matrix
D	Internal diameter
d_f	Function of momentum equation coefficient
E	Modulus of elasticity, Energy
e	Thickness of pipe wall, internal energy
F_{vap}, F_{cond}	Constants in vapour generation and condensation rate expressions
f	Darcy Weiback friction coefficient
f_g	Gas mass fraction
f_v	Vapour mass fraction
f_x, f_y, f_z	Body force per unit mass in x, y, z directions
G	Shear modulus
G_b	Generation of turbulence kinetic energy due to buoyancy
G_k	Generation of turbulence kinetic energy due to mean velocity gradients

g	Acceleration due to gravity
H	Pressure head
I_t	Moment of inertia of pipe
$[J]$	Jacobian matrix
J	Determinant of Jacobian matrix
J'_f	Mass flux correction through face f
$\hat{J}^*$	Assumed mass flux through face f due to the influence of velocities in the adjacent cells
J^*_f	Assumed mass flux through face f
J_f	Mass flux through face f
J_t	Polar moment of inertia of pipe
K	Bulk modulus of fluid
K^*	Equivalent Bulk modulus of fluid
K_o	Reference bulk modulus
k	Thermal conductivity, Turbulent kinetic energy
$[k]$	Structural stiffness matrix
L	Length of the pipe
M_x, M_y, M_z	Bending moment in x, y, z directions
$[M]$	Structural mass matrix
$[N]$	Shape function matrix
n	Bubble number density, density exponent, unit normal
n_b	Number of bubbles per unit volume of liquid
N_{faces}	Number of faces enclosing cell
P_B , P_b	Bubble pressure

P_v	Vapour pressure
P_o	Reference liquid pressure
p^*_{co} , p^*_{c1}	Guessed pressure field within the two cells on either side of the face
P, p	Pressure
p'_{co} , p'_{c1}	Pressure correction within the two cells on either side of the face
Q	Discharge
Q_x, Q_y, Q_z	Shear force in x, y, z directions
$\dot{q}$	Rate of volumetric heat addition per unit mass
R	internal radius, phase change rate
R_B	Bubble radius
R_e, R_c	Vapour generation and condensation rates
S	Surface area
S_m , S_k, S_ε	source terms
T	Surface tension, Temperature
t	time
u_x, u_y, u_z	Pipe displacements in x, y, z directions
$[u]$	Displacement vector
$[\dot{u}]$, $\vec{V}$	Velocity vector
$[\ddot{u}]$	Acceleration vector
U_x, U_y, U_z	Fluid velocity in x, y, z directions
V	Fluid velocity, cell volume
$V^2/2$	Kinetic energy per unit mass
Y_m	Contribution of the fluctuating dilatation in compressible turbulence to the overall dissipation rate

α	Vapour volume fraction, Newmark integration parameter
β	Newmark integration parameter
Γ	Diffusion coefficient
γ	Shear strain
δ	Kronecker symbol
ε	Dissipation rate, normal strain
η ,ξ, ζ	Natural coordinates
θ_x, θ_y, θ_z	Rotation of pipe in x, y, z directions
κ^2	Shear coefficient of pipe wall
λ	Bulk viscosity coefficient
μ	Molecular viscocity
ν	Poisson's ratio
ρ	Density, mixture density
σ	Stress, Turbulent Prandtl number
τ	Shear stress
φ	Scalar quantity

ABBREVATIONS

ALE	Arbitrary-Lagrangian- Eulerian
AMG	Algebraic Multi-Grid
CB	Convolution Based
CFD	Computational Fluid Dynamics
CHT	Constant Head Water Tank
CSD	Computational Solid Mechanics
CV	Control Valve
DGCM	Discrete Gas Cavity Model
DNS	Direct Numerical Simulation
DVCM	Discrete Vapour Cavity Model
FEM	Finite Element Method
FSI	Fluid-Structure Interaction
FV	Finite Volume
FVM	Finite Volume Method
GI	Galvanized Iron
HDPE	High-Density PolyEhylene
IAB	Instantaneous Acceleration–Based
LES	Large Eddy Simulation
MDPE	Medium Density PolyEthylene
MOC	Method of Characteristics
PDE	Partial Differential Equations
PISO	Pressure-Implicit with Splitting of Operators
PVC	PolyVinyl Chloride

QAV	Quick Acting Valve
QUICK	Quadratic Upwinding Interpolation of Convective Kinetics
RANS	Reynolds Averaged Navier-Stokes simulation
RNG	Re-Normalisation Group
SIMPLE	Semi Implicit Method for Pressure Linked Equations
SIMPLEC	Semi-Implicit Method for Pressure Linked Equations-Consistent
SST	Shear Stress Transport
UPVC	Unplasticized PolyVinyl Chloride

ABSTRACT

Sudden changes in operating conditions in a piping system, like closing or opening of the valve, starting and stopping of the pump, induce hydraulic transient. The hydraulic transient manifests as pressure fluctuations inside the pipe, which travels back and forth until the available energy from the abrupt changes in flow condition gets dissipated. The pressure fluctuations (water hammer) cause pressure rise/drop alternatively in the piping system. When low pressure prevails for a long time and goes below the vapour pressure of the fluid, the system is subjected to cavitation. The cavitation is the formation, growth and collapse of vapour bubbles in a flowing fluid and results into very high-pressure fluctuations. Although the modelling using one-dimensional continuity and momentum equations can predict the maximum water hammer pressure accurately, the simulated flow characteristic, viz., the pressure wave, deviates from the measured. In many instances, this deviation between the simulated and computed pressure wave is reduced by incorporating some concepts like variable unsteady friction, artificial viscosity and diffusive terms in the governing equations. While the system undergoes water hammer and cavitation, the piping system experiences severe dynamic forces because of fluid-structure interaction. Fluid induced structural motion and structure induced fluid motion, and the underlying coupling mechanisms are referred to as fluid-structure interaction (FSI). Several attempts have been carried out to incorporate the FSI into numerical models by using one-dimensional structural equations. The study of FSI in a practical problem, considering the prominent physical features of the problem, is not yet present in the literature. Moreover, the influence of support conditions on transient flow was not dealt with in detail. Hence, the present study investigates, both numerically and experimentally, the effect of fluid-structure interaction on the damping of pressure fluctuations because of the closure the valve in a reservoir-pipe-valve system.

The current study includes an experimental investigation into the effect of valve closure and spacing of anchors on transient cavitating flow through the pipes of three different materials. The materials considered in the study are mild steel (MS), unplasticized polyvinyl chloride (UPVC) and high-density polyethylene (HDPE). The experiments with different flow rates of fluid and different closure times of the valve in the piping system proved that the first pressure

peak in water hammer under sudden closure condition does not depend on the closure time of the valve; whereas the occurrence of cavitation and the pressure rise due to cavitation are highly influenced by the closure time of the valve. The pressure rise due to cavitation varies drastically with a decrease in closure time. The water hammer pressure in the piping system, for both elastic and visco-elastic materials included in the study, remains unaltered with the change in the number of fixed anchors attached to the system. As the rigidity of the piping system is increased by adding more number of fixed anchors, the chance of occurrence of cavitation and the resulting pressure rise are increased, whereas the lateral acceleration of the piping system decreases significantly during the experiments. Hence, the spacing of anchors in any piping system should be decided by considering the lateral acceleration of the piping system and pressure rise due to cavitation. For industries where vibration has to be limited, anchors can be provided closely, by taking precautionary measures to avoid the failure due to cavitation.

The current study also includes a numerical investigation into the effect of fluid-structure interaction (FSI) on transient flow characteristics in a piping system and the influence of spacing of anchors, on transient flow. The current study proved that the proper accounting of fluid-structure interaction (FSI) in the transient analysis can predict the pressure variation with reasonable accuracy, without any additional artificial methods mentioned earlier. Numerical simulations of four different problems from two different experimental setups, published in literature and the one conducted in the study have been used for assessing the effect of FSI on the damping of the pressure wave. It is found that the model accounting the fluid-structural system predicts of the damping of the pressure wave in the quasi- rigid pipe system better, whereas the incorporation of FSI does not yield any improvement for a completely rigid system like a pipe buried in concrete. In general, the piping system will not be rigid and hence, the study incorporating FSI has a significant role in the transient analysis in practical piping systems to predict the damping of pressure wave effectively. However, the huge computation load limits such studies.

Keywords: Water hammer, Sudden closure, Cavitation, Fluid structure interaction, Computational Fluid Dynamics, Pressure wave damping.

CHAPTER 1

INTRODUCTION

1.1. Background

Transient flow in a piping system is a transition of flow from one steady flow to another and occurs as a result of the abrupt changes in the normal operating condition like closing or opening of the valve, starting or stopping of pumps. Such abrupt changes create pressure waves of significant magnitude. The propagation and reflection of these pressure waves are referred to as hydraulic transients or water hammer (WH). Classical one-dimensional water hammer equations were commonly used to model transient flow (Chaudhry, 1979; Chaudhry and Hussaini, 1985; Hadj-Taıeb and Lili, 2000; Greyvenstein, 2002; Mitosek and Szymkiewicz, 2012; Amara et al., 2013; Shimada and Vardy, 2013; Seck et al., 2017; Martins et al., 2017). Though these equations correctly predicted the first pressure peak, the experimental results always show sudden damping of pressure wave contrasting the numerical results obtained from classical WH analysis (Araya and Chaudhry, 1997; Brunone et al., 2000; Mitosek and Szymkiewicz, 2012; Amara et al., 2013; Monajitha et al., 2014; Shimada and Vardy, 2013; Seck et al., 2017; Martins et al., 2017). Many researchers investigated the reasons for this deviation and identified a few factors such as fluid friction, nature of network demand, unsteady friction, leaks in pipes and elasticity of pipe material (Araya and Chaudhry, 1997; Vitkovsky et al., 2000; Brunone et al., 2000; Mitosek and Szymkiewicz, 2012; Amara et al., 2013; Monajitha et al., 2014; Shimada and Vardy, 2013; Seck et al., 2017; Martins et al., 2017) as the reasons.

The interaction between the pipe material and the fluid (Fluid structure interaction) is a physical phenomenon which does not have full representation in the classical water hammer theory. This lack of representation of fluid-structure interaction in the conventional water hammer model could be one of the possible reasons for having the deviation in the damping of pressure between that observed in experimental measurements and that from the model. Fluid induced structural motion, structure induced fluid motion, and the underlying coupling mechanisms are commonly referred to as Fluid-Structure Interaction (FSI). In conventional water hammer analysis, the elasticity of pipe is incorporated into the propagation speed of pressure

waves; and the pipe inertia and axial pipe motion are generally not taken into account. These simplifications are acceptable for rigidly anchored pipe system. However, for less restrained systems, fluid structure interaction is more significant (Heinsbroek and Tijsseling, 1994; Ferras et al., 2016a). Three liquid-pipe interaction mechanisms were generally used to model the FSI, and these are friction coupling, Poisson coupling and Junction coupling (Wiggert et al., 1987; Lavooij and Tijsseling, 1991). The Friction coupling represents the mutual friction between the liquid and the pipe. The Poisson coupling relates the pressures in the liquid to the axial (longitudinal) stresses in the pipe through the radial contraction or expansion of the pipe wall. The Junction coupling applies at specific points in a pipe system such as unrestrained valves, bends and tees.

Water hammer waves cause pressure rise/drop alternatively in the piping system. When low pressure goes below the vapour pressure of the fluid, the system is subjected to cavitation. The cavitation is the formation, growth and collapse of vapour bubbles in a flowing fluid when the pressure drops below its vapour pressure. Research area on cavitation is vast and includes gaseous cavitation, vaporous cavitation and column separation. Simpson and Bergant (1994a) summarized the previous experimental investigations in the field of water hammer with column separation. Generally, the pressure caused by water hammer with cavitation is significantly higher than that consequent to water hammer alone. Hence, investigations considering the effect of cavitation on piping system also become essential.

1.2. The relevance of the Topic

The study on fluid structure interaction in liquid-filled pipe system dates back to the nineteenth century; the fundamental theoretical basis for FSI in straight liquid-filled pipes was proposed by Skalak (1954). In classical water hammer theory, an equivalent bulk modulus K^* was initially included to represent the effect of pipe material and the thickness of the pipe. Later, different structural parameters were included in the WH analysis. Accordingly, several mathematical models are available in the literature to represent FSI in WH analysis. During a transient flow event in a fluid-filled piping system, the generated pressure wave propagates in the fluid and induces the axial, flexural, rotational, radial and torsional actions in the piping system. Even though many researchers included FSI in their study, most of them coupled the axial

motion equations of the pipe alone, with the fluid equations, in the analysis (four-equation model) (Lavooij and Tijsseling, 1991; Li et al., 2003; Ferras et al., 2017). The researchers who used all the aforementioned actions in the form of the fourteen-equation model (Wiggert et al., 1987; Mittal and Tezduyar,1995; Heinsbroek,1997) including the lateral and torsional equations, considered these one dimensional (1-D) equations as uncoupled with the other four equations. Moreover, the interaction of all the equations is coupled at the junctions only.

The load imparted on the piping system during the process of water hammer and cavitation is transferred to the support mechanisms such as anchors, thrusts, and blocks. Limited investigations have been carried out to study how the forces consequent to water hammer and cavitation are transmitted from the piping system to the pipe anchors and support mechanism and vice versa. Similarly, the studies seeking the influence of the support condition/ anchoring system on the transient cavitating flow are limited. Most of the investigations on FSI in piping system (Vardy and Fan, 1986; Heinsbroek and Tijsseling, 1994; Ferras et al., 2017) ignored the effect of cavitation in their theoretical work and made arrangements for avoiding cavitation in their experimental works. Vardy and Fan (1986 and 1989) carried out tests on FSI without cavitation on four different pipe systems in a test rig built in the Hydraulics Laboratory, University of Dundee (UK). Tijsseling and Fan (1991, 1992 and 1994) carried out experiments in the same experimental setup by considering cavitation. They carried out the experiments in a horizontal pipe, pipe with elbow and T pipe. All the tests were conducted in closed pipes suspended freely in a horizontal plane, thus avoiding the effect of support conditions and the transients were generated by the impact of solid steel rod on one of the pipe ends. Heinsbroek and Tijsseling (1994) conducted an experimental investigation on the effect of support rigidity on conventional water hammer analysis. Experimental set up consists of seven straight pipes connected by six 90^{o} bends suspended by steel cables and supported by springs at the bends. This experiment has limited practical application owing to its deviation from the practical system. Ferras et al. (2017) developed a 1-D FSI solver for a modified form of 4-equation model, capable of describing the resistance to movement of anchor blocks and its effect on the transient pressure wave propagation in straight pipelines. However, the effect of fixed anchors on the transient cavitating flow has not been explored so far. Moreover cavitation is not considered in the experiments conducted by Heinsbroek and Tijsseling (1994) and Ferras et al. (2017).

1.3. The motivation for the Research Work

Several cases of steel and concrete penstock failure have been reported (Adamkowski, 2001). Adamkowski (2001) reported that a penstock failure in the Oigawa Power station, Japan in 1950 caused by water hammer as a result of the sudden closure of a butterfly valve. A detailed study of penstock failure in Lapino Power plant in December 1997 by Adamkowski (2001) revealed that the leading cause of failure was the excessive pressure rise due to water hammer. Moreover, the increase in pressure caused by water hammer in a piping system and its damping behviour can be influenced by the anchoring conditions of the piping system. Hence, the study of FSI is also vital in piping systems of nuclear reactors where the collapse of the system may lead to radiation which is the most hazardous situation. Such studies are significant in chemical industries also where failure creates environmental issues.

Disruption of water supply is a common issue in Kerala, which is attributed by the pipe bursting because of water hammer and cavitation. The transient analysis with FSI can be utilized to assess the risk of failure of the existing pipes under different working conditions. Besides, the induced vibrations during transient flow in a liquid-filled piping system are also a crucial area to be investigated as it affects the pipe connections, fittings and flow regulating instruments. Hence, FSI analysis plays a critical role in the understanding of the acceleration of the piping system under dynamic loads and can be used as an aid to reduce the vibration of the piping system.

1.4. Objectives of the Research Work

The lack of representation of fluid-structure interaction in the classical water hammer theory could be one of the possible reasons for the inability in predicting the damping of pressure accurately. In FSI, there is an interface surface which is common for both the fluid and the solid domain. The governing equations of both the fluid and the solid must be satisfied at this interface. Similarly, fluid and solid boundary conditions must also be satisfied at this interface. A set of coupling conditions, which initiates the transfer of data between the fluid and solid domain, accomplishes this compatibility. During the transient condition in the fluid-filled piping system, the pressure waves propagate in the fluid and induce the axial, flexural, rotational, radial and torsion actions in the piping system. Even though many researchers included FSI in their

study, most of them coupled the axial motion equations of the pipe alone, with the fluid equations, in the analysis. The researchers who used the fourteen equation model, including the lateral and torsion equations, considered these 1-D equations as uncoupled with the other four equations. The interaction of all the equations is coupled at the junctions only. The studies which incorporate two-way coupling of the structural and fluid system in the FSI analysis in 3-D were not yet addressed in full respect for a practical problem. Moreover, the study of FSI in a practical problem, considering the prominent physical features of the problem, is not present in the literature.

Moreover, most of the experimental investigations on transient flow reported in the literature neglected cavitation and made arrangements to avoid cavitation during experiments. The studies with cavitation and FSI were conducted on suspended pipe systems, with closed pipes suspended freely in a horizontal plane, so that the effect of supporting conditions could be excluded. Limited experiments have been reported so far considering water hammer with cavitation incorporating the impact of fixed anchors. Hence, the effect of fixed anchors attached to the piping system on transient cavitating flow characteristics, in a reservoir-pipe-valve system is selected as the area of the present experimental investigation. The objectives of the present study are fixed accordingly as

1. To assess the effect of valve closure time, flow velocity, material property and number of fixed anchors on transient cavitating flow through a pipe by conducting experiments in a reservoir-pipe-valve system.
2. To simulate the transient flow for evaluating the effect of FSI on the damping of pressure wave.
3. To examine the effect of number of fixed supports on transient flow through pipes by numerical simulation.

1.5. Organization of the Thesis

The thesis work comprising six chapters altogether as described below

- The introduction (Chapter 1) provides an overview of transient flow, cavitation and fluid structure interaction and the importance of modelling transient flow with fluid structure interaction. The scope and objective of work are also given at the end of this chapter.
- The literature review (Chapter 2) provides historical background and overview of essential concepts related to the present research area. It is divided into four subsections, viz., water hammer, cavitation, computational fluid dynamics, and fluid structure interaction. The theoretical and experimental researches carried out in the area are included in this chapter.
- Chapter 3 - materials and methods have four main parts. The first part provides the governing equations of fluid dynamics, structural dynamics and cavitation. The numerical methods used for the solution of concerned governing equations are given in the second part. The third part describes the numerical implementation procedure using the software. The last part includes the experimental setup and details of the experiment conducted as a part of the current study.
- In chapter 4, the results and discussions of the current experimental investigation are presented. The experimental results are presented as the influence of different variables adopted for the study, on transient flow characteristics.
- In chapter 5, the results and discussions of the numerical investigation are presented. This chapter has two main parts. The first part is the investigation on the effect of FSI on the wave damping of pressure. The second part includes the particulars of numerical modelling of the current experimental study to determine the influence of several fixed anchors on transient flow characteristics.
- Summary and conclusion of the research are presented in chapter 6.

1.6. Summary

This chapter gives an introduction about the transient cavitating flow and its significance in practical situations. It also describes the basic principles of Fluid Structure Interaction. Further, it details the scope and objectives of the present study and the thesis outline.

CHAPTER 2

REVIEW OF LITERATURE

2.1. General

For any piping system, a sudden change in operating conditions like closing or opening of the valve, starting and stopping of the pump induce transient flow. The hydraulic transient manifests as pressure fluctuations inside the pipe which travels to and fro until the available energy from the abrupt changes in flow condition gets dissipated. Finally, the flow attains another steady state. These phenomenon (water hammer wave) cause pressure rise/drop alternatively in the piping system. When the pressure drop prevails for a long time and drops to the vapour pressure of the fluid, the system is subjected to cavitation, which is the formation, growth and collapse of vapour bubbles in a flowing fluid. During these processes, viz., the water hammer and cavitation, the piping system experiences severe dynamic forces due to fluid-structure interaction. A general review of these phenomena is discussed in the following sections.

2.2. Water Hammer

Abrupt changes in the flow condition like closing or opening of the valve, starting or stopping of the pumps, are unavoidable situations in hydraulic systems and cause water hammer. An approximate equation (Eqn. 2.1) for the maximum pressure resulting from the water hammer (known as Joukowsky pressure) was derived in the second half of the 19th century (Bergant et al., 2006).

$$\Delta p = \rho c \Delta V \tag{2.1}$$

Where Δp is the maximum pressure due to the change in velocity ΔV, ρ is the mass density of fluid and c the velocity of sound in the fluid. Further, 1-D water hammer equations were derived, based on the conservation of mass (continuity equation) and momentum (equation of motion).

The 1-D continuity equation and the equation of motion for representing the process of water hammer are as shown in Eqn. 2.2 (Wylie et al. 1993).

$$\frac{\partial H}{\partial t} + \frac{c^2}{gA}\frac{\partial Q}{\partial x} = 0$$

$$\frac{\partial Q}{\partial t} + gA\frac{\partial H}{\partial x} + \frac{f}{2DA}Q|Q| = 0 \tag{2.2}$$

where H is the pressure head, Q is the discharge, t is the time, g is the acceleration due to gravity, A is the area of cross section, f is the Darcy Weisbach friction factor and D is the internal diameter.

Hughes (1963) studied the effect of a valve closure on water hammer waves in a fully developed laminar viscous flow by conducting experimental and numerical studies in a closed conduit. The researcher proposed a one-dimensional model that incorporated dispersion and dissipation of pressure wave during transient flow and validated the model successfully against the experimental data. Holmboe and Rouleau (1967) investigated the behaviour of pressure transients during a valve closure by conducting experiments in a pressurized tank-pipe-valve system. The pipe was embedded in concrete during the experiment to reduce the vibration of the system and to avoid the effect of support condition on transient flow. The experimental results match well with the results of one-dimensional numerical analysis. However, such a system with embedding concrete is not feasible in most of the practical cases. Streeter and Wylie's (1967) classic text book elaborates on the Method of Characteristics (MOC) to solve the water hammer equations numerically. The MOC uses the compatibility relations that are valid along the positive and negative characteristic lines.

Chaudhry and Hussaini (1985) presented three explicit finite difference schemes – MacCormac, Lambda and Gabutti schemes for the analysis of transient flow through the pipe. All the three schemes have a predictor step and a corrector step and are second-order accurate both in space and time. The study showed that the advantage of second-order accurate schemes over first-order accurate schemes was negligible when the courant number was around one. Sibetheros et al. (1991) analysed the hydraulic transient by using the MOC with spline interpolation function and proved that the numerical analysis of water hammer problems by using that method gave better accuracy than the MOC with linear interpolation.

Kono et al. (1992) analysed numerically the failure pattern of pipes, consequent to a sudden closure of a valve, by using the MOC method and compared the pattern with a real broken penstock. The pipe stresses were calculated by using the Finite Element Method (FEM) and the position at which plastic deformation initiated was also identified.

Research on similar lines contributed substantially to the health monitoring of existing water distribution systems. The work of Ligget and Chen (1994) proposed an inverse transient analysis method for the health monitoring of an existing water distribution systems. A considerable amount of data were collected from the existing water distribution system and was used in the transient analysis algorithm to calibrate the system. The primary application of this method was the identification of leaks and thefts in the distribution system. Araya and Chaudhry (1997) developed a numerical model for the prediction of pressure wave in an unsteady flow, by introducing an energy dissipation factor in the momentum equation. The results of this model agreed well with the experimental results of Holmboe and Roleau (1967). Hadj-Taieb and Lili (2000) utilised the finite difference conservative method - Newton Raphson iterative method- along with MOC for the modelling of water hammer in gas-liquid mixture flowing through a deformable pipe. The developed model was validated by using the experimental results of Chaudhry et al. (1990). The results from the finite difference conservative method closely agreed with the test results. The researchers found that the numerical oscillations could be reduced by adopting small space and time steps, and also by bringing the Courant number near unity.

Brunone et al. (2000) measured the velocity profiles in transient flows by conducting experiments on polyethylene pipe and found strong resemblance with the theoretical models proposed by Araya and Chaudhry (1997). However, it is interesting to note that the measured velocity profile was unsymmetrical with respect to the centre of cross section at certain stage of the transient event. The upper half of the velocity profile showed a positive flow while the lower half showed a negative flow. Further, they used the unsteady friction concept in a numerical model and evaluated the “decay” coefficient to match the damping of pressure waves. Vitkovsky et al. (2000) conducted a numerical study based on unsteady friction model suggested by Brunone et al. (2000). The researchers introduced variable-unsteady friction (variable k model) and tested the model with the experimental results from Bergant and Simpson (1995). They found that the variable-unsteady friction (variable k model) model

showed better agreement with the experimental results than the constant unsteady friction model.

Adamkowski (2001) used the transient analysis with the classical water hammer equations, combined with material testing, and stress analysis to identify the reason for the penstock failure at Lapino Power plant. The researcher found that the bursting of the pipe was because of the excessive pressure rise consequent to water hammer after a rapid cut off in the flow. The study recommended that the factors like the rate of flow cut off and the resulting maximum pressure rise, stresses in the geometrically unsymmetrical elements, and the quality of the welded or riveted joints, should be considered for the design of hydropower plants. Greyvenstein (2002) presented an implicit finite difference method that used a pressure correction approach with a time-step-weighing factor. The method could be used for liquid and gas flows, steady and transient flows and isothermal and non-isothermal flows. The developed numerical scheme was compared with the two-step Lax-Wendroff method and the second-order MOC. It is found that the results from the developed method with optimum value of time-step-weighing factor was in good agreement with that from the second-order two-step Lax-Wendroff method.

Bourdarias and Gerbi (2002, 2008) developed a three-dimensional numerical model for compressible flow in deformable pipes and concluded that a significant part of energy was absorbed by the deformable pipe material and hence, the pressure generated during the water hammer is smaller in the pipes than in rigid and quasi-rigid pipes. The compressibility of water was modelled by using linearized pressure law. According to Karney and Filion (2003), there are six causative energy-dissipation mechanisms for damping the pressure fluctuations in a piping system, viz., fluid friction, the nature of network demand, the presence of leaks, the complexity of looped pipe, unsteady friction, and the presence of surge protection devices. But, most of these mechanisms (except first and fifth one) are irrelevant in the case of a single short pipe system, normally modelled in an experimental setup. Hence, it is appropriate to look for other mechanisms which cause the damping of pressure wave in a single piping system.

Ghidaoui et al. (2005) conducted a review of the research works that were performed previously on the water hammer phenomenon. Around 134 studies were reviewed by emphasizing one-dimensional and two-dimensional mass and momentum equations, their solution methods, turbulence models and boundary conditions. Bergant et al. (2006)

reviewed all the general aspects of water hammer from the beginning to the late 20th century. A detailed survey of all available numerical models and all experimental works conducted so far in the field were included in this review.

Shen et al. (2006) simulated the flow near the entrance of a pipe by using multi-grid Finite Volume (FV) technique to reduce the computational cost. In this model, the equations were first solved on a very coarse grid, and these results were used for selecting a better initial guess for the subsequent finer grid. This process was repeated until the required accuracy was obtained. The process of incremently reducing the size of mesh could diminish the CPU time substantially. Leon et al. (2007) also used a second-order accurate finite volume scheme for modelling the transient flow. The performance of the proposed model was numerically tested by modelling smooth and sharp transients. It was found that the proposed model was superior to the MOC scheme and the previously developed FV schemes. The FV model was extended to include two-phase flow by Leon et al. (2008). The researchers formulated a second-order accurate finite volume shock-capturing scheme for modelling one-phase and two-phase transient flows. The proposed model was compared with the MOC scheme and the experimental results of Chaudry et al. (1990). The results showed that the performance of the single-phase flow model greatly depended on the Courant number. When the adopted Courant number was close to unity, the MOC gave better results, whereas when that was below 0.95, the proposed FV model gave better results. It was found that the proposed scheme was more efficient for the two-phase flow than the MOC.

Ahmadi and Keramat (2010) studied the effect of valve closure time on the water hammer pressure numerically by adopting two-valve closure times 30 ms and 50 ms. The researchers reported that when closure time is less than '*2L/c'* (ratio of two times length to celerity of pressure wave), the valve closure time does not affect the maximum pressure rise. In that condition (sudden closure), the maximum pressure is related to the Joukowsky equation. When valve closure time is higher than '*2L/c'* (gradual closure) the pressure rise is less than the Joukowsky pressure.

The deviations of the numerical results from the experimental results in water hammer studies were a topic of research for several decades. Stephens et al. (2011) pointed out that most of the existing numerical transient models predicted the first water hammer pressure peak accurately but failed to predict the further phase lag or damping of pressure wave accurately. The researchers concluded that the reasons for this mismatch might be the

presence of entrained air, unsteady friction, friction losses and mechanical damping. A transient model incorporating mechanical damping was able to predict the field results accurately. Mitosek and Szymkiewicz (2012) suggested a modification of the governing equations for unsteady pipe flow, on the basis of the results of many experiments carried out in steel and high-density polyethylene (HDPE) pipes of various lengths. The researchers proposed an approximate model for the elastic behaviour of the liquid and the pipe materials that account for the variable pressure wave velocity. The numerical tests showed that the proposed approach leads to a better agreement between the computational and experimental results. Also, the compressibility of water and the elasticity of the material of the pipe wall have major roles to play in the wave attenuation.

Amara et al. (2013) also identified the deviation of numerical results from experimental results while simulating water hammer events. The researchers suggested a modification in the finite difference MacCormack scheme, by introducing an artificial viscosity and dissipation constant, to minimise the error between numerical and experimental results. The researchers used the two-step Runga - Kutta splitting technique for solving the governing equations. The adapted MacCormack scheme gave better results compared to the original one. Meanwhile Shimada and Vardy (2013) conducted a few simulations to assess the influence of grid type, size and shape while using fixed-grid MOC for modelling water hammer events. The performances of a diamond grid and rectangular grid in the analysis of water hammer were assessed. The changes in grid type did not alter the numerical results though the grid types had their advantages and disadvantages.

Influence of various factors on flow characteristics were also studied by conducting transient flow analysis to find out the reason for pressure wave damping. Mansuri et al. (2014) numerically investigated the effect of pipe roughness and reservoir water levels on the pressure waves during various transient events in a piping system. The effect of pipe wall roughness was studied by giving different values for Darcy's Weisbach friction factor ranging from 0.002 to 0.1. The results indicated that the pressure wave damped more with an increase in the friction factor, but the reduction is only marginal. This behaviour suggested that the other mechanisms contributed to the deviation between the predicted and experimental results of pressure wave. Monajitha et al. (2014) also found that the experimental pressure wave damps out quickly compared to the numerical simulation. Generally, the 1-D numerical model simulates the first peak in the transient pressure variation

accurately, but it cannot capture the quick decay exhibited by the experimental pressure signals (Mitosek and Szymkiewicz, 2012; Monajitha et al., 2014). This difference between the observed and the calculated pressure characteristics during a transient flow may be due to the lack of representation of actual experimental conditions that range from the losses due to air entrainment to the losses due to pipe wall hysteresis.

Mitosek and Szymkiewicz (2016) studied the influence different factors on the damping of pressure wave and tried to establish a relation between the pipe length and the speed of pressure wave in a reservoir-pipe-valve system. Experiments were conducted for different pipe lengths ranging from 12 m to 177.4 m, and the periods of pressure waves were measured from the pressure wave cycle, and thus the wave celerity of each pipe length was calculated. The researchers found that the celerity of the pressure increased with the pipe length and was attributed to the effect of reservoir in case of pipes of small length. Following the numerical studies on the effect of valve closure time on transient flow, Kodura (2016) investigated the effect of valve closure time on peak of water hammer pressure by conducting experiments in steel and polyethylene pipelines. Four closure times were selected for the experiment, of which one was sudden closure and the remaining three were gradual closure. The researcher compared the performance of existing numerical models for predicting the pressure variation during gradual closure of valve and found that the predicted pressure peak is lower than the actual pressure peak obtained from the experiments. Seck et al. (2017) conducted a numerical investigation by using water hammer equations in conservation form, incorporating dynamic friction instead of quasi-steady friction. The researchers compared the developed numerical model with an analytical solution, experimental results and a quasi-steady friction model and found that the dynamic friction model predicted the wave attenuation better than the quasi-static model. However, there is further room for improvement as there was an appreciable deviation of simulated pressure wave, even after implementation of the dynamic friction model, viz, the Brunone's model (Brunone et al. 1991) modified by Bergant (Bergant et al., 2001), from the measured one. These deviations always point towards the need for attempting alternative approaches to account pressure wave damping.

From the literature review in the area of water hammer, it is found that the classical water hammer equations can be successfully used for the analysis, design, health monitoring and failure analysis of piping systems. The review also reveal the fact that one-dimensional

classical water hammer equations predict the first pressure rise accurately, but fail to model the damping of pressure waves. Several researchers tried to reduce this deviation in the damping of pressure wave by incorporating the various concepts like unsteady friction, the variable unsteady friction, the artificial viscosity and the dissipation constant into the 1-D model. However, there is further room for improvement as there was an appreciable deviation of simulated pressure wave, even after implementation of these strategies, as seen in the study by Seck et al. (2017). These deviations always point towards the need for attempting alternative approaches and higher dimensional models.

2.3. Cavitation

Water hammer waves cause pressure rise/drop alternatively in the piping system. When low pressure prevails for a long time, the system is subjected to cavitation. Research area on cavitation in transient flow itself is very wide including gaseous cavitation, vaporous cavitation and column separation. Among these, transient vaporous cavitation is mainly included in this study. Transient vaporous cavitation is the formation, growth and collapse of vapor bubbles in a flowing liquid of a closed conduit in a region where the pressure of the liquid drops to its vapour pressure. If the vapour pressure exists for a large period time, the liquid column will be separated into two liquid columns with an intermediate vapour pocket. Such a condition is referred as column sparation and the area containing vapour is referred as cavity.

Tarasevich (1980) derived the equations for the calculation of water hammer pressure and the maximum pressure due to the collapse of cavity by assuming column separation during cavitation. Simpson and Bergant (1994a) summarized the previous experimental investigations in the field of water hammer with column separation. Further, these researchers conducted experiments in a copper pipe line with two flow visualization polycarbonate blocks. The researchers recommended the usage of a flush mounted pressure transducer with high overall natural frequency, to capture sharp pressure pulses. Simpson and Bergant (1994b) conducted a numerical study of column separation and compared six cavity models including Discrete Vapour Cavity Model (DVCM) and Discrete Gas Cavity Model (DGCM). These comparisons of column separation models were carried out in two horizontal pipeline systems (both short and long pipelines) with a valve at the downstream end. The effect of parameters like wave speed, friction factor, initial velocity, diameter of the pipe and length

of the pipe, on the maximum pressure rise was also included in this investigation. The researchers recommended the model DGCM to simulate column separation accurately. Later in 1999, the researchers (Bergant and Simpson, 1999) proposed a classification for column separation flow regimes as active column separation and passive column separation. In active column separation flow regime, the maximum pressure at the valve is governed by column separation. In passive column separation flow regime, the maximum pressure at the valve is not altered by the column separation and is equal to the water hammer pressure itself.

Mitosek (2000) experimentally investigated the cavitation phenomena in elastic and visco-elastic pipes during transient fluid flow. Three pipe materials were considered for the tests, viz., steel, Medium Density PolyEthylene (MDPE) and Unplasticized PolyVinyl Chloride (UPVC). Experiments were repeated for two different pipe lengths, with different inlet pressure. The researcher found that the frequency of cavitation pressure oscillations depends on pipe wall elasticity and duration of oscillation. Similarly, the maximum increase in cavitation pressure depends on the pressure wave velocity and the period through which cavitation prevails.

Singhal et al. (2002) conducted a comprehensive study on the transient vaporous cavitation and developed an analytical model for its representation. In order to compute the change in fluid property during phase transition, the vapour transport equation was used. The expression for phase change rate was derived from a reduced form of Rayleigh-Plesset equation for bubble dynamics (Singhal et al., 2002). This model considers all the first order effects including phase change, bubble dynamics, turbulent pressure fluctuations and presence of non-condensable gases in the fluid. The model has the capability to account for N- number of phases; species transport effects, provision for giving slip velocities between the phases, and thermal and compressibility effects in both phases.

The model was derived from the basic continuity equations for multiphases, constitutitve relationship, and Rayleigh-Plesset buble dynamics equation (as given in the equation 2.3)

$$\frac{\partial}{\partial t}(f_v \rho) + \nabla.\left(f_v \rho \vec{V}_v\right) = \nabla.(\Gamma \nabla f_v) + R_e - R_c \tag{2.3}$$

where f_v is the vapour mass fraction, R_e and R_c are the vapour generation and condensation rates and Γ is the diffusion coefficient. The rate of mass exchange is given by the following equations 2.4 and 2.5 (Singhal et al., 2002).

$if P \leq P_v$

$$R_e = F_{vap} \frac{\max\left(1.0, \sqrt{k}\right)\left(1 - f_v - f_g\right)}{\sigma} \rho_l \rho_v \sqrt{\frac{2}{3}\frac{(P_v - P)}{\rho_l}}$$

(2.4)

$if P \geq P_B$

$$R_c = F_{cond} \frac{\max\left(1.0, \sqrt{k}\right) f_v}{\sigma} \rho_l \rho_v \sqrt{\frac{2}{3}\frac{(P - P_v)}{\rho_l}}$$

(2.5)

where F_{vap} *and* F_{cond} are the constants in vapour generation and condensation rate expressions, k is the turbulent kinetic energy, f_g is the gas mass fraction, f_v is the vapour mass fraction, P_B is the bubble pressure and P_v is the vapour pressure.

Schnerr and Sauer (2001) proposed a model with the same approach as Singhal et al. model to derive an exact expression for the net mass transfer from liquid phase to vapour phase. The expression for the vapour volume fraction is of the form (Eqn. 2.6) (Schnerr and Sauer, 2001)

$$\frac{\partial}{\partial t}(\alpha \rho_v) + \nabla.\left(\alpha \rho_v \vec{V}\right) = \frac{\rho_v \rho_l}{\rho} \frac{D\alpha}{Dt}$$

(2.6)

Schnerr and Sauer (2001) used the following expression to relate vapour volume fraction and the number of bubbles per unit volume of liquid as given in equation 2.7 (Schnerr and Sauer, 2001).

$$\alpha = \frac{n_b \frac{4}{3}\pi {R_B}^3}{1 + n_b \frac{4}{3}\pi {R_B}^3}$$

(2.7)

where n_b is the number of bubbles per unit volume of liquid and R_B is the bubble radius. This expression was used to derive the net bubble formation and transfer rate and resulted in the following relations (Eqn. 2.8 and 2.9) (Schnerr and Sauer, 2001).

$$R = \frac{\rho_v \rho_l}{\rho} \alpha(1-\alpha) \frac{3}{R_B} \sqrt{\frac{2}{3} \frac{(P_v - P)}{\rho_l}} \tag{2.8}$$

$$R_B = \left(\frac{\alpha}{1-\alpha} \frac{3}{4\pi} \frac{1}{n}\right)^{\frac{1}{3}} \tag{2.9}$$

where R is the mass transfer rate of the bubble.

This model has the characteristics that the mass transfer rate is proportional to $\alpha_V(1-\alpha_V)$ and the function $f(\alpha_v, \rho_v, \rho_l) = \frac{\rho_v \rho_l}{\rho} \alpha(1-\alpha)$ approaches zero when $\alpha=0$ and $\alpha=1$ and has the maximum value in between. Moreover, this model requires the user to input only the number of spherical bubbles per unit volume of the liquid, thus simplifying the user input.

Historical review by Bergant et al. (2004, 2006) includes a detailed survey of the numerical models and experimental work conducted in the field of water hammer with column separation. Transient vaporous cavitation is only included in this review and other two types gaseous cavitation and steam condensation were not considered. From the survey, the researchers concluded that the DVCM model could validate the test results. Based on Singal et al.(2002) model, Zwart et al. (2004) conducted further studies and proposed a modified cavitation model known as Zwart-Gerber-Belamri model. Singhal et al.(2002) model is the basic model of bubble dynamics and represent many advanced factors, which in practical situation can be neglected or assumed. In the Zwart-Gerber-Belamri model, all the bubbles in the system are assumed to have same size, and hence the total inter-phase mass transfer rate per unit volume (R) is calculated using the bubble number densities (n). Therefore, the rate of change of mass of a single bubble is given by the equation 2.10 (Zwart et al., 2004).

$$R = n \times \left(4\pi {R_B}^2 \rho_v \frac{DR_B}{Dt}\right)$$

(2.10)

The main difference between this relation and the Singhal et al. (2002) relation is that, the mass transfer rate is dependent on both liquid phase and vapour phase densities in the former, while it is dependent only on the vapour phase density in the latter,.

Various cavitation models available in literature viz., column separation model, Adamkowski's model, gas vapour cavitation model and bubbly cavitation model, were compared for their efficiency by Urbanowicz and Zarzycki (2008). Among these four models, the column separation model, Adamkowski's model and bubbly cavitation model are very good in the simulation of cavitation. Adamkowski's model found to be the best model among the three models which correctly simulates the pressure amplitude of the experimental results. Lee et al. (2008) conducted a numerical investigation to study the effect of air entrainment in the wave speed by introducing a variable wave speed model. The researchers considered free gas in liquid along with vaporous cavitation bubbles in the model. Numerical study showed that the presence of gas in fluid amplifies the first pressure peak and fasten the energy dissipation.

Brunone et al. (2009) experimentally investigated the transient flow in a pipe caused by the rapid opening of the downstream valve in the pipe system. This scenario replicates the maintenance of piping system, in which the upstream valve of the pipe system will be closed and the downstream valve will be opened after that. The experiments were conducted in HDPE pipe installation with different initial pressure. The experimental analysis revealed that the water column separation was more severe near the inlet. Adamkowski and Lewandowski (2009, 2012) developed a new discrete vapour cavity model (DVCM) by incorporating unsteady friction and compared it with the existing DVCM model. Experiments were conducted in a copper pipe with two visualizing segments made of plexi-glass pipe and found that generated vapour due to cavitation was distributed along the pipe, with maximum concentration close to the valve. The proposed model was found to be better in predicting pressure amplitude, damping ratio and frequencies. Keramat et al. (2010) developed a model for the analysis of column separation in visco-elastic pipes. The column separation was modelled with DVCM model and visco-elasticity was modelled with Kelvin-Voigt elements. The researchers concluded that the retarded behaviour of visco-elastic pipes strongly

dampens the pressure waves. The proposed model was tested satisfactorily against test results of Soares et al. (2009) and Covas et al. (2004).

Sumam et al. (2010) presented an alternate approach for modelling transient vaporous cavitation using a one-dimensional model. Cavitating flow was simulated using continuity and momentum equations for water vapour mixture and transport equation was used for vapour phase. A pressure under-relaxation strategy was employed for developing the model. The model could simulate the flow characteristics of the published and experimental results reasonably well. The researchers also emphasised the need for using a fine time step (10^{-5}s) for predicting the sharp pressure peaks generated in cavitation. Influence of visco-elasticity of pipe material on transient cavitating flow was a topic of interest for many researchers. Lind and Philips (2012) numerically evaluated the influence of visco-elasticity on the collapse of vapour bubbles as a result of cavitation near a wall boundary. During the study, the researchers noticed the occurrence of oscillations during bubble collapse and found that the collapse and perturbation of bubbles are more, close to the boundary wall. Bombardieri et al. (2014) experimentally investigated the water hammer phenomena during the priming of pre pressurized and evacuated pipelines and verified by using one-dimensional two-phase flow numerical simulation. The researchers concluded that the mismatch between the numerical and experimental results was resulted from the lack of representation of cavitation and condensation in the model.

Geng et al. (2017) modelled transient cavitating flow by using a combination of the MOC (for water hammer) and the FVM (for cavitation using openFOAM). Based on the study, the researchers suggested to reinforce the pipe at the outlet where the cavitation pressure is the maximum. Pezzinga and Santoro (2017) studied two different cavitation models, viz., bubble-flow models and shallow-water model in both 1-D and 2-D by using the MacCormack numerical scheme. The researchers found that 1-D model overestimated the head values and failed to predict the correct shape of the variation of pressure head, while 2-D model predicted both accurately.

Many investigators (Barten et al., 2008; Soares et al., 2009; Sumam et al. 2010) modelled the transient vapourous cavitation in a pipe by using 1-D flow and transport equations and obtained reasonable accuracy. Pezzinga and Santoro (2017) compared the performance of the 1-D and 2-D model for transient cavitation and found that performance of the latter was better. However, there is further scope for improvement as the deviation in the

energy dissipation was observed. This observation points towards the need for using a higher dimension model for modelling the transient cavitation. Lind and Phillips (2012) observed that the collapse and perturbation of bubbles in a cavitating flow in pipe are more close to the boundary wall. This observation also reinforce the need for using higher dimension models.

2.4. Computational Fluid Dynamics (CFD)

Recently, many attempts have been made to use the Computational Fluid Dynamics (CFD) models for the analyses of problems of transient flow in a piping system. Here, the governing equations are the same conservation equations but in its full form considering almost all processes like friction, boundary layer, three-dimensional variability of flow variables. Thus, the fluid flow is governed by the Partial Differential Equations (PDE) that depict the conservation laws of mass, momentum and energy, and state equation. CFD is the art of replacing a set of PDE by a set of algebraic equations which can be solved by using efficient linear equations solvers. Most of the CFD solvers are based on Finite Volume Method (FVM) in which the domain is discretised into a finite set of control volumes. General conservation equations for mass, momentum and energy are solved on these set of control volumes.

Bakker and Marshall (2006) reviewed the CFD methodology and illustrated the different steps in developing a model by using the CFD. The boundary conditions available in the CFD software, the criteria for selecting appropriate boundary conditions and details of FVM were well explained by the researcher. Salvador et al. (2007) made use of Singal et al. model available in ANSYS Fluent for predicting the cavitation pressure, which considers two phases- liquid and vapour along with small fraction of non condensable gases. Some simple geometry pipes were considered for the study, viz., a circular orifice, a rectangular orifice, a circular nozzle and a rectangular venturi. The model could predict the experimental results to satisfactory level.

Sahu et al. (2009) created a CFD model of the piping system for fully developed laminar flow in FLUENT and studied the variation of velocity and friction factor along the axis of the pipe. The friction factor obtained from the numerical study matched well with the experimental result, which indicated the capacity of the software to predict flow characteristics. Jinping et al. (2010) studied the effectiveness of the SIMPLE (Semi Implicit Method for Pressure Linked Equations) algorithm available in CFD software to model water

hammer phenomenon by taking experimental results from Bergant and Simpson (1994). The results established the capability of the model to simulate transient flow.

Bhandari and Singh (2012) numerically investigated the variation of axial velocity and the skin friction in the transient flow through the pipe by using a CFD software. From the study, the researchers found that the axial velocity initially increases along the pipe length and reaches a constant value, while the skin friction decreased along the pipe length and reached a constant value. Kozubkova et al. (2012) compared different cavitation models available in the ANSYS Fluent by considering the numerical simulation of flow in a cone. Singal et al. model and Zwart–Gerber–Belamri models were considered for comparison. The researchers found that the Zwart–Gerber–Belamri model showed larger cavitation region with low frequency.

Saemi et al. (2014) investigated the water hammer phenomena in both laminar and turbulent flows with the help of the CFD software ANSYS FLUENT. The transient analysis was conducted by using two different turbulence models, viz., Re-Normalisation Group (RNG) k-ε model and k-ω Shear Stress Transport (SST) models. Two experiments were conducted in a copper pipe for validating the numerical models; one with Reynold's number (Re) 82 to simulate the laminar flow and the other with Re as 5700 to model the turbulent flow. The researchers realised that both models predict the flow with acceptable accuracy, but the k-ω SST model predicted pressure peak better than the other. Martins et al. (2014) presented a procedure for selecting an efficient mesh in a 3-D-CFD model, for attaining both computational accuracy and the minimum computational time, in terms of three non-dimensional parameters. The authors of the paper arrived at these parameters by comparing the computed velocity profile with the available exact profile for the laminar flow and the semi-empirical profiles for turbulent flows.

Transient analysis using the CFD was found to be very useful in the design of surge protection devices also. Lahane et al. (2015) numerically simulated the water hammer event, created in a rectangular pipe as a result of the valve closure at the inlet, by using CFD software ANSYS Fluent and identified the critical locations where surge protection devices are to be provided to withstand the adverse effect of water hammer. The study conducted by Ahmadi and Keramat (2010) on the effect of valve closure time on the transient flow were extended by Smitha and Miji (2016) by using the CFD software ANSYS FLUENT. The researchers used the experimental results of Mitosek and Szymkiewicz (2012) to validate the

results. From the two numerical simulations, it was confirmed the fact that when the valve closure time is less than *'2L/c'*(sudden closure condition), the pressure rise due to water hammer is the same as Joukowsky pressure whereas the pressure rise reduces with the increase in valve closure time in the case of gradual closure.

Wang et al. (2016) effectively simulated the flow in a reservoir-pipe-valve system with pipe elevated at the downstream end by using a 2-D cavitation model in the CFD software ANSYS Fluent, and found it as a better model in predicting the experimental results than 1-D discrete vapour cavity model. The Schnerr-Sauer cavitation model and SST k-ω turbulence model were used in the study. Unsteady Reynold's Averaged Navier – Stokes equations were solved for the mixture of liquid and vapour with a time step size of 0.0001s. The researchers reported that the 2-D-CFD model was better for predicting the formation of bubbles along the top of the pipe wall, which was represented by the 1-D model. However, neither the experiment nor the numerical study discussed about the high frequency oscilations normally present in a transient cavitating flow. Mitosek and Szymkiewicz (2000) indicated that the high frequency oscillations in a cavitating flow can be captured by the measuring system in an experimental setup only if the sampling time is less than or equal to 10^{-5} s. This could be the reason for getting matching results even when the sampling time and simulation time step is less than or equal to 10^{-4} s.

Mostafa et al. (2016) numerically studied the cavitation phenomenon on hydrofoil using Singal et al. model and CFD. Three different turbulence models were used to compare the performance of the numerical models in capturing the boundary layer characterstics properly. It was found that the RNG k-ε model with enhanced wall treatment was better to model the turbulence and boundary layer characteristics. Martins et al. (2016) carried out a detailed analysis of the flow characteristics of the transient flow by using a 3-D-CFD model. The highly refined mesh sizes as specified in Martins et al. (2014) renders the analysis of practical problems almost impossible as a result of huge computation time. Computation time increases exponentially with decrease in the size of elements. Jansson et al. (2017) numerically studied the cavitation induced during the transient flow and compared the results from the simulation with that from the experiments conducted in a oil filled pressurised tank-pipe-valve system. The two-dimensional numerical study was conducted by using CFD, in which the researchers used Schnerr- Sauer cavitation model with a very fine mesh and with

time step of 1 μs. Large amplitude hydraulic transients due to bubble collapse were well predicted by the CFD model.

Martins et al. (2017) compared the performance of two types of unsteady friction models for simulating the energy dissipation characteristics of transient flow viz., the instantaneous acceleration–based (IAB) and convolution based (CB) 1-D flow models, by utilising a two-dimensional CFD model with high spatial and temporal resolutions. The researchers concluded that the convolution-based UF models better describe the pressure signal than the instantaneous acceleration–based ones because they take into account a set of previous time steps. Martins et al. (2018) used a CFD model for laminar transient flow (using ANSYS FLUENT) through a piping system, to study the instantaneous pressure and velocity distribution along the pipe radius and found that the wall shear stress and axial velocity components near to the pipe wall are strongly related. Although the CFD models are used for analysing the transient flow in a piping system, their capability in predicting the damping of pressure wave has not been explored.

From the discussions in this section, it is realised that CFD is a powerful tool for transient flow analysis. But its capability for modelling the damping of pressure wave has not been explored yet. The interaction between fluid and pipe can easily be achieved by CFD analysis of transient flow with fluid-structure interaction (FSI). For incorporating FSI in transient flow analysis, different numerical and analytical methods have been developed so far. Hence, the next section discusses the different research works conducted till now for the modelling of transient flow with FSI.

2.5. Fluid Structure Interaction (FSI)

The fluid pressure produced as a result of transient flow event induces motion in the structural components of the piping system, which in turn, changes the flow conditions. Most of the studies on water hammer consider the fluid system alone, without considering the effect of deformation of the pipe material and its mutual interaction; and this lack of representation could be one of the possible reasons for the deviation in the damping of the pressure wave during transient flow. In classical water hammer theory, an equivalent bulk modulus K^* (Eqn. 2.11) is included to represent the effect of pipe material and thickness of pipe and elastic properties of the pipe material (Bergant et al., 2006; Tijsseling and Anderson, 2006; Wiggert et al., 1987).

$$K^* = \frac{K}{\left(1 + \frac{DK}{eE}\right)}$$

(2.11)

where K is the bulk modulus of fluid, D is the internal diameter of the pipe, e is the thickness of the pipe wall, and E is Young's modulus of the pipe material. But this representation of the elasticity of the pipe material may not be sufficient to simulate the actual behaviour of the system during a water hammer event with high pressure, as the pipe can deform in case of large pressure and thus changing the boundary condition of the fluid. This change in boundary condition can have a substantial effect on the pressure damping and hence, shall be considered in the analysis for getting more realistic results. Probably, ignoring this effect leads to acceptable results for rigid pipes, but the incorporation of FSI into the model becomes essential for flexible pipes. In such cases, the dynamic analysis of both the fluid and the structure has to be carried out together.

2.5.1 Four-Equation model and Fourteen-Equation model

Two mathematical models are commonly used in the literature for the analysis of FSI, viz., four-equation model and fourteen-equation models. In four-equation model, the liquid one-dimensional equations (Eqn. 2.2) and pipe axial motion equations (Eqn.2.12) are used for the analysis.

$$\frac{\partial \dot{u}_x}{\partial t} - \frac{1}{\rho_t}\frac{\partial \sigma_x}{\partial x} = 0$$

$$\frac{\partial \dot{u}_x}{\partial x} - \frac{1}{E}\frac{\partial \sigma_x}{\partial t} = -\frac{\nu R}{Ee}\frac{\partial P}{\partial t}$$

(2.12)

where u_x is the pipe displacement component in x direction, σ_x is the pipe stress component in x direction, E is the modulus of elasticity of pipe material, e is the pipe wall thickness, R is the internal radius of pipe, P is the pressure and ν is the Poisson's ratio.

The fourteen-equation model uses 1-D flow equations along with all the structural equations including axial, bending and torsion equations, which treats the pipe as a slender

member. Lateral bending equations in y direction is given in Eqn.2.13 and similar four equations are there in z direction also. Torsion equations are given in Eqn. 2.14.

$$\frac{\partial \dot{u}_y}{\partial t} + \frac{1}{\rho_t A_t + \rho_f A_f}\frac{\partial Q_y}{\partial x} = 0$$

$$\frac{\partial \dot{u}_y}{\partial x} + \frac{1}{\kappa^2 G A_t}\frac{\partial Q_y}{\partial t} = -\dot{\theta}_z$$

$$\frac{\partial \dot{\theta}_z}{\partial x} + \frac{1}{E I_t}\frac{\partial M_z}{\partial t} = 0$$

$$\frac{\partial \dot{\theta}_z}{\partial t} + \frac{1}{\rho_t I_t}\frac{\partial M_z}{\partial x} = \frac{1}{\rho_t I_t} Q_y$$

(2.13)

$$\frac{\partial \dot{\theta}_x}{\partial t} - \frac{1}{\rho_t J_t}\frac{\partial M_x}{\partial x} = 0$$

$$\frac{\partial \dot{\theta}_x}{\partial x} - \frac{1}{G J_t}\frac{\partial M_x}{\partial t} = 0$$

(2.14)

where A_f is the cross-sectional area of fluid, A_t is the cross-sectional area of pipe, G is the shear modulus, J_t is polar moment of inertia of pipe, M_x, M_y, M_z are the bending moments in x, y, z directions, Q_x, Q_y, Q_z are the shear forces in x, y, z directions, u_x, u_y, u_z are the pipe displacements in x, y, z directions, θ_x, θ_y, θ_z are the rotation of pipe in x, y, z directions, κ^2 is the shear coefficient of pipe wall and, ρ_t and ρ_f are the densities of the pipe and the fluid respectively.

Wiggert et al. (1987) introduced a numerical model for the analysis of transient flow through pipes, which accounted for the coupled motion of fluid and pipe. The researchers tested the developed numerical model by using the results of the experiment conducted in a system of three pipes connected orthogonally in series. The researchers considered 1-D flow equations along with all the structural equations including axial, bending and torsion

equations, treating the pipe as a slender member. The fourteen governing equations were classified into four groups, with four equations each in three groups and two torsion equations in the fourth group. The 1-D flow equations and two equations corresponding to axial motion of the pipe were coupled together at every point and solved. While the lateral motion equations and torsion equations were not coupled together at every point but were instead coupled at pipe junctions only, through boundary conditions. Hence, the coupling system in this 1-D model was only partial. Lavooij and Tijsseling (1991) incorporated FSI by including axial motion equation of the pipe with the 1-D fluid flow equations into the model. The researchers considered three different coupling mechanisms in the model viz., Poisson coupling, junction coupling and friction coupling. The researchers used the MOC to solve 1-D fluid equations, and Finite Element Method (FEM) to solve the structural equations.

Experimental study on water hammer incorporating the effect of piping system and its support system is not common in literature. Heinsbroek and Tijsseling (1994) experimentally investigated the effect of rigid vs flexible supports on transient flow characteristics by conducting experiments on seven straight pipes that were connected by six 90^{o} bends, suspended by steel cables and supported by springs at the bends. It was found that the influence of support anchors on the transient behaviour of the system is small for anchor with rigidity more than the axial stiffness of one meter of pipe. But for flexible support system, FSI is more important and to be considered for the determination of equivalent stress in the piping system. The researchers found that the maximum stress developed in the flexible systems was higher than that in the rigid system. Meanwhile, the forces acting on the support were less for the flexible system.

Heinsbroek (1997) used two different numerical procedures for solving the FSI problems. The first method used a combination of the MOC (for fluid) and FEM (for structural) and the second used the MOC for both. The fourteen-equation model was used for the study. Numerical simulation was carried out with the help of FLUSTRIN code developed by the DELFT HYDRAULICS. The study was conducted by using the experimental results of Heinsbroek and Tijsseling (1994). By comparing the results of numerical and experimental studies, it was found that Bernoulli- Euler theory along with MOC-FEM numerical procedure was better choice for the considered FSI problems. With the experimental setup of Heinsbroek and Tijsseling (1994), the same researchers investigated the influence of movement of bends on a 3-D suspended pipeline with a total of 6 bends - restrained and

unrestrained (Tijsseling and Heinsbroek, 1999). Pressure head history was plotted for 16 cases by changing the conditions of bend. It was found that the pressure peak exceeded the value calculated by the Joukowsky equation. Maximum stress in the pipe was found to be the lowest when most of the bends are restrained. Tijsseling (1996) carried out a detailed review of the mechanisms used in the modelling of FSI and concluded that 1-D fourteen-equation model describing longitudinal, lateral and torsional motion for the liquid filled pipe system is generally sufficient to represent the fluid-structure interaction. Wiggert and Tijsseling (2001) also conducted a detailed review on the essential mechanism that causes FSI in the liquid filled flexible piping system. One additional feature of flexible pipes compared to rigid pipe is its visco-elasticity.

Visco-elasticity is the property of materials that exhibit both viscous and elastic characteristics during deformation. Under applied load, these materials exhibit instantaneous elastic strain followed by gradual retarded strain. The polymers are visco-elastic in nature but this factor is neglected in the hydraulic transient analysis by most of the researchers. Visco-elastic behavior of pipe material causes damping of pressure wave and increases the rate of energy dissipation. Pezzinga (2002) experimentally tested the effectiveness of inserting an HDPE pipe downstream of the pump for suppressing surges in a piping system. The experimental conditions were numerically simulated by a 1-D and quasi- 2-D models which incorporated the visco-elasticity of the pipe by mean of Kelvin–Voigt model. The proposed model could predict the experimental results better than the conventional elastic model.

Apart from the numerical methods adopted earlier, Li. et al. (2003) proposed a new analytical solution for the FSI four equation model, based on D' Alembert wave solution. The proposed model was validated with the test results of a suspended closed tube setup of Vardy and Fan (1989). This analytical model diminished the error in numerical method. Covas et al. (2004, 2005) presented a mathematical model incorporating visco-elasticity of the pipe material and unsteady friction, and validated the model with the data from a hydraulic transient experiment conducted in a polyethylene pipe system. Pressure and circumferential strain data were collected by conducting the experiments for ten different flow rates. Creep compliance function of the polyethylene pipe was estimated by conducting creep tests in pipe specimens. For modelling the unsteady friction, the head loss was decomposed to steady state component and unsteady state component. Linear visco-elasticity model was used for

modelling visco-elasticity, which included instantaneous strain and gradual retarded strain. The researchers observed that the pressure wave was highly attenuated and dispersed in time due to the visco-elasticity of the pipe material.

Tijsseling and Vardy (2004) distinguished seven types of fluid flow with time scale as no flow, steady flow, quasi-steady flow, rigid column, water hammer with 1-D-FSI, 2-D-FSI and 3-D-FSI. The researchers have presented governing equations for all of them. The importance of friction, elasticity, inertia and Poisson's coupling at different time scales are investigated using a numerical model. Jo (2004) classified FSI problems into two, viz., weakly coupled and strongly coupled FSI systems. The researcher stated that if the deformation of the structure is very less or negligible, the influence on the fluid domain will be less and they are weakly coupled. In contrast if the deformation is more in structure, the fluid and the structure domains are strongly coupled. Governing equations and their coupling mechanism are also explained by the researcher. Stella et al. (2005) incorporated the computational solid mechanics (CSD) along with the CFD and developed a new methodology for the analysis of FSI problems. CFD solver FLUENT and CSD solver ADINA were used in this study. The researchers conducted a study on hot flow through a flexible pipe and found that the elasticity of the pipe material influences the distribution of heat flux along the pipe. This study illustrates the possibility of such coupling.

Tijsseling (2007) developed a four-equation model for FSI analysis, by averaging hoop and radial stresses for thick-walled pipes. The researchers coupled the liquid 1-D equations, and the axial and the radial motion equations of the pipe through boundary conditions. An experiment was conducted on a closed steel straight pipe suspended freely, excited by hitting at one end of the pipe by a solid rod. Etlender et al. (2007) presented an FSI model for transient flow in flexible hoses. FVM was used for the discretisation of fluid and FEM was used for the discretisation of pipe structure, as thin shell. Iterative-staged-algorithm was used for FSI coupling. The researchers concluded from the study that the wall flexibility substantially influenced the propagation speed and damping of pressure waves.

Ahmadi and Keramat (2008) investigated the effect of junction coupling at valves and junctions of a piping system. A combination of the MOC and the FEM methods were used for the analysis of fluid and pipe equations respectively and were implemented by using MATLAB. The results showed that the junction coupling effects depended mainly on rigidity of the piping system. Jiang et al. (2009) numerically conducted the FSI analysis to identify

the influencing parameters of structural deformation during water hammer and found that the major influencing parameters were the pipe length, the fluid velocity, the pipe thickness and the fluid density whereas the less influencing parameters were the pipe diameter, the elastic modulus, the Poisson's ratio and the fluid viscosity. Henclik (2010) presented a new solution algorithm for the four-equation model, and used this for studying a reservoir-pipe-valve system with a number of rigid supports. Numerical investigations proved that Poisson's effect was the factor that influenced the pressure variation resulting from a transient event in a relatively rigid restraint pipe.

Keramat et al. (2012) considered the FSI and the visco-elasticity together for the modelling of the transient flow in a piping system. Visco-elasticity was modelled by using the Kelvin–Voigt model and the FSI by using four-equation model. Two modelling strategy were used for the numerical solution . viz., the MOC–FEM approach and the full MOC approach. Poisson's and junction coupling were considered in both methods. Numerical results were compared and found to be satisfactory with the available experimental results. Xu et al. (2012) studied the causes and effects of vibration in a marine pipe system during a transient event. Transient flow incorporating FSI through a fluid filled pipe elbow was used for the numerical simulation by using ADINA software. From the numerical study, the researchers concluded that the deformation was maximum at the elbow, and hence, the protection against vibration is most important near elbows. Meanwhile, the fluid velocity highly influenced the pipe vibration and deformation. As the velocity increased pipe vibration and deformation also increased. Wilcox (2012) conducted transient mechanical analysis of the piping system for partial closing of the valve by using the AFT impulse software and CEASAR II software. The researcher reported that the unbalanced forces occurred at the locations, where there are changes in direction of flow or changes in area of cross section, can be evaluated by using this method of analysis.

Hou et al. (2012) reviewed the recent development in the area of FSI and reported the challenges faced by the researchers working in the area of FSI. The researchers realised that the FSI problem in its full complexity pose significant challenges to the present numerical computation methods, and only a few works have been reported with such investigation considering all the important aspects. Li et al. (2014) conducted vibration analysis of liquid filled pipe lines using finite element method (FEM) considering the pipe as a plane beam element. Lagrangian interpolation function, first order Hermite interpolation function and

Ritz method were used for developing the numerical model in the MATLAB. Simao et al. (2014, 2015) studied the dynamical behaviour of a pipe system during a water hammer event by using 3-D-CFD analysis for fluid and FEM analysis for structure. Water hammer experiments were conducted in GI and PVC pipe installations supported on iron supports. The number of supports and position of supports were not disclosed in this paper. Three support conditions were simulated - pipe with frequent expansion joint, pipe against longitudinal movement throughout its length and pipe against longitudinal movement at the upper end. The wave velocity was calculated by incorporating these support conditions in the equation. From the numerical study, the researchers calculated the displacement of the pipe at various locations for different conditions. That information was found to be very useful for the design of piping system.

Wu et al. (2015) considered a pump along with the piping system and used the CFD software - FLUENT to model the pump and MOC to model the pipeline system. In the study, the MOC code was kept as a master programme and Fluent code as a slave code. The proper interaction between the models was established by using a separate coupling code. The model could predict the experimental results reasonably good. Zhu et al. (2014) conducted a coupling analysis with FSI to find out the flow erosion and the pipe deformation of an elbow pipe with gas-solid flow. Finite volume method was used to discretise the solution domain. All the simulations were carried out in CFD package ANSYS workbench 14.0. ANSYS Fluent was used to analyse the fluid part and ANSYS mechanical was used to analyse solid part viz., the pipe. From the numerical study, it was observed that the pipe deformation increased with the increase in the inlet flow rate and the curvature to diameter ratio.

Maajel et al. (2015) reviewed recent work conducted in the field of FSI and reported the essence of investigations in the recent fifteen years. The FSI analysis of actual industrial piping system is very complicated due to the presence of too many supports which have to be analysed individually. Hence, it is not viable or economical to build such models. Ferras et al. (2016a) studied the damping mechanism in transient flow through the experiments conducted in a straight copper pipe, a coil of copper pipe and polyethylene pipes. They qualitatively assessed the relative importance of the three phenomena that frequently affect the characteristics of transient pressure wave, namely the FSI, the pipe-wall visco-elasticity and the unsteady friction. They concluded that the most influencing factor in a quasi-rigid pipe (like a copper pipe) is the FSI whereas that in polyethylene pipe is the visco-elasticity.

Ferras et al. (2016b) implemented a 1-D FSI model incorporating the unsteady friction by using the Brunone's, and the Trika's models, and the dry friction for the pipe-support interaction by using the Coulomb's model. The performance of the model was good in predicting the wave damping. Interestingly, the model underestimates the damping effect when the FSI and the unsteady friction alone were used whereas the model overestimates the damping effect when the Coulomb's friction was also included along with the FSI and the unsteady friction (as evident from the comparison of pressure wave). Nonetheless, the approach of nesting the Coulomb model in the FSI friction coupling does not allow for a fully satisfactory description of the observed pressure signal. Ferras et al. (2017) developed a 1-D FSI solver, for a modified form of 4-equation model, capable of describing the resistance to movement of anchor blocks and its effect on the transient pressure wave propagation in straight pipelines. The model takes care of the FSI by means of the 4-equation model, assuming that the predominant effect of FSI is due to axial motion alone and neglecting other forms of actions. The 1-D model is capable of representing anchor blocks taking into account the inertia of the block and the dry friction with the surrounding ground and has practical applications where it is possible to estimate the inertia of the support condition. All these models use 1-D equations for representing the FSI.

Mohan (2016) attempted to model the transient flow incorporating FSI by using a 3-D-CFD model. But, the results of Mohan (2016) indicated that the first pressure peak did not match correctly, rather the first pressure peak was overestimated and shape of the first pressure peak distorted. Moreover, the stabilised support reactions actually differ from the actual static support reactions. It seems that the model did not account for the gravity load. Hence, the model proposed by Mohan (2016) could not capture the basic characteristics; viz., first peak in water hammer and its shape, the reliability of the model was at stake. However, the model indicated a direction towards the damping of pressure wave. Hence, it is appropriate to study the effect of FSI on the damping of pressure wave along with its ability to predict the characteristics of the flow, viz., first peak of water hammer pressure, shape of water hammer pressure and velocity profiles such that reliability of model is well established.

Review of the literature mentioned above on the transient flow analysis with FSI showed that, even though many researchers included FSI in their study, most of them coupled the axial motion equations of the pipe alone, with the fluid equations, in the analysis. The researchers who used the fourteen equation model (1-D model), including the lateral and

torsion equations, considered these equations as uncoupled with other four equations. All the equations were coupled at the junctions only. Moreover, the study of FSI in a practical problem, considering all prominent physical features of the problem, is not present in the literature. CFD analysis of transient flow through pipes, by incorporating FSI, for studying the pressure wave damping are limited in the literature.

Similarly, there are many experimental studies available in the field of water hammer and cavitation, but the studies seeking the influence of support condition/ anchoring system on the transient flow are limited. Although Heinsbroek and Tijsseling (1994) studied the influence of support system flexibility on transient flow, the researchers used a system which was suspended using steel wires, which is rare in practical cases. Ferras et al. (2017) investigated the effect of anchor blocks in the transient flow through straight pipe lines by using four equation model, but the anchor blocks were assumed to be moving along with pipe. Thus, the effect of fixed anchors on the transient cavitating flow has not been explored so far.

Though there are many experimental studies available in the field of water hammer and cavitation, the studies seeking the influence of support condition/ anchoring system on the transient cavitating flow in a practical reservoir-pipe-valve system are limited. If the piping system is not anchored well, it will be flexible and experience excessive vibration during transient flow. The presence of more anchors makes the system rigid and obviously the vibration of the system get reduced. But its impact on the fluid flow characteristics has not been investigated so far. Hence, the present study aims to investigate the effect of fixed anchors on different flow characteristics associated with transient flow in piping systems.

2.6. Summary

The literature review included the works related to the transient flow and the damping of pressure wave, CFD models for the transient flow, FSI and its coupling with fluid model and then cavitation. The review reveals the fact that one-dimensional classical water hammer equations predict the first pressure rise accurately, but fail to model the damping of pressure waves. The lack of representation of fluid-structure interaction in the classical water hammer theory could be one of the possible reasons for the inability in predicting the damping of pressure accurately. CFD analysis of transient flow through pipes, by incorporating FSI, for studying the pressure wave damping are limited in the literature. It may be noted that the

forces acting on the system while considering the FSI is unsymmetrical and therefore, a three dimensional analysis of the system is imperative. Hence, the present study aims to assess the effect of FSI on the damping of pressure wave, by developing a 3-D model with all prominent physical features of the system, with proper interaction between the equations at all nodes and at every time step. Similarly, the experimental studies seeking the influence of support condition/ anchoring system on the fluid flow characteristics during transient cavitating flow in a practical reservoir-pipe-valve system are limited. Hence, the present study also aims to investigate the effect of fixed anchors on different flow characteristics associated with transient cavitating flow in piping systems.

CHAPTER 3

MATERIALS AND METHODS

3.1. General

Classical one-dimensional water hammer equations are most commonly used to model transient flow. Although these equations correctly predict the first pressure peak, a deviation in the damping behaviour of pressure fluctuation is observed between the numerical and the experimental results in such simulations (Araya and Chaudhry, 1997; Brunone et al., 2000, 2004; Mitosek and Szymkiewicz, 2012; Amara et al., 2013; Shimada and Vardy, 2013; Seck et al., 2017; Martins et al., 2017). The pressure fluctuations consequent to transient flow also induce motion/deformation/vibration in the structural components of the piping system, which in turn, change the flow conditions. Most of the studies on water hammer consider the fluid system alone, without considering the effect of deformation of the pipe material and its mutual interactions. This lack of representation is probably one of the reasons for the deviation in the damping of the pressure wave mentioned earlier. Water hammer waves, during its to and fro motion, cause pressure rise and drop alternatively in the piping system. When the pressure drops to vapour pressure, the system can be subjected to cavitation. Research area on cavitation includes gaseous cavitation, vaporous cavitation and column separation. The present study deals with transient vaporous cavitation.

The current study uses a three-dimensional mathematical model which describes both the transient flow in pipes and consequent deformation/motion of the structure, viz., the pipe. This chapter describes the fundamental governing equations, the assumptions, and initial and boundary conditions that are required for the solution of the problem under consideration. Further, it also elucidates the various turbulence models and cavitation models. The solution procedure for the fluid model uses the finite volume method (FVM) and that for the structural part utilises the finite element method (FEM). The chapter includes the fundamental principles of FVM and FEM.

3.2. Governing Equations

Fundamental governing equations of fluid dynamics, solid dynamics, cavitating flow and turbulence are included in this section.

3.2.1. Assumptions

Three-dimensional model of fluid and pipe were selected for the study on FSI. For cavitation modelling, 2-D axi-symmetric model was used. In the numerical investigation of water hammer with cavitation, only transient vaporous cavitation is considered. The following assumptions were used for the study (Niyogi et al., 2006; Anderson and Wendt, 1995; Modi and Seth, 1985; Timošenko and Goodier, 1951; Ameen, 2005).

- The fluid medium is considered to be a continuum
- The liquid is Newtonian liquid.
- For steady flow analysis, the fluid is considered as incompressible.
- For transient flow analysis, the fluid is considered as compressible.
- The pipe material is assumed as homogeneous, isotropic and linearly elastic.

3.2.2. Governing Equations for Fluid Flow

The fundamental governing equations of fluid dynamics are the continuity, momentum and energy equations. They are the mathematical statements of three fundamental physical principles viz., conservation of mass, momentum and energy.

3.2.2.1. Continuity Equation (Conservation of mass):

The law of conservation of mass states that the total mass moving into the system is equal to the sum of total mass moving out of the system and the change in storage within the system. This conservation relation in partial differential form is given by the Eqn.3.1 (Niyogi et al., 2006; Anderson and Wendt, 1995; Fluent Theory Guide, 2012; ANSYS user's manual, 2013).

$$\frac{\partial \rho}{\partial t} + \frac{\partial (\rho U_x)}{\partial x} + \frac{\partial (\rho U_y)}{\partial y} + \frac{\partial (\rho U_z)}{\partial z} = S_m \tag{3.1}$$

where ρ - the density of flowing fluid

U_x, U_y, U_z - fluid velocity components in x, y and z directions

t - time

S_m - source term.

This equation is valid for all flow problems including compressible and incompressible flows.

3.2.2.2. Momentum Equation (Conservation of momentum)

Momentum equation, also known as the Navier-Stokes Equations (N-S equation), is governed by the principle of conservation of momentum, which states that the total momentum in a system remains conserved. The complete Navier-Stokes Equations in conservation form are given in Eqn.3.2. The three equations represent the conservation of momentum in three directions (Niyogi et al., 2006; Anderson and Wendt, 1995; Fluent Theory Guide, 2012; ANSYS user's manual, 2013).

$$\frac{\partial (\rho U_x)}{\partial t} + \frac{\partial (\rho U_x^2)}{\partial x} + \frac{\partial (\rho U_x U_y)}{\partial y} + \frac{\partial (\rho U_x U_z)}{\partial z} = -\frac{\partial p}{\partial x} + \frac{\partial}{\partial x}\left(\lambda\left(\frac{\partial U_x}{\partial x} + \frac{\partial U_y}{\partial y} + \frac{\partial U_z}{\partial z}\right) + 2\mu \frac{\partial U_x}{\partial x}\right)$$
$$+ \frac{\partial}{\partial y}\left[\mu\left(\frac{\partial U_y}{\partial x} + \frac{\partial U_x}{\partial y}\right)\right] + \frac{\partial}{\partial z}\left[\mu\left(\frac{\partial U_x}{\partial z} + \frac{\partial U_z}{\partial x}\right)\right] + \rho f_x$$

$$\frac{\partial (\rho U_y)}{\partial t} + \frac{\partial (\rho U_x U_y)}{\partial x} + \frac{\partial (\rho U_y^2)}{\partial y} + \frac{\partial (\rho U_y U_z)}{\partial z} = -\frac{\partial p}{\partial y} + \frac{\partial}{\partial x}\left[\mu\left(\frac{\partial U_y}{\partial x} + \frac{\partial U_x}{\partial y}\right)\right] +$$
$$\frac{\partial}{\partial y}\left(\lambda\left(\frac{\partial U_x}{\partial x} + \frac{\partial U_y}{\partial y} + \frac{\partial U_z}{\partial z}\right) + 2\mu \frac{\partial U_y}{\partial y}\right) + \frac{\partial}{\partial z}\left[\mu\left(\frac{\partial U_z}{\partial y} + \frac{\partial U_y}{\partial z}\right)\right] + \rho f_y$$

$$\frac{\partial(\rho U_z)}{\partial t}+\frac{\partial(\rho U_x U_z)}{\partial x}+\frac{\partial(\rho U_y U_z)}{\partial y}+\frac{\partial(\rho U_z{}^2)}{\partial z}=-\frac{\partial p}{\partial z}+\frac{\partial}{\partial x}\left[\mu\left(\frac{\partial U_x}{\partial z}+\frac{\partial U_z}{\partial x}\right)\right]+\frac{\partial}{\partial y}\left[\mu\left(\frac{\partial U_z}{\partial y}+\frac{\partial U_y}{\partial z}\right)\right]$$
$$+\frac{\partial}{\partial z}\left(\lambda\left(\frac{\partial U_x}{\partial x}+\frac{\partial U_y}{\partial y}+\frac{\partial U_z}{\partial z}\right)+2\mu\frac{\partial U_z}{\partial z}\right)+\rho f_z$$

(3.2)

where p - pressure

f - body force per unit mass

μ - molecular viscosity

λ - bulk viscosity coefficient.

3.2.2.3. Energy Equation (Conservation of energy)

The energy equation is based on the law of conservation of energy which states that energy can neither be created nor be destroyed, but can only be converted from one form to another. Hence, the total energy flowing into the system should be equal to the sum of total energy flowing out of the system and the change in internal energy. This principle can be represented mathematically as Eqn.3.3 (Versteeg and Malalasekera, 2007; Anderson and Wendt, 1995; Fluent Theory Guide, 2012; ANSYS user's manual, 2013).

$$\frac{\partial}{\partial t}\left[\rho\left(e+\frac{V^2}{2}\right)\right]+\nabla.\left[\rho\left(e+\frac{V^2}{2}\vec{V}\right)\right]$$
$$=\rho\dot{q}+\frac{\partial}{\partial x}\left(k\frac{\partial T}{\partial x}\right)+\frac{\partial}{\partial y}\left(k\frac{\partial T}{\partial y}\right)+\frac{\partial}{\partial z}\left(k\frac{\partial T}{\partial z}\right)-\frac{\partial(U_x p)}{\partial x}-\frac{\partial(U_y p)}{\partial y}-\frac{\partial(U_z p)}{\partial z}$$
$$+\frac{\partial(U_x\tau_{xx})}{\partial x}+\frac{\partial(U_x\tau_{yx})}{\partial y}+\frac{\partial(U_x\tau_{zx})}{\partial z}+\frac{\partial(U_y\tau_{xy})}{\partial x}+\frac{\partial(U_y\tau_{yy})}{\partial y}+\frac{\partial(U_y\tau_{zy})}{\partial z}$$
$$+\frac{\partial(U_z\tau_{xz})}{\partial x}+\frac{\partial(U_z\tau_{yz})}{\partial y}+\frac{\partial(U_z\tau_{zz})}{\partial z}+\rho\vec{f}\vec{V}$$

(3.3)

where e - internal energy

τ - stress components (normal and shear)

$V^2/2$ - kinetic energy per unit mass

$\dot{q}$ - rate of volumetric heat addition per unit mass

k - thermal conductivity

$\vec{V}$ - velocity vector

T - Temperature

3.2.3. Governing Equations for the Piping System

In the transient analysis accounting FSI, dynamic analysis of the piping system is also required to be carried out. In the early numerical investigations, the pipe was modelled with one-dimensional elements with a hollow circular cross-section. Axial, lateral and torsional vibrations were considered in the analysis and the model considered was referred to as fourteen-equations model. The governing equations corresponding to each of these structural responses (fourteen-equation model) are given in section 2.4.1. But, the current study utilised a three-dimensional model, and the governing equations used for the analysis were differential equations of motion (Eqn.3.4), constitutive relations (Eqn.3.5), strain displacement relations (Eqn.3.6) and compatibility conditions (Eqn.3.7).

3.2.3.1. Differential Equations of Motion

Differential equations of motion of a deformable body represent the relation between the internal stress field induced in the body to the body forces acting including inertial force of the body. By using the conservation of momentum principle, the equations of motion can be represented as given in equation 3.4 (Timošenko and Goodier, 1951; Boresi et al., 1985; Ameen, 2005).

$$\frac{\partial \sigma_{xx}}{\partial x} + \frac{\partial \tau_{yx}}{\partial y} + \frac{\partial \tau_{zx}}{\partial z} + B_x = 0$$
$$\frac{\partial \tau_{xy}}{\partial x} + \frac{\partial \sigma_{yy}}{\partial y} + \frac{\partial \tau_{zy}}{\partial z} + B_y = 0$$
$$\frac{\partial \tau_{xz}}{\partial x} + \frac{\partial \tau_{yz}}{\partial y} + \frac{\partial \sigma_{zz}}{\partial z} + B_z = 0 \qquad (3.4)$$

$\sigma_{xx}, \sigma_{yy}, \sigma_{zz}$ - normal stresses in x,y,z directions

$\tau_{xy}, \tau_{yz}\ \tau_{xz}$ -shear stresses on three faces

B_x, B_y, B_z -Body forces in x, y, z directions including inertia force per unit volume

3.2.3.2. Stress-strain relation – Constitutive Equations- isotropic

These equations are the relations connecting stress and strain fields and reflect the properties of the material. This relation is based on generalised Hooke's law. In the case of homogeneous, isotropic and linearly elastic materials, these equations contain only two material constants Young's modulus '*E'* and Poisson's ratio '*v'* as given in Eqn. 3.5 (Timošenko and Goodier, 1951; Boresi et al., 1985; Ameen, 2005).

$$\begin{bmatrix}\sigma_{xx}\\ \sigma_{yy}\\ \sigma_{zz}\\ \tau_{xy}\\ \tau_{yz}\\ \tau_{xz}\end{bmatrix} = \frac{E}{(1+v)(1-2v)}\begin{bmatrix} 1-v & v & v & 0 & 0 & 0 \\ v & 1-v & v & 0 & 0 & 0 \\ v & v & 1-v & 0 & 0 & 0 \\ 0 & 0 & 0 & \frac{(1-2v)}{2} & 0 & 0 \\ 0 & 0 & 0 & 0 & \frac{(1-2v)}{2} & 0 \\ 0 & 0 & 0 & 0 & 0 & \frac{(1-2v)}{2} \end{bmatrix}\begin{bmatrix}\epsilon_x\\ \epsilon_y\\ \epsilon_z\\ \gamma_{xy}\\ \gamma_{yz}\\ \gamma_{xz}\end{bmatrix} \quad (3.5)$$

ε_x, ε_y, ε_z - normal strains in x, y, z directions

γ_{xy}, γ_{yz} γ_{xz} - Shear strain on three faces

3.2.3.3. Strain – Displacement relation

Under the action of forces, an elastic body undergoes deformation. If the deformation is same at all points of the body, there is no strain induced in the body and the motion in the body is said to be rigid body motion. If the displacement of the body is different at different points, two type of strains are induced in the body, viz., normal strain and shear strain. Normal strain and shear strain are related to the displacements by the relation given in Eqn. 3.6 (Timošenko and Goodier, 1951; Boresi et al., 1985; Ameen, 2005).

$$\begin{bmatrix} \epsilon_x \\ \epsilon_y \\ \epsilon_z \\ \gamma_{xy} \\ \gamma_{yz} \\ \gamma_{xz} \end{bmatrix} = \begin{bmatrix} \frac{\partial}{\partial x} & 0 & 0 \\ 0 & \frac{\partial}{\partial y} & 0 \\ 0 & 0 & \frac{\partial}{\partial z} \\ \frac{\partial}{\partial y} & \frac{\partial}{\partial x} & 0 \\ 0 & \frac{\partial}{\partial z} & \frac{\partial}{\partial y} \\ \frac{\partial}{\partial z} & 0 & \frac{\partial}{\partial x} \end{bmatrix} \begin{bmatrix} u_x \\ u_y \\ u_z \end{bmatrix} \tag{3.6}$$

u_x, u_y, u_z - pipe displacements in x, y, z directions

3.2.3.4. Compatibility Conditions

As the six strain components are functions of three displacement components as given in Eqn.3.6, they are not independent. The six strain components are connected each other as given in Eqn. 3.7 (known as compatibility conditions). A realistic strain field should satisfy these equations (Timošenko and Goodier, 1951; Boresi et al., 1985; Ameen, 2005).

$$\frac{\partial^2 \epsilon_x}{\partial y^2} + \frac{\partial^2 \epsilon_y}{\partial x^2} = \frac{\partial^2 \gamma_{xy}}{\partial x \partial y}$$

$$\frac{\partial^2 \epsilon_y}{\partial z^2} + \frac{\partial^2 \epsilon_z}{\partial y^2} = \frac{\partial^2 \gamma_{yz}}{\partial y \partial z}$$

$$\frac{\partial^2 \epsilon_z}{\partial x^2} + \frac{\partial^2 \epsilon_x}{\partial z^2} = \frac{\partial^2 \gamma_{zx}}{\partial z \partial x}$$

$$2\frac{\partial^2 \epsilon_x}{\partial y \partial z} = \frac{\partial}{\partial x}\left(-\frac{\partial \gamma_{yz}}{\partial x} + \frac{\partial \gamma_{zx}}{\partial y} + \frac{\partial \gamma_{xy}}{\partial z}\right)$$

$$2\frac{\partial^2 \epsilon_y}{\partial z \partial x} = \frac{\partial}{\partial y}\left(\frac{\partial \gamma_{yz}}{\partial x} - \frac{\partial \gamma_{zx}}{\partial y} + \frac{\partial \gamma_{xy}}{\partial z}\right)$$

$$2\frac{\partial^2 \epsilon_z}{\partial x \partial y} = \frac{\partial}{\partial z}\left(\frac{\partial \gamma_{yz}}{\partial x} + \frac{\partial \gamma_{zx}}{\partial y} - \frac{\partial \gamma_{xy}}{\partial z}\right)$$

(3.7)

3.2.4. Governing Equations for Cavitating Flow

The basic governing equations of fluid flow for a single-phase flow field depict the conservation of mass, momentum and energy for liquid phase alone. The cavitating flow involves two phases, viz., water and vapour, and hence, the governing equations should be available for both the phases. Transport of this additional phase (vapour) is governed by the vapour transport equation as given in Eqn.3.8 (Schnerr and Sauer, 2001; Singhal et al., 2002; Zwart et al.,2004).

$$\frac{\partial}{\partial t}(\alpha \rho_v) + \nabla.(\alpha \rho_v \vec{V_v}) = R_e - R_c$$

(3.8)

where $\vec{V_v}$ is the vapour phase velocity, α is the vapour volume-fraction, and the subscript v denotes the vapour phase. R_e and R_c are the source terms for the growth and collapse of the bubbles as a result of cavitation. These two variables account for the rate of evaporation of water and condensation of vapour phases. The bubble growth and collapse are governed by the bubble dynamics equation, viz., the Rayleigh-Plesset equation, which is given by Eqn.3.9 (Schnerr and Sauer, 2001; Singhal et al., 2002; Zwart et al., 2004). All the bubbles are assumed to be spherical in shape, with constant temperature and pressure inside the bubble, and distributed homogeneously within the liquid.

$$R_B \frac{d^2 R_B}{dt^2} + \frac{3}{2}\left(\frac{dR_B}{dt}\right)^2 = \left(\frac{P_b - P}{\rho_l}\right) - \frac{4\nu_l}{R_B}\dot{R_B} - \frac{2T}{\rho_l R_B}$$

(3.9)

where R_B is the bubble radius, T is the surface tension coefficient, ρ_l is the bubble density, ν_l is the kinematic viscosity of the liquid, P_b is bubble surface pressure, and P is the local far-field pressure.

When higher order terms and surface tension are neglected, the Eqn.3.9 simplifies into

$$\frac{dR_B}{dt} = \sqrt{\frac{2}{3}\frac{P_b - P}{\rho_l}} \tag{3.10}$$

This equation provides an underlying physical model to introduce the effects of bubble dynamics in the cavitation model.

3.2.4.1. Cavitation models

Based on the Rayleigh-Plesset equation for bubble dynamics, different cavitation models were in use (Schnerr and Sauer, 2001; Singhal et al., 2002; Zwart et al., 2004). The three popular cavitation models available in the literature are

a) Singhal et al. Model
b) Zwart-Gerber-Belmari Model
c) Schnerr-Sauer Model

The details of all these three available models are given in section 2.3 of the literature review. It is observed that the Schnerr-Sauer model is more robust and converges faster, as compared to the Singhal et al. model (Wang et al., 2016; Jansson et al., 2017). Moreover, the Schnerr-Sauer model is simple to use and set up as compared to the Zwart-Gerber-Belmari model. Besides, the only input required for the Schnerr-Sauer model is the number of spherical bubbles per unit volume of the liquid, thus simplifying the initialisation of the numerical model. Hence, Schnerr-Sauer model was chosen for the present study.

3.2.5. Turbulence Models

Turbulence is a three-dimensional unsteady random motion observed in fluid flow at moderate to high Reynolds number. Turbulent flow is a type of fluid flow characterized by fluctuating and chaotic property changes. These fluctuations lead to mixing of transported quantities such as momentum, energy, and species concentration, and cause the transported quantities to fluctuate as well. Although the Navier-Stokes equation is capable of evaluating the solution by taking this turbulence into account, it needs enormous computational resources to simulate and resolve such small scales of fluctuations. This type of approach is called Direct Numerical Simulation (DNS). An alternative method is to employ turbulence models to include the effect of turbulence in the flow. The Reynolds Averaged Navier-Stokes simulation (RANS) and Large Eddy Simulation (LES) are the two kinds of approaches.

In the solution of governing equations, the simulation of turbulent flow causes significant problems. Direct simulation of turbulence by the time-dependent Navier-Stokes equations (DNS) is possible only for simple flow cases at low Reynolds numbers. In the Reynolds Averaged Navier-Stokes Simulation (RANS) model, the flow variables are decomposed to mean and fluctuating parts. Then, a time averaging is operated, and two additional terms are added to the Navier-Stokes equation. This method has one equation and two-equation models. Commonly used one equation model is Spalart Allmaras model whereas that of two equation models are k–ε model and k–ω model. In these models, additional equations are solved together with Navier-Stokes equations.

The following are the different turbulence models used in Computational Fluid Dynamics.

- Spalart–Allmaras
- k–ε models
    - Standard k–ε
    - Re Normalisation Group (RNG) k–ε
    - Realizable k– ε
- k–ω models
    - Standard k–ω model

Shear Stress Transport (SST) k–ω model

- Reynolds stress model (RSM) model
- LES

k-ε turbulence model was selected for the study from the available turbulence models as it is the most general-purpose turbulence model. The k-ε turbulence models are of three types; standard k-ε model, RNG k-ε model and realizable k-ε model. The standard k-ε model is stable and numerically robust, which can be used for all general problems except for the flow over curved surfaces, the flow in rotating fluids and the flow with boundary layer separation (Fluent Theory Guide, 2012; ANSYS user's manual, 2013). In the present study, none of these conditions were prevailed or expected (boundary layer separation is not expected). Hence, the use of the unconditionally stable standard k-ε model is justifiable. Standard wall function is also used along with the standard k-ε model to simulate the boundary layer characteristics.

The turbulence kinetic energy k and its rate of dissipation ε are obtained from the following transport equations Eqn.3.11 and 3.12 (Anderson and Wendt, 1995; Fluent Theory Guide, 2012; ANSYS user's manual, 2013).

$$\frac{\partial(\rho k)}{\partial x}+\frac{\partial(\rho k u U_i)}{\partial x_i}=\frac{\partial}{\partial x_j}\left[\left(\mu+\frac{\mu_t}{\sigma_k}\right)\frac{\partial k}{\partial x_j}\right]+G_k+G_b-\rho\varepsilon-Y_M+S_k \tag{3.11}$$

$$\frac{\partial(\rho\varepsilon)}{\partial t}+\frac{\partial(\rho\varepsilon U_i)}{\partial x_i}=\frac{\partial}{\partial x_j}\left[\left(\mu+\frac{\mu_t}{\sigma_\varepsilon}\right)\frac{\partial \varepsilon}{\partial x_j}\right]+C_{1\epsilon}\frac{\epsilon}{k}(G_k+C_{3\epsilon}G_b)-C_{2\epsilon}\rho\frac{\epsilon^2}{k}+S_\epsilon \tag{3.12}$$

G_k - generation of turbulence kinetic energy due to the mean velocity gradients

G_b - generation of turbulence kinetic energy due to buoyancy

Y_M - contribution of the fluctuating dilatation in compressible turbulence to the overall dissipation rate.

$C_{1\varepsilon}$, $C_{2\varepsilon}$,$C_{3\varepsilon}$ - constants.

σ_k and σ_ε - turbulent Prandtl numbers for k and ε

S_k and S_ε - source terms.

3.2.6. Equation of state

The fluid was considered as incompressible for steady flow analysis whereas, it was considered as compressible for transient flow simulation. The compressibility of fluid was taken care of by the simplified form of the Tait equation (Eqn.3.13) (Ginell, 1961; Li, 1967; Fluent Theory Guide, 2012; ANSYS user's manual, 2013).

$$\left(\frac{\rho}{\rho_0}\right)^n = \frac{K}{K_0} \tag{3.13}$$

where $K = K_0 + n\Delta P$ and $\Delta P = P - P_0$

P_0 = reference liquid pressure, ρ_0= reference liquid density, K_0= reference bulk modulus and n= density exponent, P = liquid absolute pressure

3.3. Numerical Method

A variety of mathematical models have been used to model fluid transients considering FSI (Wiggert et al., 1987; Li et al., 2003; Tijsseling, 2007; Soares et al., 2008). The numerical procedure for solving these equations includes Method of Characteristics (MOC), a combination of MOC and Finite Element Methods, Finite Difference Method, Finite Volume Method and the like (Wiggert et al., 1987; Lavooij and Tijsseling, 1991; Heinsbroek, 1997; Li et al., 2003; Tijsseling, 2007; Soares et al., 2008). Recently, many attempts have been made to use the combination of structural dynamics and Computational Fluid Dynamics (CFD) models for the analyses of problems incorporating FSI. The governing equations for the CFD model are the same conservation equations but in its full form considering almost all processes like friction, boundary layer and turbidity. CFD is the art of replacing a set of PDE by a set of algebraic equations which can be solved by using efficient linear equation solvers. Most of the CFD solvers are based on the Finite Volume Method (FVM) in which the domain is discretised into a set of finite control volumes (Versteeg and Malalasekera, 2007; Moukalled et al., 2016;

Patankar, 1980). General conservation equations for mass, momentum and energy are solved on these set of control volumes.

3.3.1. Computational Fluid Dynamics (CFD)

Study of transient flow, considering three-dimensional governing equations in its full form is computationally intensive and normally comes under the category of CFD. The basic principle of CFD is to replace the continuous problem domain with a discrete domain using grids (or elements). Instead of defining the flow variables at every point in a continuous domain, this procedure defines the flow variables only at the grid points in the discrete domain and solve for the relevant flow variables at these grid points. The value of flow variables at other locations is determined by interpolating the values at the grid points.

ANSYS Fluent is an engineering software suite that can simulate CFD and different programming algorithms for simulation and optimisation. In this study, the flow in pipes is analysed using ANSYS Fluent which use FVM for the numerical discretization.

3.3.2. Finite Volume Method

The Finite Volume method uses an integral form of the equations to be solved. The computational domain is divided into elementary volumes and the integration is performed within these elementary volumes (Versteeg and Malalasekera, 2007; Moukalled et al., 2016; Patankar, 1980). The method enables to handle complex geometry without having the equation written in curvilinear coordinates. The method also preserves the conservative property. The elementary control volumes are described by the coordinates of the vertices of the quadrilaterals (for 2-D) or hexahedral (for 3-D).

Integral forms of the governing equations are given in Eqn.3.14, 3.15 and 3.16 (Niyogi et al., 2006; Anderson and Wendt, 1995; Fluent Theory Guide, 2012; ANSYS user's manual, 2013).

Continuity equation:

$$\frac{\partial}{\partial t}\int_V \rho dV + \oint_S \rho(U_i.n)dS = 0$$

(3.14)

Momentum Equation

$$\frac{\partial}{\partial t}\int_V \rho U_i dV + \oint_S \rho U_i(U_i.n)dS = \int_V \rho f_e dV + \oint_S [-p_{n+}(\bar{\bar{\tau}}.n)]dS$$

(3.15)

Energy equation

$$\frac{\partial}{\partial t}\int_V \rho E dV + \oint_S \rho H(v.n)dS = \oint_S k(\nabla T.n)dS + \int_V (\rho f_e.v + \dot{q}_h)dV + \oint_S (\bar{\bar{\tau}}.n)dS$$

(3.16)

where $\bar{\bar{\tau}}$- viscous stress tensor

For solving the integral forms of the governing equations, the ANSYS Fluent uses any one of the two methods viz., the pressure-based solver and the density-based solver. In the density-based solver, the density and the velocities are obtained from the continuity and the momentum equations respectively. On the other hand, in pressure-based solver, the pressure is obtained by solving pressure equation which is derived from the continuity and the momentum equations in such a way that the velocity field, corrected by the pressure, satisfies the continuity (Fluent theory guide 2012). Pressure based solver is used for the current simulation as it is the widely used solver in most of the transient flow simulations (Martins et al., 2014, 2016, 2018; Ferreira et al., 2018). The pressure-based solver uses two types of solver algorithms, viz., coupled and segregated. The continuity and the momentum equations are solved together in the coupled algorithm, while these equations are solved sequentially in the segregated algorithm. The segregated algorithm is better as it is memory efficient and hence adopted in the current study (Martins et al., 2014, 2016, 2018; Ferreira et al., 2018).

3.3.3. Discretization Schemes

Discretization of solution domain is mainly classified into spatial and temporal discretization. The general transport equation is converted into algebraic equations by integrating

it in each control volume. The unsteady conservation equation of a scalar quantity ϕ in integral form can be written as Eqn. 3.17.

$$\int_{V} \frac{\partial \rho \phi}{\partial t} dV + \oint \rho \phi \vec{v}. d\vec{A} = \oint \Gamma_{\phi} \nabla \phi. d\vec{A} + \int_{V} S_{\phi} \, dV \tag{3.17}$$

$\vec{A}$ - surface area vector

Γ_{ϕ} - diffusion coefficient for ϕ

$\nabla \phi$ - gradient of ϕ

S_{Φ} - source of ϕ per unit volume

Equation 3.17 is applied to each control volume, or cell, in the computational domain. Discretization of Equation 3.17 on a given cell yields Eqn. 3.18.

$$\frac{\partial \rho \phi}{\partial t} V + \sum_{f}^{Nfaces} \rho_f \vec{v}_f \phi_f . \vec{A}_f = \sum_{f}^{Nfaces} \Gamma_{\phi} \nabla \phi_f . \vec{A}_f + S_{\phi} V \tag{3.18}$$

N_{faces} - number of faces enclosing cell

ϕ_f - value of ϕ convected through face f

$\rho_f \vec{v}_f . \vec{A}_f$ - mass flux through the face

$\vec{A}_f$ - area of face f

$\nabla \phi_f$ - gradient of ϕ at the face f

V - cell volume

3.3.3.1. Spatial Discretization

In FVM, the value of the function ϕ given in Eqn.3.17 is calculated and stored at cell centres. However, the values of the function ϕ are to be determined at the cell faces also for the discretization of the convective term. This discretization is carried out by different methods like first order upwind, second order upwind and QUICK schemes.

First-Order Upwind Scheme

The function value at any face is equated to the cell centre value of the function at the upstream side. This method is first order accurate only.

Second-Order Upwind Scheme

When second-order accuracy is desired, quantities at cell faces are computed using a Taylor series expansion of the cell-centred solution about the cell centroid. Thus, when second-order upwind is selected, the face value ϕ_f is computed using the expression Eqn. 3.19.

$$\phi_f = \phi + \nabla\phi . \vec{r} \tag{3.19}$$

where ϕ and $\nabla\phi$ are the cell-centred value and its gradient in the upstream cell, and $\vec{r}$ is the displacement vector from the centroid of the upstream cell to the centroid of the face. This formulation requires the determination of the gradient $\nabla\phi$ in each cell.

QUICK Scheme (Quadratic Upwinding Interpolation of Convective Kinetics)

In QUICK scheme, the function value at any face is calculated by taking the weighted average of three cell centre values. Two neighbouring nodes of the face under consideration and one more node at the upstream side are selected in this scheme. This method is also second order accurate.

3.3.3.2 Temporal Discretization

Temporal discretization involves the integration of every term in the differential equations over a time step Δt. The integration of the transient terms is given in Eqn. 3.20 to 3.23.

A differential equation for the time evolution of a variable ϕ is given by Eqn. 3.20.

$$\frac{\partial \phi}{\partial t} = F(\phi) \tag{3.20}$$

where F(ϕ) is a function from any spatial discretization. If the time derivative is discretized by using backward differences, the discretization results in first-order accurate temporal scheme (Eqn. 3.21).

$$\frac{\phi^{n+1} - \phi^{n}}{\Delta t} = F(\phi) \tag{3.21}$$

The second-order accurate temporal discretization is given by Eqn. 3.22.

$$\frac{3\phi^{n+1} - 4\phi^{n} + \phi^{n-1}}{2\Delta t} = F(\phi) \tag{3.22}$$

where

ϕ - a scalar quantity

n+1 - value at the next time level $t+\Delta t$

n - value at the current time level t

n-1 - value at the previous time level $t-\Delta t$

Implicit Time Integration

Implicit time integration considers the value of the function at future time level as given in Eqn. 3.23.

$$\frac{\phi^{n+1} - \phi^{n}}{\Delta t} = F(\phi^{n+1}) \tag{3.23}$$

This is referred to as "implicit" integration since ϕ^{n+1} in a given cell is related to ϕ^{n+1} in neighbouring cells through $F(\phi^{n+1})$ as given in Eqn. 3.24.

$$\phi^{n+1} = \phi^{n} + \Delta t \times F(\phi^{n+1}) \tag{3.24}$$

This implicit equation can be solved iteratively at each time level before moving to the next time step. The implicit scheme is unconditionally stable.

3.3.4. Pressure-Velocity Coupling

ANSYS Fluent has five different pressure velocity coupling algorithms viz., SIMPLE, SIMPLEC, PISO, Coupled, and Fractional Step (FSM). Among these SIMPLE, SIMPLEC, PISO and Fractional Step (FSM) are pressure based segregated algorithms.

3.3.4.1. SIMPLE

SIMPLE (Semi-Implicit Method for Pressure Linked Equations) was used as pressure velocity coupling method. Out of the many algorithms, the SIMPLE was chosen for this study as this algorithm mainly influences the convergence rate (Ferreira et al., 2018; Martins et al., 2018). The SIMPLE algorithm uses a relationship between the velocity and the correction in the pressure to enforce mass conservation and thereby obtains the pressure field.

If the momentum equation is solved with a guessed pressure field p^*, the resulting face flux, $J_f{}^*$, computed from Equation 3.25.

$$J_f^* = \hat{J}_f^* + d_f(p_{c0}^* - p_{c1}^*) \tag{3.25}$$

The resulting face flux, $J_f{}^*$does not satisfy the continuity equation. Consequently, a correction J_f' is added to the face flux J_f^* so that the corrected face flux J_f given by Eqn.3.26,

$$J_f = J_f^* + J_f' \tag{3.26}$$

According to SIMPLE algorithm

$$J_f' = d_f(p_{c0}' - p_{c1}') \tag{3.27}$$

where

J'_f - Mass flux correction through face f

$\hat{J}^*_f$ -Assumed mass flux through face f due to the influence of velocities in the adjacent cells

J^*_f -Assumed mass flux through face f

J_f -Mass flux through face f

p^*_{co}, p^*_{c1} -Guessed pressure field within the two cells on either side of the face

d_f -Function of momentum equation coefficient

p'_{co}, p'_{c1} -Pressure correction within the two cells on either side of the face

Then, SIMPLE algorithm substitutes the flux correction equations into the discrete continuity equation to get a discrete pressure correction equation in the cell as Eqn. 3.28.

$$a_p p' = \sum_{nb} a_{nb} p'_{nb} + b \tag{3.28}$$

where the source term b is the net flow rate into the cell as given in Eqn. 3.29.

$$b = \sum_{f}^{N_{faces}} J_f^* A_f \tag{3.29}$$

where

a_p, a_{nb} -Momentum equation coefficients

A_f -Area of face f

The pressure-correction equation (Equation 3.28) may be solved using the Algebraic Multi-Grid (AMG) method. Once a solution is obtained, the cell pressure and the face flux are corrected using equations 3.30 and 3.31.

$$p = p^* + \alpha_p p' \tag{3.30}$$

$$J_f = J_f^* + d_f (p'_{c0} - p'_{c1}) \tag{3.31}$$

Here α_p is the under-relaxation factor for pressure. The corrected face flux, J_f, satisfies the discrete continuity equation during each iteration.

In the current study, the second order upwind scheme was used for the solution of density and momentum equations, whereas first order upwind scheme was used for turbulent kinetic energy and turbulent dissipation rate. Convergence criterion adopted was absolute with the following residual values: 0.000001 for Continuity equation, 0.00001 for x velocity, y velocity, z velocity, turbulent kinetic energy and turbulent energy dissipation factor. Stability criterion was satisfied by lowering the Δt and the desirable level of accuracy was maintained by using good quality mesh.

3.3.5. Finite Element Method

In the transient analysis accounting FSI, the dynamic analysis of the piping system was also required to be carried out and was implemented by using the Finite Element Method (FEM). The governing equations of structural dynamics are solved for the discretised geometry along with the differential equations of motion, the constitutive equations, the strain displacement relation and the compatibility conditions. A 3-D twenty node hexahedron element was used for modelling the piping system. This element is a solid element with 20 geometric nodes (Fig. 3.1), with three translational degrees of freedom at each node, in the global coordinate system. The discretised form of dynamic equation was given in Eqn. 3.32 (Chopra, 1995).

$$[M][\ddot{u}] + [C][\dot{u}] + [k][u] = F(t) \tag{3.32}$$

where $[M]$ - mass matrix,

$[C]$ - damping matrix

$[k]$ - stiffness matrix

$[\ddot{u}]$ - acceleration

$[\dot{u}]$ - velocity

$[u]$ - displacement

$F(t)$ - force with respect to time

Lagrangian interpolation polynomials for 3-D elements were used as the shape functions for 20 node hexahedron elements with respect to the natural coordinates from -1 to +1

(Zienkiewicz et al., 1977; Cook et al., 1974; Cook, 2007). The shape functions of the 20-node hexahedron (Fig. 3.1) are given in equation 3.33.

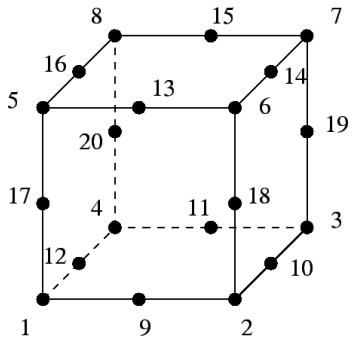

Fig. 3.1 3-D 20 node element with node numbers

$$N_i = \frac{1}{8}(1+\xi_i\xi)(1+\eta_i\eta)(1+\zeta_i\zeta)(\xi_i\xi+\eta_i\eta+\zeta_i\zeta-2) i = 1,2,\ldots,8$$

$$N_i = \frac{1}{4}(1-\xi^2)(1+\eta_i\eta)(1+\zeta_i\zeta) i = 9,11,13,15$$

$$N_i = \frac{1}{4}(1+\xi_i\xi)(1+\eta^2)(1+\zeta_i\zeta) i = 10,12,14,16$$

$$N_i = \frac{1}{4}(1+\xi_i\xi)(1+\eta_i\eta)(1+\zeta^2) i = 17,18,19,20$$

(3.33)

where ξ_i , η_i , ζ_i = natural coordinates of the element node with respect to the local coordinate system, $-1 \leq \xi \leq 1$, $-1 \leq \eta \leq 1$, $-1 \leq \zeta \leq 1$.

The element stiffness matrix is given as equation 3.34.

$$[\boldsymbol{k}] = \int_{\boldsymbol{V}} [\boldsymbol{B}]^{\boldsymbol{T}} [\boldsymbol{D}][\boldsymbol{B}] \boldsymbol{dV}$$

(3.34)

where $[\boldsymbol{B}]$ - strain displacement matrix

$[\boldsymbol{D}]$ - matrix for constitutive relation for linear elastic material.

The element mass matrix is evaluated on the basis of the consistent formulation as given in equation 3.35.

$$[\boldsymbol{M}] = \int_{\boldsymbol{V}} \boldsymbol{\rho_s} [\boldsymbol{N}]^{\boldsymbol{T}} [\boldsymbol{N}] \, \boldsymbol{dV}$$

(3.35)

where $[\boldsymbol{N}]$ - matrix of shape function of 20 node hexahedral elements.

The ANSYS Structural uses the following procedure. The mass and stiffness matrices are assembled from the element matrices.

Stiffness Matrix in terms of natural coordinates is given as equation 3.36.

$$[\boldsymbol{k}] = \int_{-1}^{+1}\int_{-1}^{+1}\int_{-1}^{+1}[\boldsymbol{B}]^{\boldsymbol{T}}[\boldsymbol{D}][\boldsymbol{B}]\boldsymbol{J}\, \boldsymbol{d\xi d\eta d\zeta} \tag{3.36}$$

Where $\boldsymbol{J}$ is the determinant of Jacobian Matrix [J] given as equation 3.37.

$$[J] = \begin{bmatrix} \frac{\partial x}{\partial \xi} & \frac{\partial y}{\partial \xi} & \frac{\partial z}{\partial \xi} \\ \frac{\partial x}{\partial \eta} & \frac{\partial y}{\partial \eta} & \frac{\partial z}{\partial \eta} \\ \frac{\partial x}{\partial \zeta} & \frac{\partial y}{\partial \zeta} & \frac{\partial z}{\partial \zeta} \end{bmatrix} \tag{3.37}$$

The direct numerical integration in time domain of the second order differential equations of motion is carried out by the Newmark- β method, considering its stability characteristics.

3.3.5.1. Numerical Integration- Newmark-β Method

For the numerical integration of dynamic equation, an implicit direct integration method known as Newmark-β method which is unconditionally stable, is commonly used. The ANSYS structural uses this method and a brief description of the procedure is given below. The dynamic equilibrium equation at any time t_n is given by

$$[M][\ddot{u}_n] + [C][\dot{u}_n] + [k][u_n] = F(t)_n \tag{3.38}$$

The Newmark-β method uses the finite difference expansions in the time interval Δt. At the next time step n+1, the velocity is given by

$$\{\dot{u}_{n+1}\} = \{\dot{u}_n\} + [(1-\alpha)\{\ddot{u}_n\} + \alpha\{\ddot{u}_{n+1}\}]\Delta t$$

(3.39)

Displacement is given by

$$\{u_{n+1}\} = \{u_n\} + \{\dot{u}_n\}\Delta t + \left[\left(\frac{1}{2} - \beta\right)\{\ddot{u}_n\} + \beta\{\ddot{u}_{n+1}\}\right]\Delta t^2$$

(3.40)

Where α and β are Newmark integration parameters. The values used in the study for α and β are 0.5 and 0.25 respectively.

Δt = $t_{n+1} - t_n$

$\{u_n\}$ - nodal displacement vector at time t_n

$\{\dot{u}_n\}$ - nodal velocity vector at time t_n

$\{\ddot{u}_n\}$ - nodal acceleration vector at time t_n

$\{u_{n+1}\}$ - nodal displacement vector at time t_{n+1}

$\{\dot{u}_{n+1}\}$ - nodal velocity vector at time t_{n+1}

$\{\ddot{u}_{n+1}\}$ - nodal acceleration vector at time t_{n+1}

The dynamic equilibrium equation at any time t_{n+1} is given by

$$[M][\ddot{u}_{n+1}] + [C][\dot{u}_{n+1}] + [k][u_{n+1}] = F(t)_{n+1}$$

(3.41)

Rearranging the equations for velocity and displacement at time t_{n+1}, the equation for $\{\ddot{u}_{n+1}\}$ and $\{\dot{u}_{n+1}\}$ in terms of known velocity and acceleration; and $\{u_{n+1}\}$ can be obtained. On substituting its value in the dynamic equation 3.41, the resulting equation is in terms of $\{u_{n+1}\}$ alone in the time step n+1. Left hand side of the equation contains terms with $\{u_{n+1}\}$ and right-hand side contains the known quantities; and hence, the equation can be solved by matrix inversion method for getting the value of displacements. Once displacement is known, velocity and acceleration at t_{n+1} can be calculated by using the relations given earlier. The simulation needs two initial conditions u_0 and $\dot{u}_0$ at time t_0.

3.3.6. Fluid-structure interaction

The FSI modelling includes multi-physics processes and links fluid dynamics and structural dynamics systems to arrive at a realistic result of the problem. The two-way coupling method is used for the analysis in which the data is passed in both directions, from fluid to structure and back. All these interactions are possible through a component “System Coupling”, inside the ANSYS Workbench.

In the FSI analysis, the pipe and fluid are modelled simultaneously, and the outer surface of the fluid is treated as the inner surface of the pipe (fluid structure interface) where the data transfer takes place. The two-way system coupling in the models requires that the interface nodes must be common for both fluid and structure systems, though the methods of solution for both the systems are different viz., FVM for fluid and FEM for structure. It means that each node in the structural system should have a corresponding node at the outer boundary of the fluid.

Several methods are available for linking FVM and FEM models. When creating an FSI model, the most important part is the connection of two independent mesh domains with different formulation. The CFD modelling (FVM) utilises an Eulerian mesh while FEM uses a Lagrangian mesh. The Lagrangian mesh is movable mesh while the Eulerian mesh is fixed in time and space for which mesh motion is activated by the dynamic mesh option in the software. The ANSYS Fluent and Structural use Arbitrary-Lagrangian-Eulerian (ALE) method for transferring the information between the fluid and solid domains (Donea et al., 1982; Lohner et al., 2006). The flow chart of the FSI phenomenon using ALE is given in Fig. 3.2.

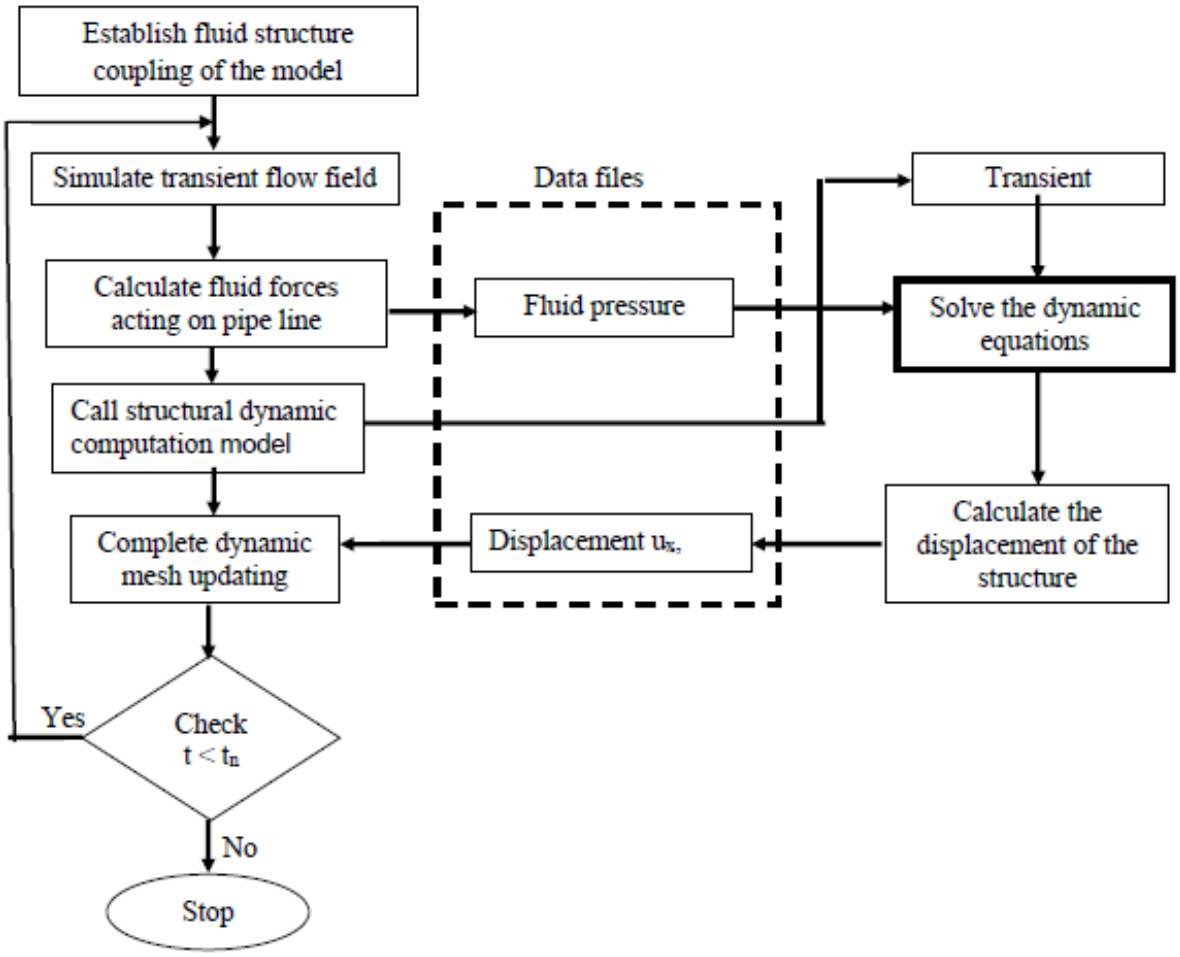

Fig. 3.2 Flow chart of the ALE method used for FSI problems in ANSYS

3.3.7. Creation of Geometry and Mesh

The geometry was created in the Design Modeler platform inside the ANSYS Fluent. While creating the mesh, different mesh options have to be specified in three directions; radial, circumferential and longitudinal directions. In circumferential direction, element size or number of divisions could be specified whereas in radial direction fine mesh was selected near the boundary and coarse mesh towards the centre. In the longitudinal direction sweep option was used by giving element size. The mesh quality was then checked for different parameters like aspect ratio, skewness, orthogonal quality and element quality. Refinement in the mesh was carried out until a good quality mesh was obtained. In the transient analysis with FSI, the

meshing of fluid was carried out inside the ANSYS Fluent after suppressing the pipe element and the meshing of the pipe was carried out inside the ANSYS Structural after suppressing the fluid part. Mesh synchronisation was implemented by providing the same commands for both the fluid and the pipe during the meshing process.

3.3.8 Initial conditions

The liquid filled pipe system was assumed to be in steady state initially. A constant head reservoir provided at the upstream boundary maintained a constant head always at that position which was considered as a pressure inlet. Transient event was created by a quick acting valve at the downstream end with a closing time at the order of 20 to 50 ms. The discharge during the closing time was assumed to vary linearly.

3.4. Implementation of Numerical method

Numerical procedure used in the software ANSYS Workbench is briefly explained as three parts

- Numerical study of Water Hammer
- Numerical study of Water Hammer with FSI
- Numerical study of Water Hammer with Cavitation

The details of these modelling procedure/selected options for three different cases are given in Table No. 3.1, 3.2 and 3.3.

Table 3.1 Details of numerical study of Water Hammer

	Process	Input commands	Remarks
Pre processor	Creation of geometry	In Design modeler	Fluid alone to be modelled
	Meshing	Radial direction : Inflation option Circumferential direction : Edge sizing Longitudinal direction : Sweep method	Several Trials till good quality mesh is obtained
Solver	Steady Flow	Solver type : Pressure based solver Time : Steady Viscous model : Standard k-ε model Standard wall function Material : Incompressible fluid	Residual value for convergence: 10^{-6}
	Boundary conditions	Inlet : Pressure inlet (Pa) Outlet : Mass flow outlet (kg/s) Interior water : Interior Outer face : Wall	
	Solution methods	Pressure velocity coupling: SIMPLE Discretization : Pressure: Second order Density: Second order upwind k and ε: First order upwind	On convergence Check the results of steady flow
	Transient state analysis	Material : Compressible fluid Outlet : From constant mass flow to zero within the closure time of valve	Monitor the required results

Table 3.2 Details of numerical study of Water Hammer with FSI

	Process	Input commands	Remarks
ANSYS Fluent-Pre processor	Creation of geometry	In Design modeler	Fluid and pipe to be modelled together
	Meshing	Mesh fluid only- Same as Table 3.1	
Solver-Setup	Steady Flow	Same as Table 3.1	
	Boundary conditions	Inlet : Pressure inlet (Pa) Outlet : Mass flow outlet (kg/s) Interior water : Interior Outer face : Fluid structure interface	
	Solution methods	Create Dynamic mesh zones Inlet and outlet : Stationary Fluid outer wall: System coupling	
ANSYS Structural	Engineering data	Select material from Engineering data base	
	Geometry	Share geometry with Fluent	
	Model-Meshing	Mesh pipe only	Maintain mesh compatibility
	Setup	Create supports	Using available support conditions
		Inner surface of pipe : Fluid solid interface	At the interaction surface data will get transferred
System Coupling	Share setup	Fluent and structural setup to be connected to the setup of System coupling.	
		Create two data transfers between fluid and structure Start the simulation	Same time step as Fluent and Structural

Table 3.3 Details of numerical study of Water Hammer with Cavitation

	Process	Input commands	Remarks
Pre processor	Creation of geometry	2D Axi-symmetric in Design modeler	Fluid alone
	Meshing	Radial direction : Edge sizing with bias and smooth transition Longitudinal direction : Edge sizing	Several Trials till good quality mesh in terms of mesh parameters is obtained
Solver	Steady Flow	Solver type : Pressure based solver Multiphase model: Mixture model Primary phase : Water Secondary phase : Vapour	
	Boundary conditions	Inlet : Pressure inlet (Pa) Outlet : Mass flow outlet Centerline : Axis Outer face : Wall	
	Solution methods	Pressure velocity coupling: SIMPLE Discretization: pressure: PRESTO! Density : Second order upwind α, k and ε : First order upwind	On convergence Check the results of steady flow
	Transient state analysis	Water : Compressible liquid Vapour: Ideal gas Multiphase model: Phase interaction, Cavitation :Schnerr-Sauer model	Create Solution monitors

3.5. Experimental setup

The current investigation used the data from two published literature (Mitosek and Szymkiewicz, 2012 and Holmboe and Roleau, 1967). Experiments from two setups, designated as experiment setup A and B available in the literature, were used to study the effect of FSI on damping of pressure wave. There is only one set of investigation in the experimental setup A which is designated as case 1. In contrast, there are two sets of experiments in the experimental setup B, which are designated as case 2(a) and case 2(b) in the remaining part of the thesis. However, the experiments those were conducted as part of the current study in the Water Flow laboratory of FCRI Palakkad is designated as the Experiment setup C. Details of all the experimental setup (both available in the literature and in the present experimental study) are described in the subsequent sections.

3.5.1. Experimental Setup A: Case 1

The current study used an experimental study by Mitosek and Szymkiewicz (2012), as a case study for verifying the effect of FSI on pressure wave damping. Their experimental setup (designated as A), given in Fig. 3.3 included a pipeline, a pressurised tank and a ball valve at the end of the pipe. Details of that experimental setup are given as follows. The pipe was a straight-steel pipe with dimensions and characteristics as length 72 m, internal diameter 0.042 m, pipe wall thickness 0.0033 m, roughness height 0.0008 m, wave velocity 1245 m/s, initial pressure head 51 m, initial velocity 0.41 m/s and average valve closure time as 0.021 s. The pipe was rigidly fixed to the floor with holders; spaced 2 m apart along the length. The inlet to the pipe (1) was located deep below the water level to eliminate air suction. The valve (4) was operated manually. The closure time ranged from 18 ms to 25 ms in all tests. A measuring system consisting of piezoelectric transducers (5), a signal amplifier (6), and a computer (7) with a data acquisition (20 MHz) card, recorded the pressure. A reservoir (2) fed water to the tested pipe (1). The initial pressure head, H_o, at the pipe outlet and the discharge were controlled using pressure-reducing valves (3). The pressure head was adjusted to avoid column separation during water hammer. Once the flow stabilised to an initial steady-state, rapid manual closure of the valve (4) created the transient event. The time recorder (8) was used for recording the closing time with an

accuracy of 1 ms. At the same instant, the valve (3) in front of the tank was also closed. A constant stream temperature of 14°C prevailed during the test.

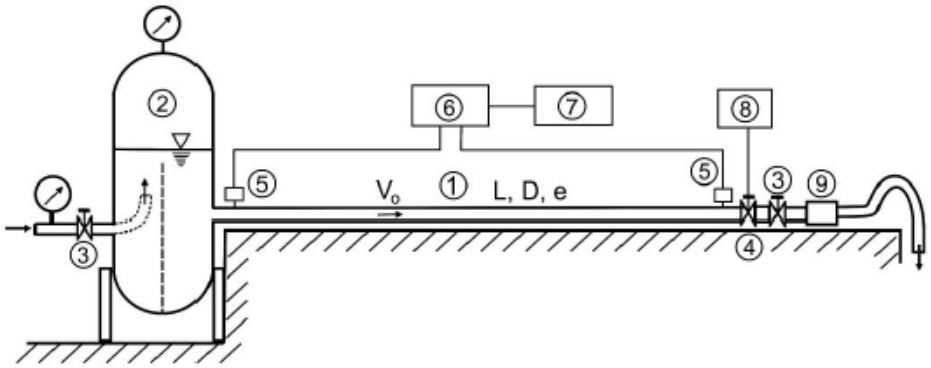

Fig. 3.3 Experimental set up A from literature (Mitosek and Szymkiewicz, 2012) (1) inlet to the pipe, (2) reservoir, (3) pressure-reducing valves, (4) manually operated valve, (5) piezoelectric transducers, (6) signal amplifier, (7) computer, (8) time recorder, (9) electromagnetic flow meter

3.5.2. Experimental Setup B: Case 2(a)

This study utilised the transient flow experiment from Holmboe and Roleau (1967) as the second case study (Fig.3.4a) and designated as experiment B. Details of that experimental setup are given as follows. The experiment setup B consisted of a constant head tank, a copper pipe and a rapid closure valve. The pipe had a length of 36.09 m and an internal diameter of 0.025 m. For conducting the experiment in turbulent flow condition, the used fluid was water with a density of 1000 kg/m^3 and viscosity of 0.00086 Ns/m^2. The analysis used a wave velocity of 1350 m/s. The Reynolds number was maintained at 6166, which indicated that the flow was turbulent (Araya and Chaudhry, 1997; Holmboe and Roleau, 1967). From the available data, the flow velocity was calculated as 0.212 m/s, which was then used for the present numerical modelling. A quick acting valve was used to create transient events. The pressure was measured at the outlet and at the middle of the pipe. To alleviate the effect of vibration during the experiment in transient flow, the pipe was embedded in concrete throughout its length, as shown in Fig. 3.4b

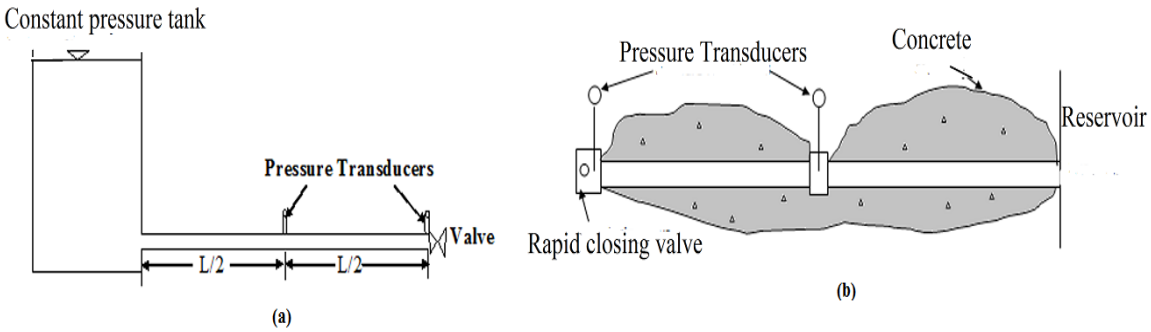

Fig.3.4 Experimental setup B from literature (Holmboe and Roleau, 1967)

3.5.3. Experimental Setup B: Case 2(b)

The Laminar flow condition was also used in the experimental setup B. The current study utilised the data from the second experiment in the laminar flow condition (Holmboe and Roleau (1967)), as another case study (case 2(b)). As in the earlier cases, the transient flow was created by the rapid closure of the valve. For keeping the flow in laminar condition, the used fluid was oil with a density of 878.4 kg/m^3 and viscosity of 0.03484 Ns/ m^2. The analysis used a wave velocity of 1324 m/s and maintained a Reynolds number of 82, as provided by Araya and Chaudhry (1997). From the provided data, the flow velocity was calculated as 0.13 m/s, and was used in the present numerical modelling. Quick acting valve and pressure transducers were provided, as explained in case 2(a).

3.5.4. Experimental Setup C

As a part of the current investigation, a laboratory-scale experimental installation was set up to study the effect of different parameters like closure time of valve, number of fixed anchors, changes in the flow velocity and material properties of the pipe on transient cavitating flow characteristics. Various types of materials viz., elastic, visco-elastic and hyper-elastic materials are used in the piping system for water distribution and for other industries. Cast iron, ductile iron, steel, galvanized iron, copper, asbestos cement and plastic are the commonly used pipe materials. Selection of pipe material depends on the various parameters like the nature of fluid conveyed; the maximum expected pressure, the durability of the material and the resistance to chemical attack. Mild steel (MS) pipe has a wide range of application, especially, for conveying

water under high pressure. They are stronger and lighter in weight than the cast iron and the asbestos cement pipes. Three varieties of plastic pipes are available viz., Unplasticized Poly Vinyl Chloride (UPVC), plasticized poly vinyl chloride (PVC) and Chlorinated PVC pipes (CPVC). The UPVC pipes are used in low temperature and low strength applications. Another type of modern pipe material is High Density Poly-Ethylene (HDPE), which is probably the most durable material available in the market. Plant roots can never grow into this type of pipe and hence, the HDPE pipes are most suitable for sewer lines and underground water lines. In order to assess the influence of the mechanical behaviour of the pipe material on the flow characteristics, the present study selected three pipe materials viz., MS, UPVC and HDPE. The properties of the material and the fluid used for testing are given in Table 3.4. The inlet flow rate, the number of fixed anchors and the closure time were also varied to study their effect on the transient cavitating flow characteristics.

Table 3.4 Fluid/Material Properties

Property/Material	Water	Mild Steel	UPVC	HDPE
Density (kg/m^3)	998.2	7850	1430	960
E (GPa)	-	200	3.0	1.035
Viscosity μ (Ns/m^2)	0.001004	-	-	-
Bulk Modulus (K) (GPa)	2.2	-	-	-

The test was conducted at the Fluid Control Research Institute, Palakkad, Kerala, with custom made setup as detailed in this section. Experiments were conducted in a reservoir-pipe-valve installation, as shown in Fig. 3.5 (the experimental setup C). The mild steel pipe used in the experiment was of length 30.30 m. The internal and external diameters of the pipe were 52.4 mm and 60.3 mm, respectively. Two 0-30 bar pressure transducers (Fig. 3.6) were attached to the pipe at a distance 0.085 m from the centre of Quick acting valve (QAV) and 20 m from the centre of QAV respectively to monitor the variation of pressure at these locations. A control valve (CV) situated at the downstream side of the pipe maintained the different flow rate required for the study. A digital flow-meter (TFM, Fig. 3.7) ensured the required flow rate through the pipe. The pipe was fed from a constant head water tank (CHT, Fig. 3.8) with a head of 17m. Before the closing of the valve for generating transient, steady flow was ensured inside the pipe by running the system with constant discharge for a sufficient period.

The pressure-actuated QAV (Fig. 3.9) mounted at the downstream section of the pipe (upstream of the flow control valve) created the sudden closure of the flow. A pressure gauge, a supplementary control mechanism attached to it, controlled the time of closure. Three different pressure values were used to control the QAV to close it at three different closure times. Fig.3.10 shows the arrangement for measuring the time of closure in the quick acting valve. The closure time of QAV was measured using an optical sensor.

Four different anchoring conditions were utilised for the study, viz., no anchors, two fixed anchors (at ends), three anchors (one each at ends and one at centre); and five anchors (one each at ends, one each at quarter span and one at the centre). The experiment was conducted for five flow rates. The second setup consisted of 2″ UPVC pipe of length 30.13 m. The internal and external diameters of the UPVC pipe were 51.2 mm and 60.2 mm respectively. The third set up consisted of 2″ HDPE pipe of length 30 m. The internal and external diameters of the HDPE pipe were 47.07 mm and 59.85 mm respectively.

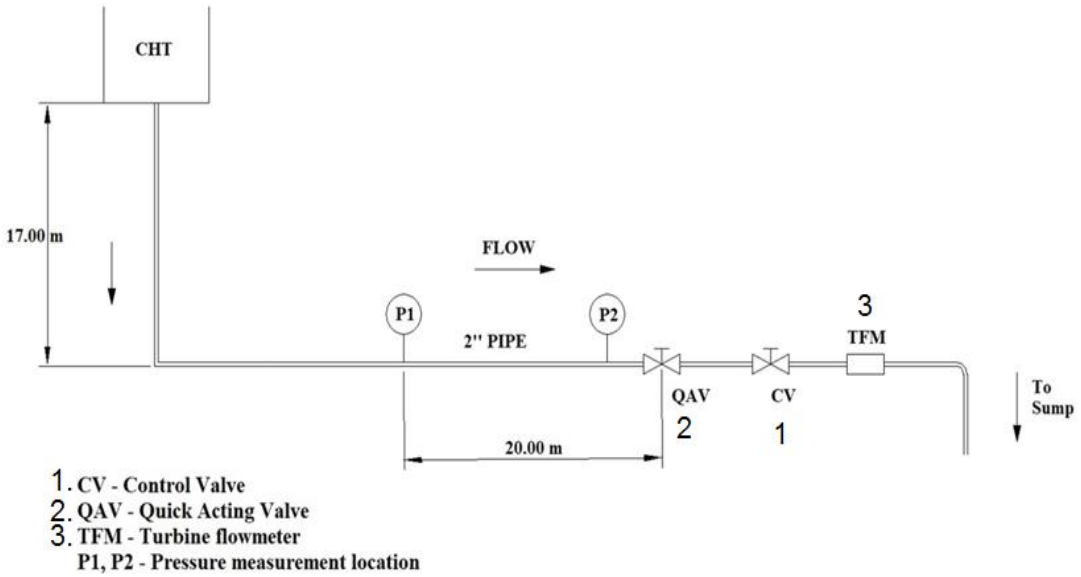

Fig 3.5 Schematic Sketch of the Experimental Setup C

The details of the experimental cases with varying flow rate, closing time, material and anchoring conditions are shown in Table 3.5.

Table 3.5 Different cases of experiments

Sl.No.	Material	Anchoring Condition	Closure time of the valve (ms)	Velocity (m/s)	Flow Rate (m^3/hr)
1 to 60	Mild Steel	No anchor	50	0.540	4.23
		Two anchor	40	0.445	3.53
		Three anchor	31	0.362	2.82
		Five anchor		0.273	2.12
				0.181	1.41
61 to 120	UPVC	No anchor	50	0.8	5.93
		Two anchor	40	0.7	5.20
		Three anchor	31	0.6	4.45
		Five anchor		0.5	3.70
				0.4	2.96
121 to 132	HDPE	Two anchor	40	1.2	7.517
		Three anchor		1.0	6.264
		Five anchor		0.8	5.011
				0.6	3.759

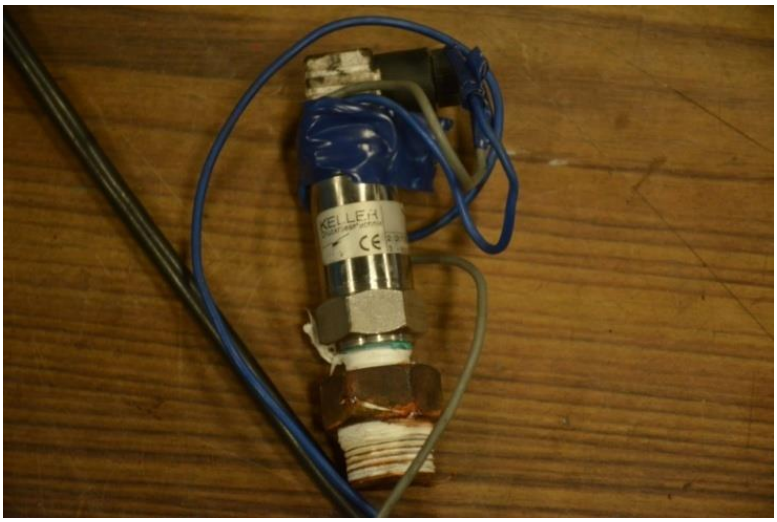

Fig. 3.6- Pressure Transducer Range 0-30 bars

Data Acquisition system (Fig. 3.11) measured the pressure variation at a sampling frequency of 100 kHz. The pressure gauges were calibrated for both positive and negative pressures to yield accurate measurements. Fig. 3.12 shows the switch to create a transient event by the closure of QAV.

Fig 3.7 Digital Flow meter used in the study

Fig 3.8 Over Head Water Tank used in the study with 17 m head

Fig. 3.9 Pressure actuated Quick Acting Valve (QAV)

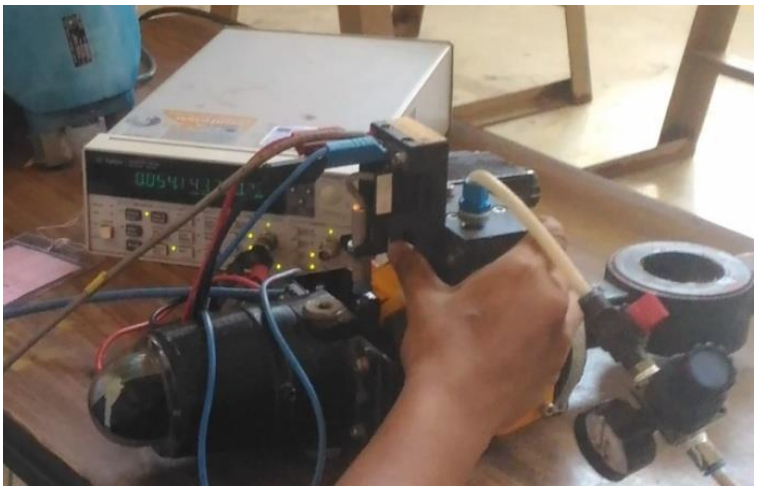

Fig. 3.10 Arrangement for the determination of closure time of Quick Acting Valve

The flow rates for different materials were chosen to ensure that the maximum pressure rise inside the pipe does not exceed 2 times the pressure rating of the pipe, and the cavitation pressure does not exceed 3 times the pressure rating of the pipe. The pressure was analytically calculated by using the Joukowski equation for sudden closure, and the flow rates were selected based on

this pressure to ensure safe working pressure. The steady flow pressure test was conducted at 1.5 times the rating to ensure that there is no leakage in the pipe or at the joints.

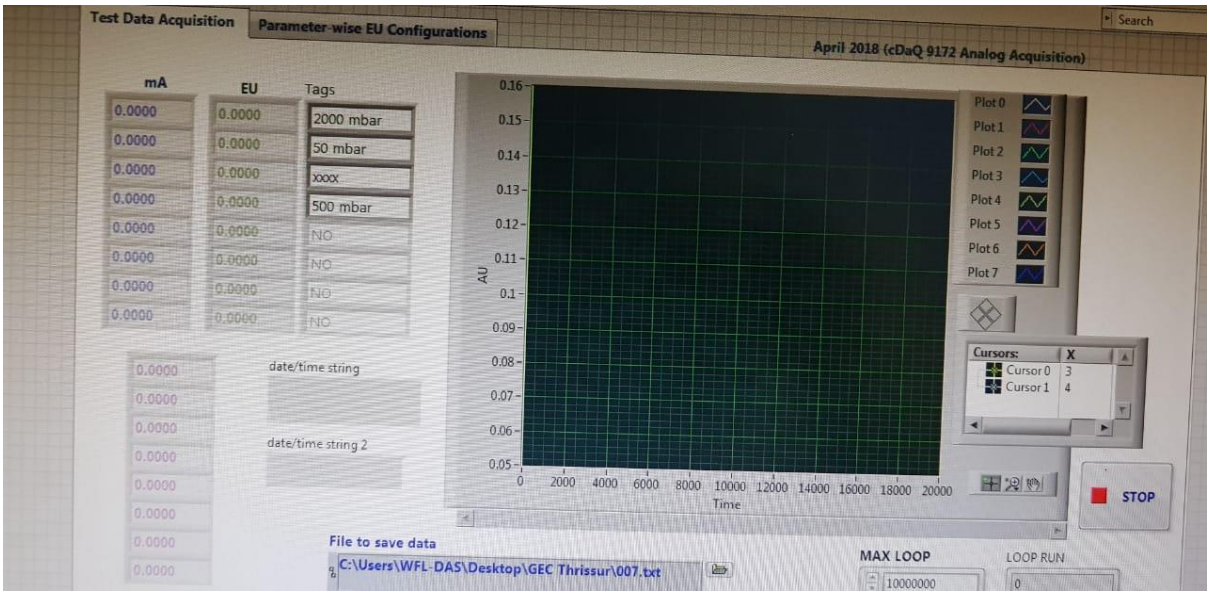

Fig 3.11 Data acquisition system with a sampling frequency of 100 kHz

Fig. 3.12 Switch of Pressure actuated Quick Acting Valve (QAV)

3.5.5. Anchoring conditions

Four different anchoring conditions were used in the setup to study the effect of the anchors on the flow. The anchors were custom designed based on classic theories of mechanics**,** to ensure complete fixity.

3.5.5.1. No anchor condition

The first support condition selected for the experimental study was no anchor condition. In this support condition, no fixed anchor or constraint was attached to the system. The pipe was laid down on the test floor and was free to move. The inlet was clamped to the water main from the CHT and the outlet was driven to an underground sump, the pipe was free to move. However, the flanges did not allow the pipe to rest completely on the floor, and hence it is simply supported at regular intervals. The negative y directional displacement was restrained as the pipe was laid on floor. This support condition was adopted for MS and UPVC pipes. The pipes are tested for flow rates (as specified in Table 3.1) for no anchor conditions (Fig. 3.13). For the HDPE pipe, this support condition was not selected because it was very difficult to fix HDPE pipe in position without any anchors.

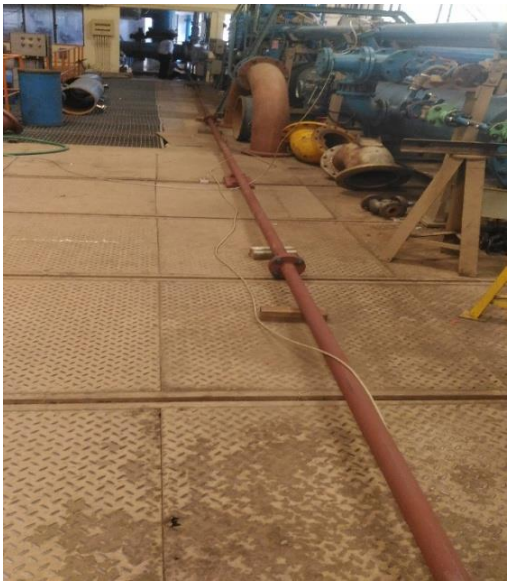

Fig 3.13 Experimental setup – MS pipe - No anchor case

3.5.5.2. Two anchor condition

The second support condition selected for the experimental study was with two fixed anchors one at each end. In this support condition, two fixed anchors or constraints are attached to the system. This support condition was used for all the three pipe materials selected in the study. The supports were so designed as to ensure fixity at the location of the support. Two

clamps, (each of width 60 mm), separated by a distance of 240 mm and fixed to a heavy plate, was used to ensure the fixity (Fig. 3.14 and 3.15). The base plate was further fixed to the foundation by using foundation bolts to ensure a rigid support. Each clamp was given four M10 nuts to ensure the restriction of lateral movements and deflection of the pipe. The supports were fixed at the inlet and the outlet (close to QAV).

3.5.5.3. Three anchor condition

Along with the two fixed anchors in the second case, one more fixed anchor of the same type was added to the system at the centre. This support condition was also applied for all the three pipes of different materials.

Fig 3.14 Anchors used to ensure fixity of the pipe

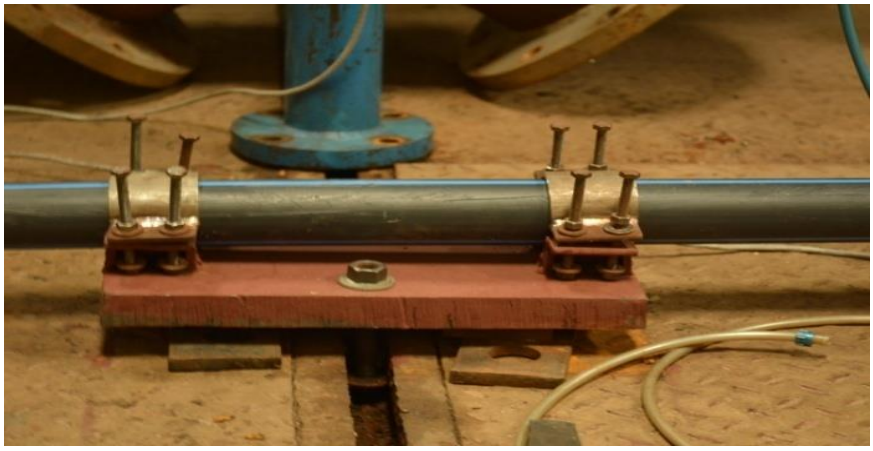

Fig. 3.15 Anchors in position

3.5.5.4. Five anchor condition

Further, two more fixed anchors were introduced to the system, at quarter spans and hence, the total number of constraints increased to five. A typical installation of HDPE is given in Fig. 3.16. For each flow rate, the precaution was taken to avoid the presence of any trapped bubble and any unexpected pressure rise due to such entrapment.

Fig. 3.16 Experimental installation for conducting experiments in HDPE Pipe

Pipes were tested under each anchoring conditions for the different severities of cavitation and also for the different severities of pressure rise, without cavitation. The mass flow was adjusted so that the peak pressure of the cavitation was captured and the pressure surge did not go beyond the limit of the design. The closure time of valve was also simultaneously checked and adjusted. The flow was opened entirely after each series of closure time, to ensure that there is no bubble or air entrapment.

3.5.6. Pipe Acceleration

An accelerometer was also used in MS pipes to measure acceleration during transient flow and was placed at the centre of the pipe for two anchor support condition. The acceleration with respect to time was monitored in lateral directions y and z. For three anchor support condition, the accelerometer was placed at quarter span, at the middle of adjacent supports. The acceleration was recorded in terms of acceleration due to gravity ‘g’.

3.5.7. Flow chart of the methodology

A flow chart showing the methodology of the experimental and numerical study included in the research is shown in Fig. 3.17. All the steps to be followed for attaining the objectives of the current research is shown schematically in the flow chart.

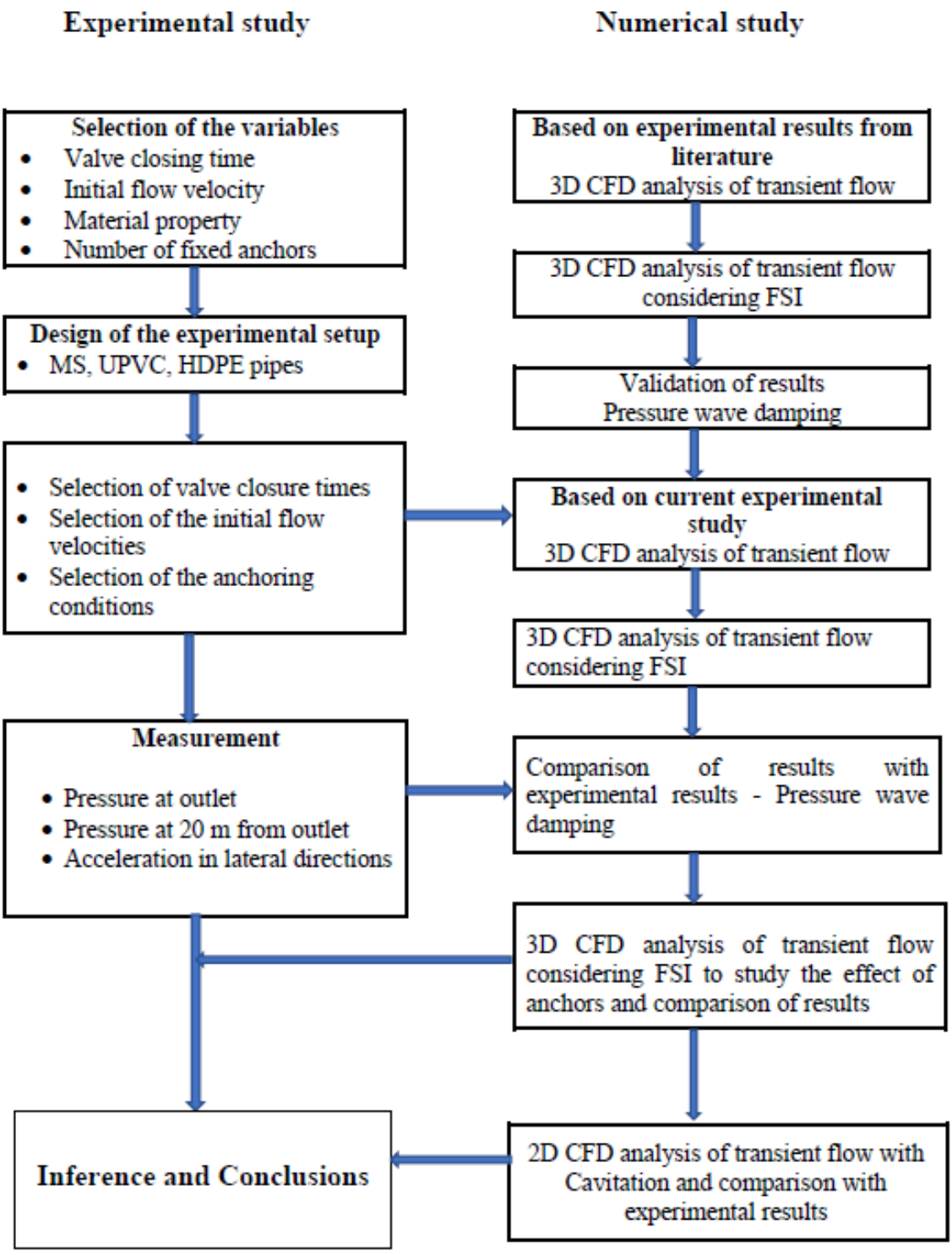

Fig. 3.17 Flow chart of the methodology

3.6. Summary

The governing equations for both fluid flow and structural actions related to the current study were discussed in the first part of this chapter. Numerical methods adopted for the analysis of water hammer, water hammer with FSI and water hammer with cavitation were discussed along with the numerical implementation procedure. The laboratory setups considered for the investigation (Experiment setup A and B, taken from literature) were also included in this chapter. The current experimental investigation (Experimental setup C) for studying the effect of different parameters like valve closure time, flow rate, number of fixed anchors and pipe material was also detailed in the last part of this chapter.

CHAPTER 4

RESULTS AND DISCUSSIONS – EXPERIMENTAL INVESTIGATION

4.1. General

Many experimental studies in the field of transient flow in a piping system dealt with the influence of the closure time of the flow-control valve on the water hammer pressure (Hughes, 1963; Kodura, 2016). However, very few studies investigated into the effect of the closure time of flow-control valve, the velocity of flow and the anchoring conditions of a piping system on the water hammer pressure, and the maximum pressure consequent to cavitation. Although the vibration accompanied by the water hammer of fluid conveying pipes was investigated both numerically and experimentally by many researchers (Zhang et al., 1999; Li et al., 2018; Wang et al., 2013; Sankarachar, 2015; Shaik et al., 2017; Hunain, 2017 and Alnomani, 2018), its effect on flow characteristics was not dealt with in those studies. If a piping system is not anchored properly, it will experience unwarranted vibration during transient flow. The provision of more anchors can make the system more rigid and obviously, the vibration of the system gets reduced. However, the impact of rigidity on the characteristics of fluid flow during a transient-cavitating event has not been investigated so far. Hence, the present study aims to examine the effect of closure time of valve, the initial flow rate of the flow, material properties of the pipe and anchoring conditions of the piping system on the characteristics of transient-cavitating flow through a piping system. The experiments were conducted in a custom-made experimental installation (explained in section 3.5.4) at the water flow laboratory of Fluid Control Research Institute Palakkad, Kerala. Based on the study, the results are presented separately as the influence of various parameters on characteristics of the transient cavitating flow.

4.2. Effect of valve-closure time on transient flow

One of the significant causes of transient flow in a pipeline is the sudden closure of the non-return valve/quick acting valve provided at the downstream end of the pipeline. The sudden closure of the valve can be actuated by a power failure or a pump trip or the like.

Experiments were conducted with various combinations of closure times and initial flow velocities so that the effect of valve-closure time and initial flow velocities on the occurrence of cavitation can be studied. The closure time of valve is a critical factor affecting the pressure peak, formed during the water hammer. It is reported by Ahmadi and Keramat (2010) that when closure time is less than $\frac{2L}{c}$, the valve-closure time does not affect the maximum pressure rise. In such a condition, the Joukowsky equation gives the maximum pressure. When the valve-closure time is greater than $\frac{2L}{c}$ the pressure rise is less than the Joukowsky pressure. Hence, the value $\frac{2L}{c}$ is used for demarcating the type of closure into two categories, viz., sudden and gradual.

The demarcating limit between the sudden closure and the gradual closure is $\frac{2L}{c}$ (Simpson and Wylie; 1991, Simpson and Bergant, 1994; Ahmadi and Keramat; 2010). By using the modulus of elasticity of pipe material and an equivalent bulk modulus of water, the wave velocity for mild steel (MS) was calculated as 1391.06 m/s. The limiting value for categorising the closure time was then calculated as 43.6 ms. Based on this calculation, three closure times were selected as 31 ms, 40 ms and 50 ms, of which 50 ms fell into the type of gradual closure and the other two, 31 ms and 40 ms, into the kind of sudden closure. For studying the effect of valve-closure time along with the change in initial flow velocities, five different initial flow velocities were adopted; which are given in Table 3.5. These initial flow velocities were selected to include different cases with and without cavitation. The steady-state pressure at the salient locations (Fig.3.4, P1 and P2) and the head loss values at the outlet (P2) for each velocity are given in Table 4.1. Pressure variations versus time are plotted at the outlet (P2) and also at 20 m from the outlet (P1) for the various cases. The variations of pressure with the three closure times for the same flow velocity are plotted in a graph to assess the effect of closure time on the occurrence of cavitation.

Fig. 4.1 shows the variation of pressure with time for an initial flow velocity 0.181 m/s and closure times as 50 ms, 40 ms and 31 ms. Out of these three closure times, first one (50 ms) works out to be gradual by the $\frac{2L}{c}$ criteria and the other two as sudden, as indicated earlier. The estimated hike in pressure for gradual closure is $\rho L a_{o,}$ where ρ is the density, L length of pipe and a_o the uniform deceleration. Thus, the estimated hike in pressure works out to be 1.1 bars and hence, the total peak pressure to be 2.8 bars. These values match with the experimental

result. Similarly, the estimated pressure hikes in sudden closure cases work out to be 2.5 bars as per the Joukowsky equation irrespective of the closure times and the corresponding peaks in the total pressure as 4.2 bars. The peak values of pressure for both the cases (with closure time as 31 ms and 40 ms) are equal (4.1 bars) and are slightly less than this value. Hence, the water hammer pressure peak is independent of the closure time when the closure comes under the category of sudden, i.e., $\mathbf{t} \leq \frac{2L}{c}$. These results match with well-established theories and facts (Simpson and Wylie, 1991; Simpson and Bergant, 1994; Ahmadi and Keramat, 2010), and thus validate the experimentation procedure and accuracy of measuring components. The variations of pressure for all the three-closure time indicate that no cavitation is present for this velocity of flow in each of the closure time. Fig. 4.2 gives the pressure variation at 20 m away from the outlet and shows how the pressure wave gets damped during the process. This damping effect also follows the general trend observed in Fig. 4.1 and hence, once again reinforces the aforementioned fact regarding the accuracy of experimentation.

Table 4.1 Steady-state pressure at the key locations and the pressure loss at outlet

Sl. No.	Initial flow Velocity (m/s)	Pressure at 20 m from outlet (P1) (Bars)	Pressure at outlet (P2) (Bars)	Pressure loss at outlet (P2) (Bars)
1	0.181	1.6965	1.6895	0.01050
2	0.273	1.6945	1.6839	0.01608
3	0.362	1.6941	1.6827	0.01730
4	0.445	1.6918	1.6759	0.02413
5	0.540	1.6878	1.6641	0.03590

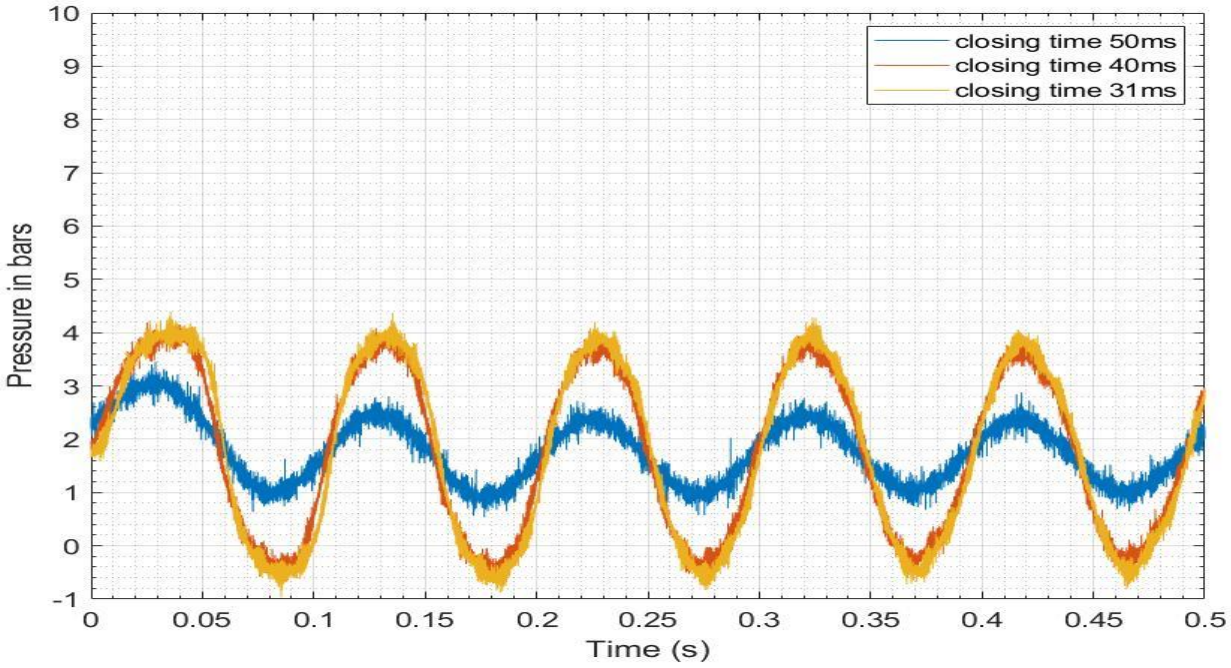

Fig. 4.1 Pressure variation at the outlet for different closure time (v= 0.181 m/s)

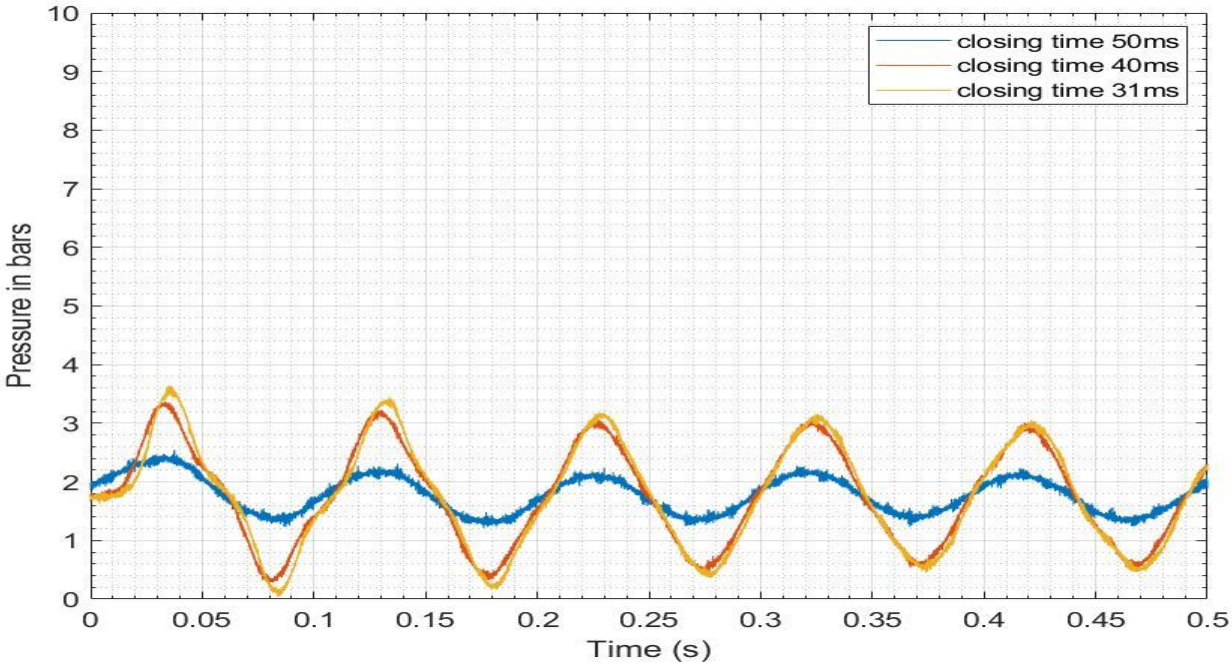

Fig. 4.2 Pressure variation at 20 m from the outlet (v= 0.181 m/s)

The experiment was repeated for an initial velocity of 0.273 m/s for all the three closure times. Here again, the characteristics of the first pressure peak for both sudden and gradual closure of the valve are similar to that for the flow velocity of 0.181 m/s. However, the curves of pressure variation indicate the occurrence of cavitation for closure times 40 ms and 31 ms as shown in Fig.4.3. The pressure drops to vapour pressure for both the cases. Duration of

cavitation periods is from 0.070 s to 0.11 s when the time of closure is 40 ms and 0.065 s to 0.11 s when it is 31 ms. Thus, the water changes from its liquid to vapour state during this period (bubble formation period) and these vapour bubbles collapse at 0.11 s, generating a sudden pressure rise up to 9.4 bars. The pressure rise reaches above 30 bars in the case of closure time of 31 ms. As the time of closure decreases, both the duration of the cavitation and the pressure hike after vapour collapse increase. It indicates the importance of closure time and its link to the occurrence of cavitation. The pressure hike as a result of cavitation was found to be much higher than that of water hammer pressure (3 to 10 times). Thus, it is always advisable to avoid the occurrence of cavitation. Hence, the assessment of operating time for flow control devices is vital for preventing the occurrence of cavitation in any piping system.

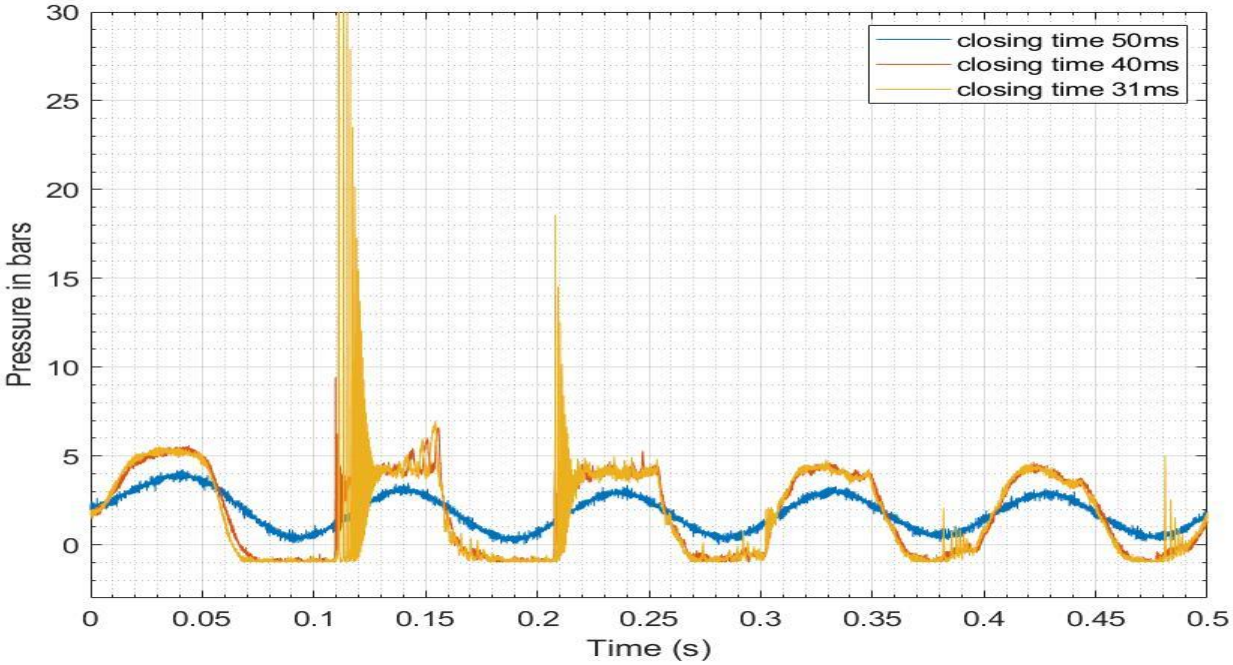

Fig. 4.3 Pressure variation at the outlet (v= 0.273 m/s)

An enlarged view of the pressure variation during the cavitation is shown in Fig.4.4 to have a better understanding of the process. Fig.4.4 shows that the pressure hike as a result of cavitation in case of closure time of 31 ms is more than three times that of 40 ms closure time. Unlike the water hammer pressure, the pressure hikes increase drastically with the decrease in closure time. The magnitudes of these hikes are significant in the context that pipes used in the piping system are normally tested for 1.5 times the static pressure. Although the closure times of 40 ms and 31 ms are classified as sudden closure and the water hammer pressures are equal, the pressure rises as a result of vapour collapse are not comparable (Table 4.2). Unlike the magnitude of water hammer pressure, the occurrence of cavitation and pressure rise due to

bubble collapse depend very much on the valve-closure time. It is seen from the Table 4.2 that the increase in pressure due to cavitation is more than 200% when there is only a 20% decrease in closure time. However, the development of a relation connecting these factors is not possible as some of the recorded pressures are more than 30 bar (deviating from the assumption made earlier for selecting the range of transducer), the maximum limit of transducer; and hence, exact value of pressure in that case could not be recorded.

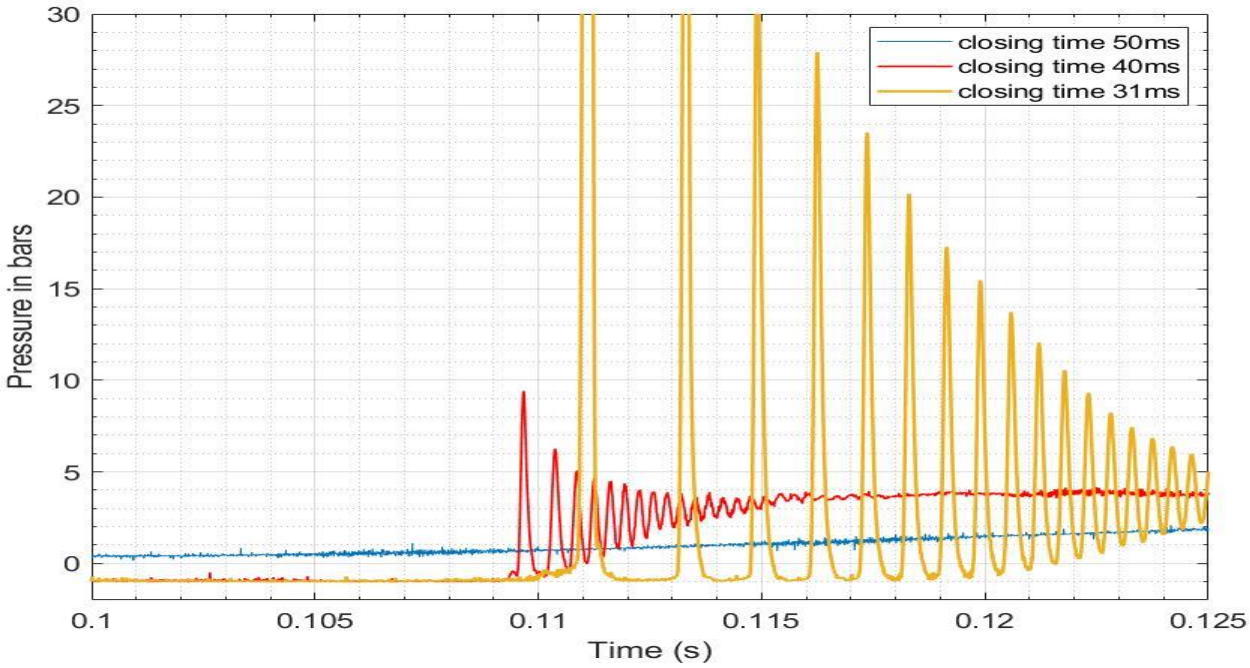

Fig. 4.4 Pressure variation at the outlet (v= 0.273 m/s) - enlarged view

To verify the occurrence of cavitation away from the outlet, the pressure variation at 20 m from the outlet was also plotted (Fig. 4.5). It shows that the second peak in the pressure wave is slightly higher than the first one and thus indicates the occurrence of cavitation not only near the outlet but also at 20 m from the outlet. However, the severity of the cavitation effect is small at 20 m when compared with that at the outlet of the pipe. The severities of the events in the case of 31 ms and 40 ms are almost equal at 20 m, whereas it is not the case in the pressure variation at the outlet. However, this fact has to be verified in the subsequent cases. As expected, there was no cavitation for the case 50 ms closure time (gradual closure) even when the flow velocity was increased from 0.181 m/s to 0.273 m/s.

Table 4.2 Details of peak pressure at the outlet for different flow rates

Velocity (m/s)	Closure time (ms)	First pressure peak (Bars)	Second pressure peak (Bars)	Third pressure peak (Bars)	Cavitation Yes/No
0.181	50	3.15	2.55	2.45	No
	40	4.1	3.85	3.8	No
	31	4.1	4.0	3.95	No
0.273	50	4.2	3.5	3.3	No
	40	5.55	9.4	5.25	Yes
	31	5.55	>30	18.5	Yes
0.362	50	5.1	4.1	3.8	No
	40	6.3	12.8	9.0	Yes
	31	6.3	>30	>30	Yes
0.445	50	6.0	4.8	4.4	No
	40	7.5	15	16.5	Yes
	31	7.5	>30	>30	Yes
0.540	50	7.2	6	5.1	No
	40	8	>30	>30	Yes
	31	8	>30	>30	Yes

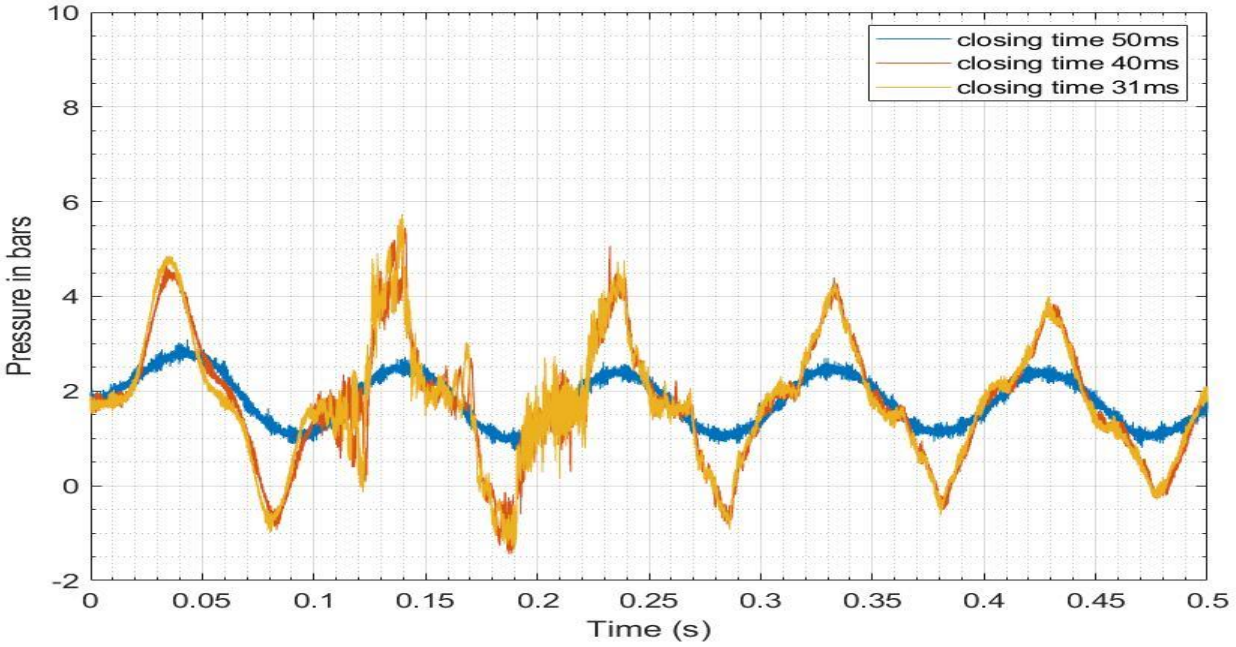

Fig. 4.5 Pressure variation at 20 m from the outlet (v= 0.273 m/s)

In order to reinforce the fact regarding the reduction in severity of pressure with the distance from the source, the curves of pressure variation at 20 m from the outlet of the pipe for the flow rate of 0.362 m/s are shown in Fig. 4.6. As in the previous case, the second pressure peaks in the pressure variation curve of sudden closure cases are higher in magnitude than the first water hammer pressure peak, indicating the presence of cavitation.

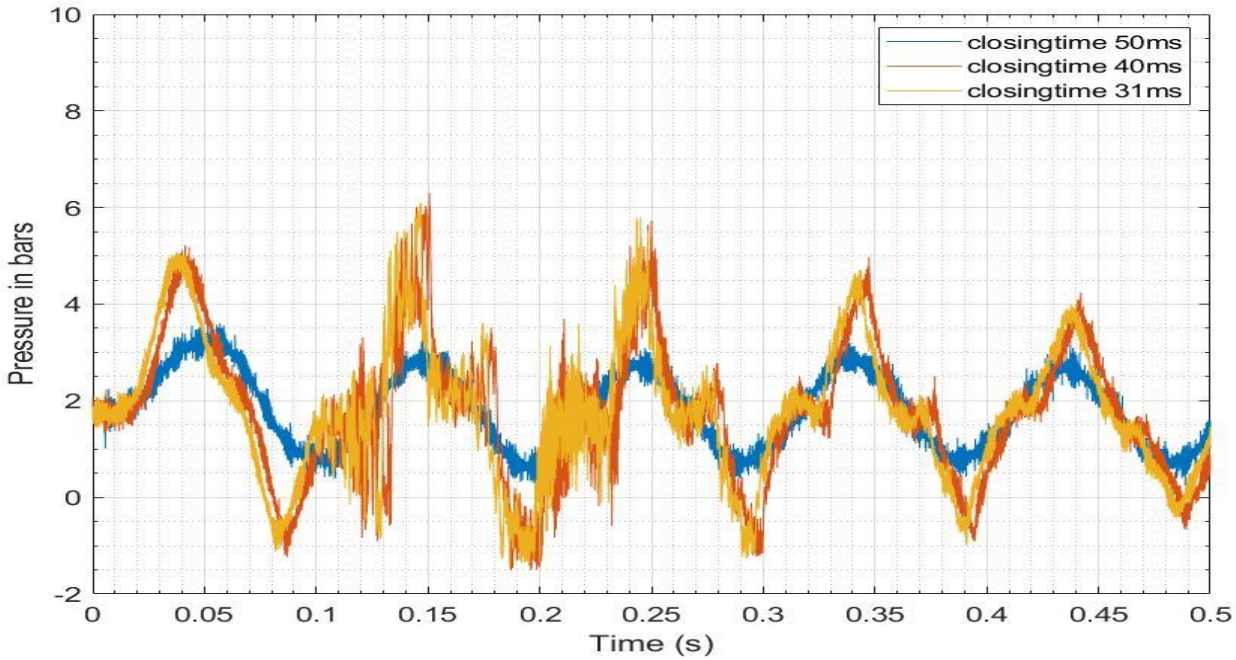

Fig. 4.6 Pressure variation at 20 m from the outlet (v= 0.362 m/s)

Here again, the severities of the events in case of 31 ms and 40 ms are almost equal though it is not so in case of pressure variation at the outlet, which indicates that the severe high-pressure wave does not travel towards upstream; rather it gets damped there itself. The generated cavitation pressure wave is of local nature, and it oscillates within short stretches. This fact was verified for all flow rates of experiments. Moreover, the local nature of occurrence of cavitation was verified by repeated trials and observations of each case. Very high frequency of pressure wave is observed in the case of cavitation compared to that of water hammer pressure wave. The water boundary/pipe boundary near the bubble collapse area might be acting as reflecting point and hence, the pressure waves oscillate with high frequency. The water hammer pressure arising out of the closure of valve acts uniformly across a cross section and gets moved upstream and downstream through the entire length of the pipe. Unlike the water hammer pressure, the pressure rise due to cavitation occurs due to the collapse of fine vapour bubbles created. A cross-section can contain many numbers of such bubbles and their

collapse. Hence the generated pressure as a result of the collapses can move not only in longitudinal direction but also along other directions due to the change in pressure across a cross section. Lind and Phillips (2012) reported that cusping and perturbation of bubbles occur very near to the boundary. Hence, the pressure variation across a cross section can create waves in all directions. Eventually, these multiple pressure waves may either impinge each other or with the boundary and create high-frequency waves.

The results corresponding to all flow velocities for three different closure times have been prepared and presented in Table 4.2. The same pattern is repeated also for the remaining three velocities 0.362 m/s, 0.445 m/s and 0.54 m/s. From Table 4.2, it can be concluded that when the valve-closure time is sudden, the water hammer pressure is as per the Joukowsky equation and is not depended on the valve-closure time. However, the pressure increment due to cavitation is not the same for all the sudden valve-closure times for a given velocity, and the pressure due to cavitation increases drastically with the decrease in valve-closure time.

The experimental results for the velocity 0.54 m/s for the two closure times 40ms and 50 ms are given in Fig. 4.7. From Fig. 4.7, it is observed that the pressure rise as a result of cavitation increases considerably for 40 ms closure time. However, the cavitation is initiated for the case of initial velocity 0.54 m/s and closure time 50 ms, i.e., the pressure just approaches the vicinity of vapour pressure as indicated by the pressure variation curve (Fig.4.7 at time 0.0875 s). This feature is also vivid from the feeble oscillations of the second peak of the pressure variation curve corresponding to closure time of 50 ms (unlike the other case with closure time 40 ms in which the high frequency and sharp peaks are present in Fig.4.7). The resulting vapour generation and the consequent pressure rise due to the vapour collapse seems to be negligible. Hence, the second pressure peak value is less than the first water hammer peak. In order to have better insight into the flow phenomenon of cavitation, the ratios of flow velocity to closure time are tabulated in Table 4.3. The ratios give the deceleration, provided the closing is linear.

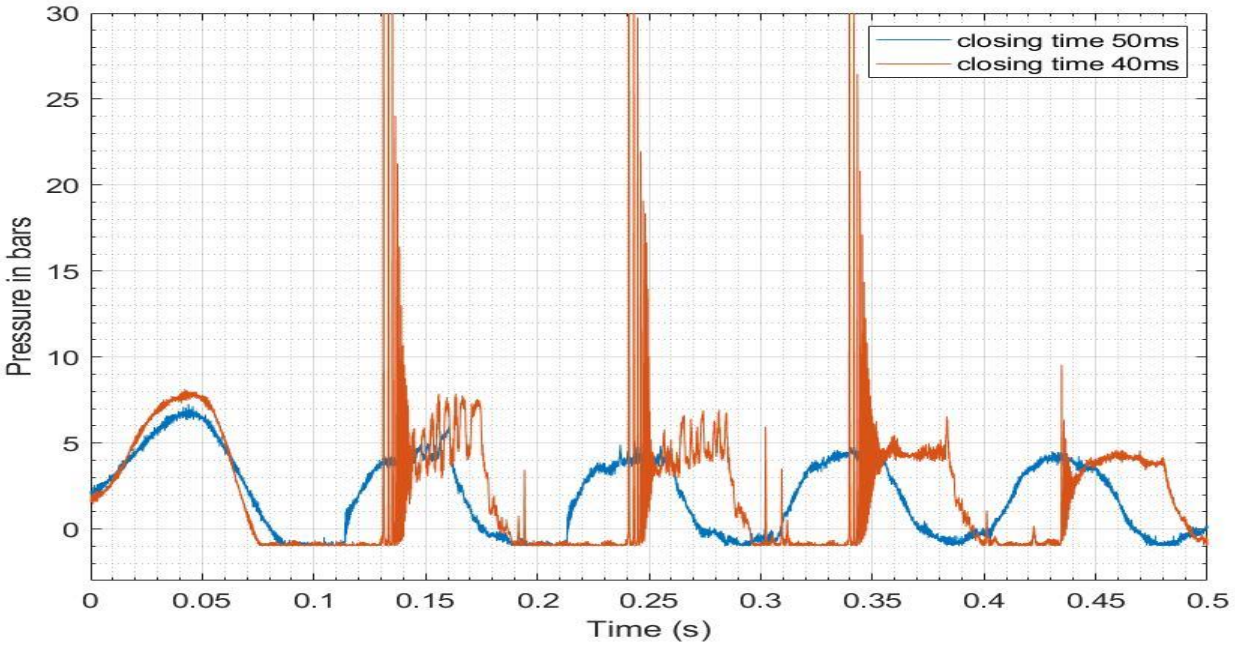

Fig. 4.7 Pressure variation at the outlet (v= 0.54 m/s)

The Table 4.3 shows that for sudden valve-closure for which closure time $\mathbf{t} \leq \frac{2L}{c}$, the occurrence of cavitation is related to the flow velocity/ valve-closure time ratio (v/t). It can be concluded from the experimental results that, the cavitation occurred when the v/t ratio is greater than 6 for sudden closure condition. But for gradual closure condition, cavitation is not initiated when the v/t ratio less than 10. When it nears 10.8, cavitation is just initiated, but the resulting vapour generation and consequent pressure rise due to the vapour collapse is negligible. However, these facts and limits shall further be verified for other gradual closure conditions.

Table 4.3 Flow velocity/valve-closure time ratio in m/s/s

Flow velocity / **Closure time**	**0.181 m/s**	**0.273 m/s**	**0.362 m/s**	**0.445 m/s**	**0.54 m/s**	
50 ms	3.62	5.46	7.24	8.90	10.80	Gradual
40 ms	4.53	6.83	9.05	11.13	13.50	Sudden closure
31 ms	5.84	8.81	11.68	14.35	17.42	
		Cavitation				

From the pressure at the outlet Vs time curve obtained for different experimental cases, an attempt is made to predict the occurrence of cavitation from the first pressure cycle itself. For that, the slopes of the recession phase of the first pressure cycle are calculated for all the flow rates and the closure times and given in Table 4.4. This slope is taken by selecting two salient points on the recession phase of the first pressure cycle with coordinates as (t_1, p_1) and (t_2, p_2) and the slope is calculated as $\frac{(p_1-p_2)}{(t_2-t_1)}$.

Table 4.4 Slope of recession phase of first pressure cycle at the outlet (bars/s)

Velocity / **Closure time**	**0.181 m/s**	**0.273 m/s**	**0.362 m/s**	**0.445 m/s**	**0.54 m/s**	
50 ms	52	98	143	182	227	
40 ms	200	353	400	500	444	Cavitation
31 ms	200	429	420	533	571	
		Cavitation				

Table 4.4 shows the variation of slope of the recession phase of first water hammer pressure cycle for different valve-closure times and initial velocities. For all the cases without cavitation, the slope is less than 300 (slope expressed in bars/s). Similarly, the slope is higher than 300 for all the cases in which cavitation occur. A gap can be easily identified between the maximum value of slope without cavitation (227) and the lowest value of the slope with cavitation (353). Thus, it can be concluded that when the slope of the decreasing phase of the first water hammer pressure cycle is higher than a value of 200, the cavitation can occur and hence, safety measures are to be resorted for reducing the effect. Now the question comes what is the use of this information? The slope of water hammer can be measured only if the transient occurs, which in turn, results in the cavitation if the condition favours. The solution to this quandary is the use of readily available simple 1-D numerical water hammer model which can easily be employed for the estimation of the water hammer cycle with great accuracy, thereby finding the slope of descending phase, and hence identifying the possibility of occurrence of the cavitation utilising the information mentioned above. It may be noted that the cavitation models are difficult to build and even if it is built, running of the model takes a lot of computer processing time. For capturing cavitation during the simulation of transient flow, very fine mesh and very small-time step are necessary even for 1-D model (Sumam et al., 2010). The 2-

D and 3-D models are computationally more expensive. Hence, this suggested method gives an easy way to identify the chance of occurrence of cavitation.

4.3. Effect of initial flow velocity on transient flow

Experiments are conducted in MS pipe for five different initial flow velocities as given in Table 3.5. The figures Fig. 4.8 to 4.10 show the variation in pressure peak with the change in initial flow velocity while the closing time and the support conditions are kept constant. The variation of pressure for various flow velocities while keeping the closure time as 50 ms and the anchoring condition as two fixed anchors are shown in Fig. 4.8. It is vivid that the peak pressure increases with the increase in initial flow velocity whereas the period of pressure waves remains same in all cases. For the initial velocity of 0.54 m/s, the cavitation is initiated (Fig.4.8 at time 0.0875 s). Feeble oscillations in pressure curve (velocity 0.54 m/s) also indicate a weak cavitation, unlike the pressure variations corresponding to the other flow velocities (Fig. 4.8). The resulting vapour generation and the consequent pressure rise due to vapour collapse seems to be negligible. Hence, the second pressure peak value is less than the first water hammer peak.

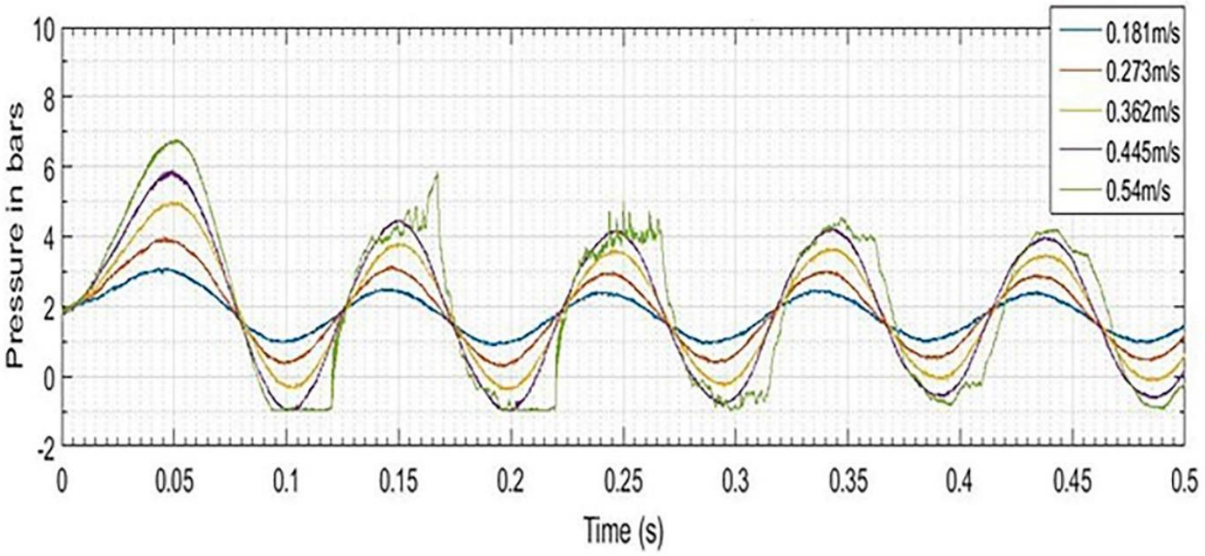

Fig.4.8 Pressure variation at the outlet for 50 ms closure time (MS pipe) and for different velocities

When the valve-closure time reduces to 40 ms, keeping all other variables constant, the pressure peak (as a result of water hammer) increases with the increase in the flow velocity as in the case of 50 ms closure time (Fig.4.9). No cavitation is present for the flow velocity 0.181 m/s. Cavitation occurs for this valve-closure time when the initial flow velocity was changed

to 0.273 m/s. For understanding the trend properly, an enlarged view of the Fig. 4.9 is prepared for the first cavitation pressure region and given in Fig. 4.10. For the flow velocity of 0.181 m/s, the water hammer pressure does not drop below vapour pressure and hence no cavitation occurs. But when the flow velocity increases to 0.273 m/s, the formation of vapour bubbles initiates at 0.07 s and the bubbles collapse at 0.1125 s and the peak pressure because of the bubble collapse is 9.4 bars. Similar trend is seen for all other flow velocities. The rise in the severity of cavitation with the increase in the initial flow velocity is vividly visible in Fig.4.10.

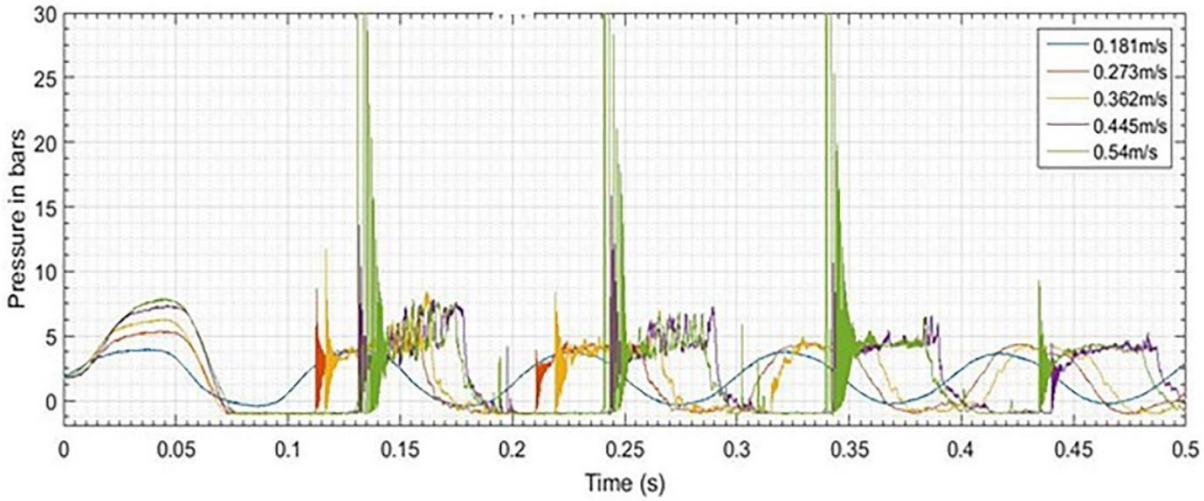

Fig. 4.9 Pressure variation at the outlet for 40 ms closure time (MS pipe) and for different velocities

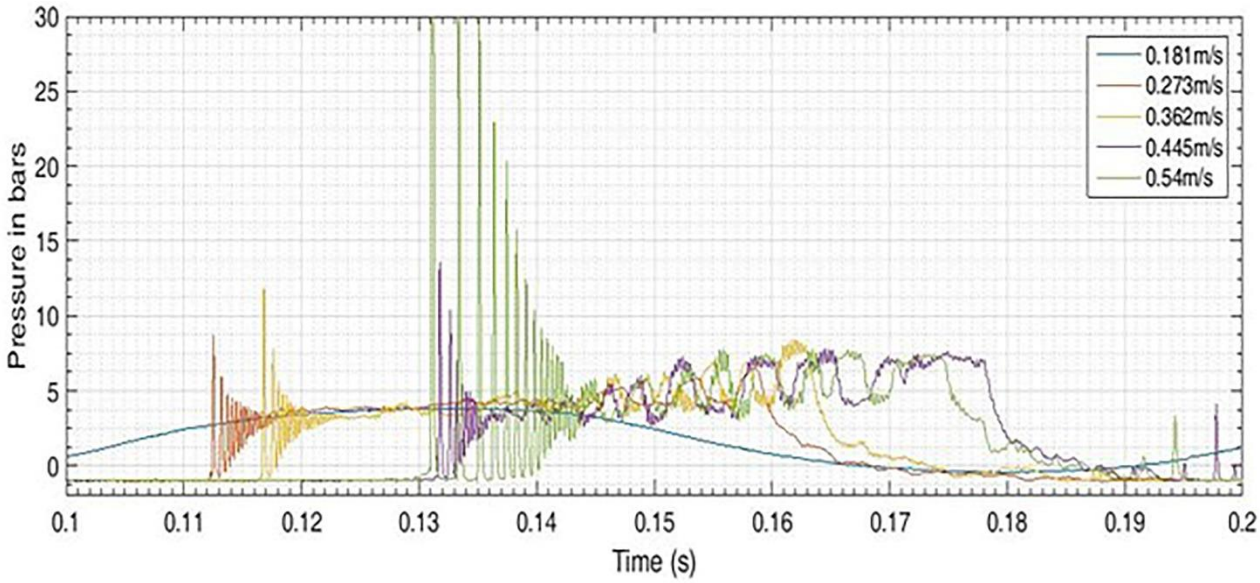

Fig. 4.10 First cavitation pressure rise at outlet for 40 ms closure time- enlarged view

It can be concluded that when the initial flow velocity increases, the cavitation period and the corresponding cavitation pressure increases drastically.

4.4. Effect of material properties on transient flow

As the mechanical behaviour of the pipe material influence the flow characteristics, the present study also assesses the effect of material properties on transient flow. Three pipe materials viz., Mild Steel (MS), Unplasticized Poly Vinyl Chloride (UPVC) and High Density Poly-Ethylene (HDPE) were used for conducting a comparative study. Initial flow velocities for the comparative study were selected in such a manner that the transient event in that flow velocity under sudden closure condition did not cause cavitation. Moreover, these velocities were selected to have almost the same water hammer pressure. The flow velocities of 0.181 m/s, 0.4 m/s and 0.6 m/s were used for MS, UPVC and HDPE respectively. In order to get rid of the variation in flow velocity and period of pressure wave, dimensionless charts were prepared by keeping the *x* axis as t/T (time/pressure wave period) and the *y* axis as the change in pressure divided by the pressure calculated from the Joukowsky formula (Fig. 4.11).

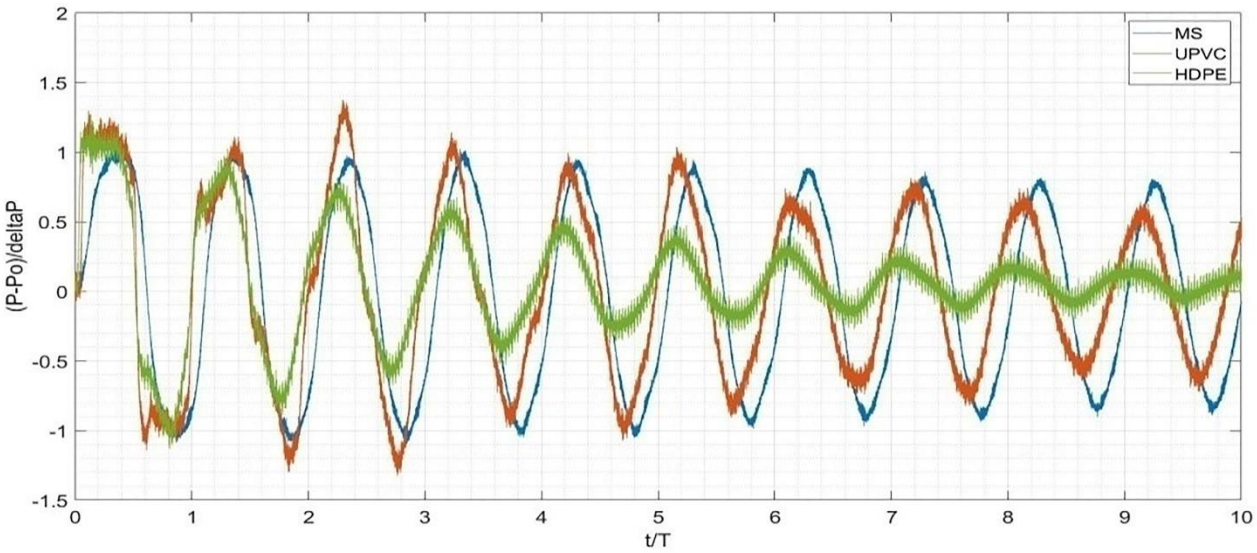

Fig.4.11 Normalised pressure at the outlet for three materials with 2 anchors

From Fig.4.11 it can be seen that WH pressure obtained from the experiment for the elastic material (MS) is the same as the pressure calculated by Joukowsky formula i.e. the ratio is 1. But, the water hammer pressures obtained from the experiment for both visco-elastic materials (UPVC and HDPE), are more than the pressures calculated by the Joukowsky formula i.e. the ratio obtained as 1.42 for UPVC and 1.34 for HDPE. For further verification, these ratios were

computed for all the cases of UPVC and HDPE pipes (Table 4.5). These data indicate that the Joukowsky formula does not predict the water hammer pressure in visco-elastic pipes correctly.

Table 4.5 Ratio of change in pressure to Joukowsky pressure (UPVC and HDPE pipes with 2 anchor condition)

Sl no	Material	Flow Velocity (m/s)	Maximum water hammer pressure ΔP (Bars)	Ratio ($\Delta P/\rho c \Delta V$)
1	UPVC (c = 430 m/s)	0.4	2.44	1.42
2		0.5	3.03	1.41
3		0.6	3.45	1.34
4		0.7	3.89	1.30
5		0.8	4.45	1.30
6	HDPE (c = 315 m/s)	0.6	2.52	1.34
7		0.8	3.15	1.25
8		1.0	3.65	1.16
9		1.2	4.14	1.10

From Table 4.5, it can be seen that the change in pressure obtained from the experiments for the UPVC pipe is much more than theoretical Joukowsky pressure for all the five flow rates (the ratio ≥ 1.3 with average value 1.36). The same is true for HDPE pipe also. However, the ratio decreases with increase in flow velocity. In any case, the ratio is greater than one. This finding has practical implication in the design as the Joukowsky formula is generally used for estimating water hammer pressure in the design calculations. Hence, proper modification has to be carried out in the pressure obtained by the Joukowsky formula while estimating the water hammer pressure for viscoelastic pipes (UPVC and HDPE).

It is interesting to note that the damping characteristics of the pressure wave for the three materials are different. To have better insight, normalised pressure plots are prepared for each material (Fig. 4.12, 4.13 and 4.14). The damping of pressure wave is different for the three materials under consideration.

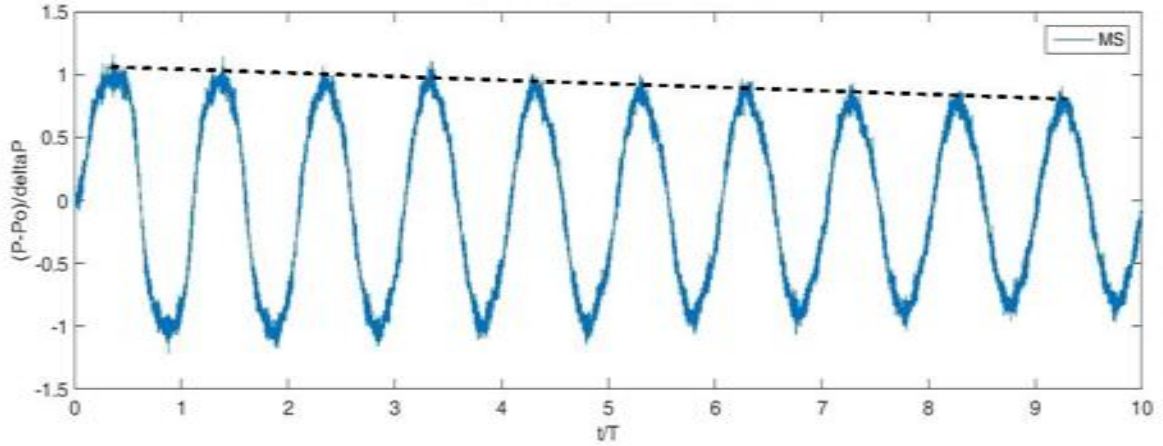

Fig.4.12 Normalised pressure at outlet (MS pipe)

Fig. 4.12 shows the damping of pressure wave (represented by the dotted line connecting the peaks) for MS pipe, with a flow velocity of 0.181 m/s. The damping is 18.2 % in 10 cycles.

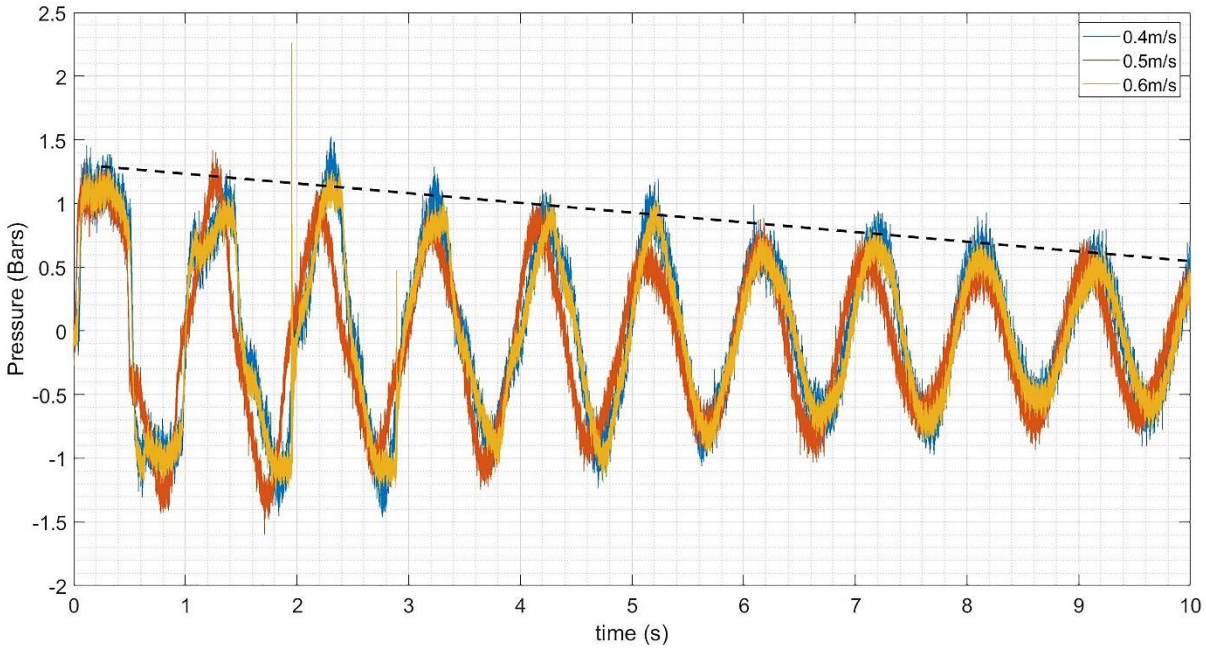

Fig.4.13 Normalised pressure at the outlet (UPVC pipe) for different velocities

Fig. 4.13 shows the normalised variation of pressure wave for UPVC pipe (under three velocities). Here the damping is 44.8 % in 10 cycles.

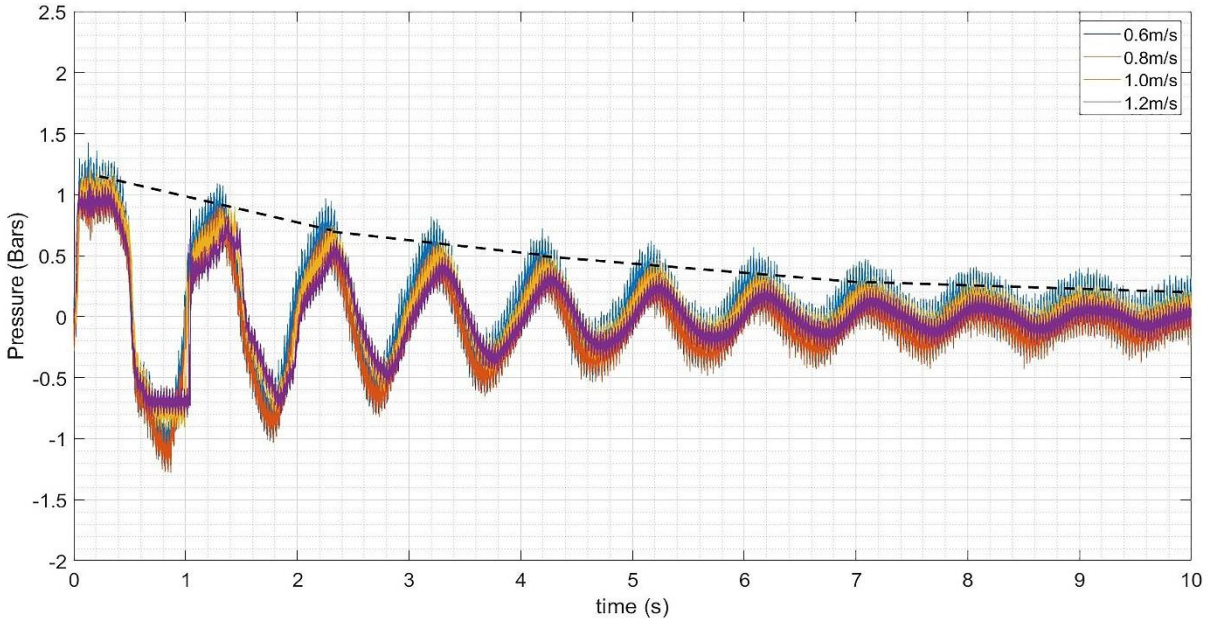

Fig.4.14 Normalised pressure at the outlet (HDPE pipe) for different velocities

Fig. 4.14 shows the normalised variation of pressure wave for HDPE pipe (under three velocities). In contrast with the other cases, the damping is 75 % in 10 cycles. It can be concluded that pressure wave damping is maximum in HDPE pipes and hence, pressure fluctuations are less dangerous for HDPE pipes. Therefore, HDPE pipes are recommended for water transmission lines where the adverse effects of sudden change in operating conditions are frequent.

4.5. Effect of Anchors on transient flow

Anchors are provided for any piping system to hold the pipes properly in position, to reduce the vibration of the pipes, and to give rigidity to the entire piping system. Anchors are normally fixed or restrained in particular direction. The anchors provided in the study were fixed which restricted the motion/deformations of pipe in all directions at these positions. The experiments were conducted to study the effect of such supports on the flow characteristics of the piping system by varying the number of fixed anchors attached to the system. This was repeated for three different materials of the pipes, viz., MS, UPVC and HDPE pipes.

4.5.1. Effect of anchors in MS pipes

As explained in the methodology, the experiments were conducted on MS pipe installation with four different anchoring conditions, viz., no anchors, two fixed anchors (at

two ends), three fixed anchors (at two ends and centre), and five fixed anchors (at ends, centre, one-fourth and three-fourth lengths). The pressure was measured at the outlet and 20 m from the outlet. For assessing the effect of anchoring conditions on transient flow characteristics, the pressure variation curves are plotted at the outlet and 20 m from the outlet, for different anchoring conditions in a single plot, keeping all other variables such as closure time, flow velocity and material proprty as constant.

4.5.1.1. Gradual Valve-closure

By taking the valve-closure time as 50ms, the pressure variation with time was compared for all the four anchoring conditions mentioned in the experimental setup (i.e. no anchor, two anchors, three anchors and five anchors) and for all the five velocities (cases as given in the Table 3.5). The pressure curves were drawn at the position of two transducers attached to the pipe (i.e., at the outlet and 20 m from the outlet). The pressure variation at the outlet was the same for all the four anchoring conditions and all the five velocities adopted in the study under gradual closure condition. A typical figure is given in Fig. 4.15 which shows the pressure variation at the outlet corresponding to a flow velocity of 0.445 m/s.

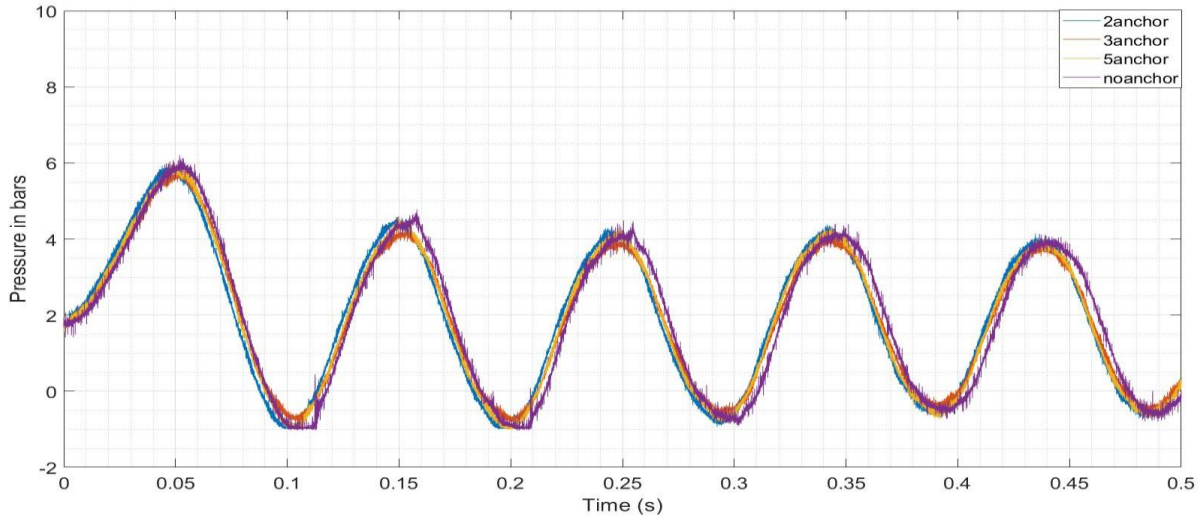

Fig. 4.15 Effect of anchors on the pressure at the outlet for a velocity of 0.445 m/s and closure time 50 ms

Pressure variation recorded by the transducer attached at 20 m from the outlet also gives similar results (Fig.4.16), for all the five flow velocities.

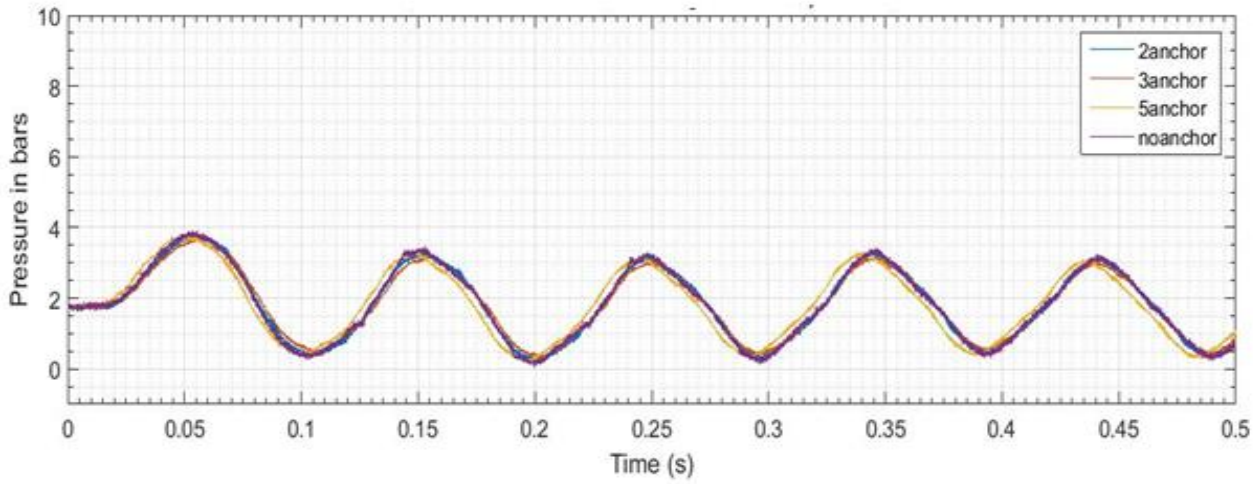

Fig. 4.16 Effect of anchors on the pressure at 20 m from the outlet (velocity of 0.445 m/s and closure time of 50 ms)

From Fig. 4.15 and 4.16, it can be found that the water hammer pressure for MS pipe is independent of number of fixed anchors attached to the system when closure time comes under the category of gradual condition.

4.5.1.2. Sudden Valve-closure

The next closure time adopted for the study is 40 ms which comes under the category of sudden closure. For this closure time, the pressure variation at the outlet and also at 20 m from the outlet were analysed for the different anchoring conditions mentioned earlier and for all the five velocities. Fig.4.17 shows the pressure variation at the outlet for a velocity of 0.181 m/s and for the four anchoring conditions. Fig. 4.17 confirms the fact that the increase in number of fixed anchors does not change the water hammer pressure even for sudden valve-closure. Similar results are available at 20 m from the outlet.

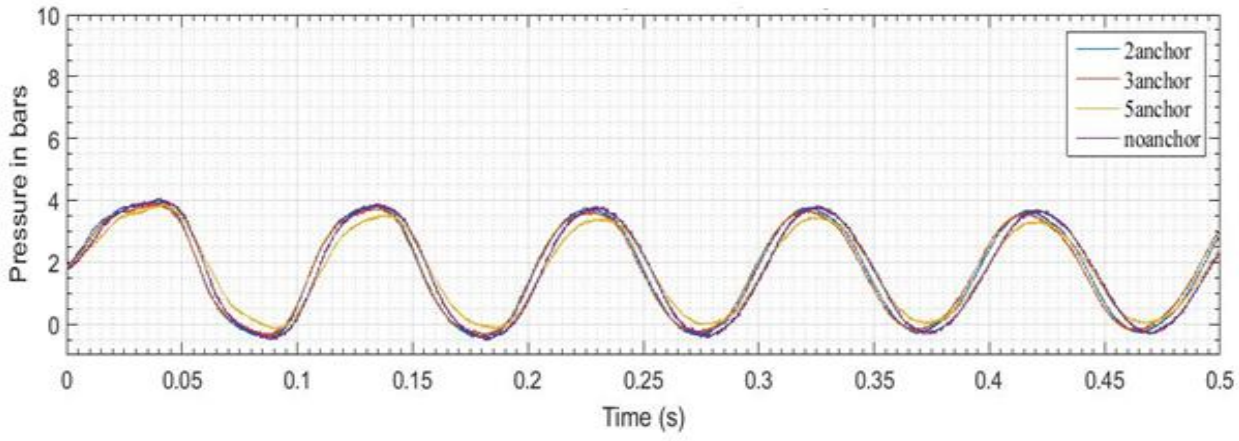

Fig. 4.17 Effect of anchors on pressure variation at the outlet for a velocity of 0.181 m/s and closure time 40 ms

The Fig.4.17 shows similar behaviour as Fig 4.15 and 4.16. The water hammer pressure and the period of pressure wave are the same for all the four anchoring conditions. The pressure peaks agree well with the respective pressure rise calculated by the Jowkousky equation for the sudden closure of the valve (calculated as 4.2 bars). For the same valve-closure time, when the velocity increases to 0.273 m/s, the pattern of pressure variation unexpectedly changes. The water hammer pressure peak (5.55 bars) is precisely the same for all the four anchoring conditions and also equal to the pressure calculated by the Jowkousky equation. The pressure variation at the outlet corresponding to a velocity of 0.273 m/s and the valve-closure time of 40 ms is given in Fig. 4.18.

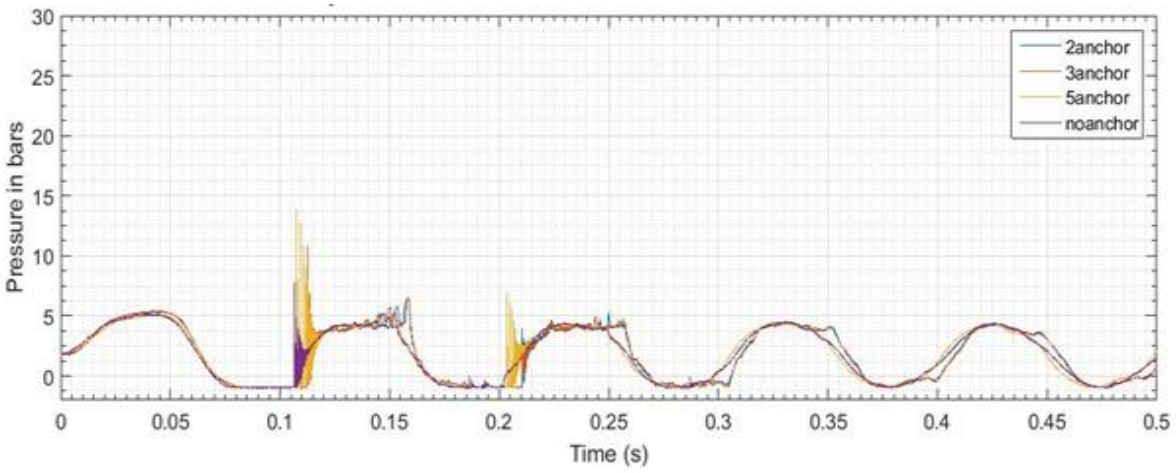

Fig.4.18 Effect of anchors on pressure variation at the outlet for a velocity of 0.273 m/s and closure time of 40 ms

Fig. 4.18 shows the increase in cavitation pressure when the number of anchors increases. The cavitation initiated at 0.075s for all the four anchoring conditions and continues up to 0.1065s in the case of no anchor. The Bubbles collapse at 0.1065s for zero anchor condition and maximum pressure rise due to bubble collapse is 7.5 bars. For the two anchors condition, the cavitation pressure is 9.4 bars. For the three anchor and the five anchor conditions, the cavitation pressures are 11 bars and 14 bars respectively. The cavitation periods are almost same in all the four cases and the pressure rise during cavitation increases with the increase in the number of fixed anchors attached to the system (Table 4.6).

The results (Fig.4.18) reveal that the increase in the number of anchors makes the pipe more rigid, which does not change the water hammer pressure peak, but creates more adverse effect during cavitation. This performance is again checked for other higher flow velocities

without changing the closure time. Fig. 4.19 shows the pressure variation at the outlet for a flow velocity of 0.362 m/s with a closure time of 40 ms.

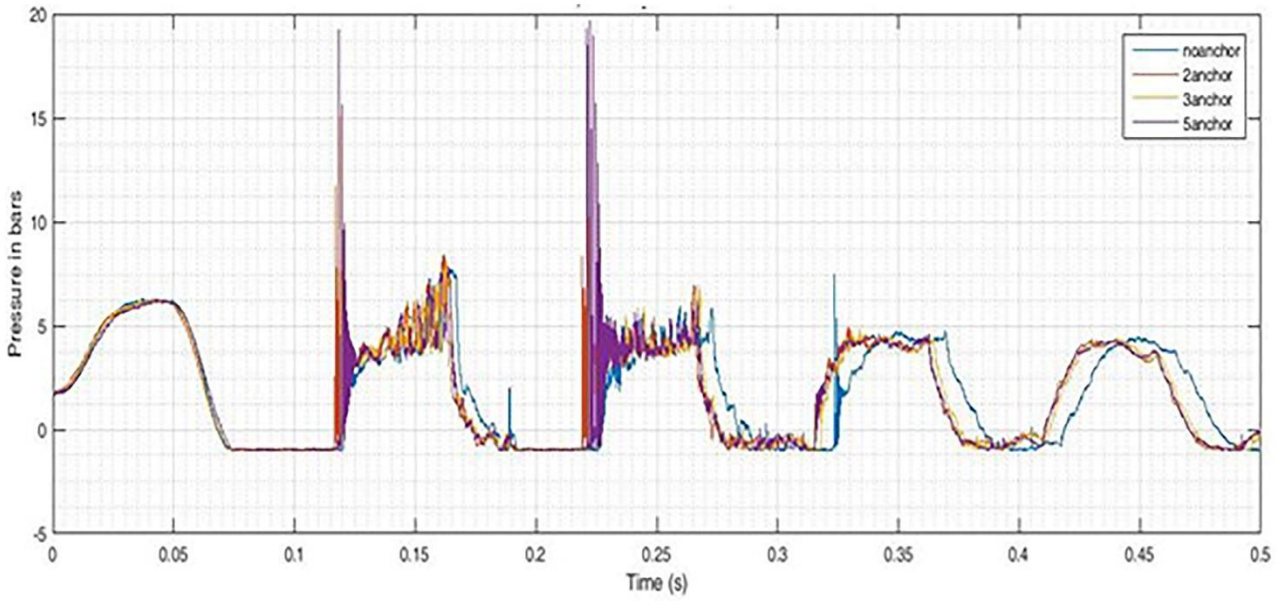

Fig. 4.19 Effect of anchors on pressure at the outlet (MS pipe) for a velocity of 0.362 m/s and closure time 40ms

It is found that the pressure curves have same pattern in both Fig.4.18 and 4.19. In both the cases, the pressure peaks as a result of water hammer do not vary with the increase in number of fixed anchors. This behaviour reinforces the fact stated in the previous section that the water hammer pressure is not affected by the change in the number of anchors. However, the second peak because of cavitation considerably changes with the increase in number of anchors. The pressure variation for all the three velocities (for which cavitation occurred) with four different anchoring conditions at 40 ms closure time are tabulated and presented in Table 4.6.

From Table 4.6, it is clear that for sudden valve-closure condition also, the number of anchors does not have any influence on the peak of water hammer pressure. However, the severity of cavitation and the pressure as a result of cavitation change radically with the increase in number of anchors. It may be noted that all the other factors, say the velocity and closing time were kept as same for each lot of experiments. Hence, the indicated change in the severity of cavitation is purely consequent to the change in the number of anchors. The reason behind this behaviour has to be analysed further.

Table 4.6 Effect of anchors on the variation of pressure for sudden closure (40 ms)

Velocity (m/s)	Anchoring condition	Water Hammer Pressure (Bars)	The period during which Cavitation occurs (s)	Cavitation duration (s)	Cavitation Pressure second peak (Bars)
0.273	No anchor	5.55	0.075 - .107	0.032	7.5
	Two anchor	5.55	0.075-0.112	0.037	9.4
	Three anchor	5.55	0.075-0.112	0.037	11
	Five anchor	5.55	0.075-0.112	0.037	14
0.362	No anchor	6.3	0.07-0.116	0.046	8.5
	Two anchor	6.3	0.07-0.116	0.046	12.8
	Three anchor	6.3	0.07-0.117	0.047	16
	Five anchor	6.3	0.075-0.117	0.047	20
0.445	No anchor	7.5	0.065-0.126	0.061	9.5
	Two anchor	7.5	0.065-0.126	0.061	15
	Three anchor	7.5	0.065-0.128	0.063	23
	Five anchor	7.5	0.065-.128	0.063	>30

The pressure variation recorded at the second transducer attached at 20 m from the outlet was also studied and the pressure variation was plotted for all the four anchoring conditions with the corresponding flow velocities. The pressure variations at 20 m from the outlet for all the four anchoring conditions do not vary much. Although this characteristic is contradictory to the results of pressure variation at the outlet, it is very much in line with the discussion had in previous section regarding the high frequency and the local reflection of the cavitation waves. A typical pressure variation curve is given in Fig. 4.20 which is for a flow velocity of 0.362 m/s and for the closure time of 40 ms.

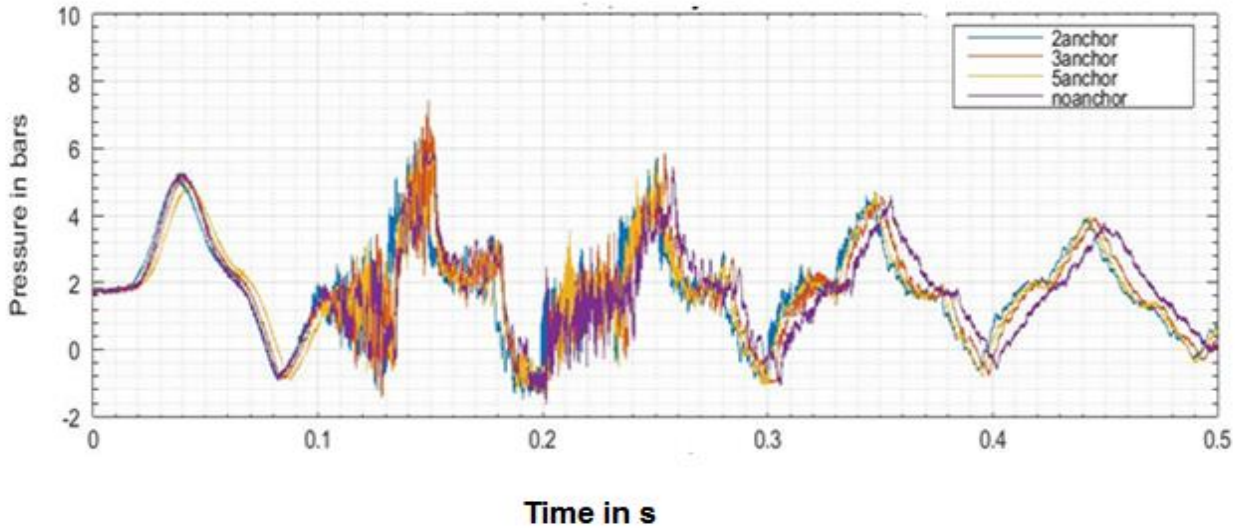

Fig. 4.20 Effect of anchors on the pressure variation at 20 m from the outlet (velocity 0.362 m/s and closure time 40 ms)

By analysing the pressure variation at the outlet and at 20 m from the outlet, for different flow velocities under sudden valve-closure condition, it can be concluded that the peak of water hammer pressure is unaltered by the presence of more number of fixed anchors. But the occurrence of cavitation and the cavitation pressure induced by bubble collapse are highly influenced by the number of anchors attached to the system. As the piping system becomes more rigid by the presence of a greater number of fixed anchors the cavitation pressure increases extensively. However, this adverse effect of cavitation is significant only at the outlet, where the transient event is initiated. This phenomenon reinforces the fact that the occurrence of cavitation and the pressure rise resulted by vapour collapse are local and hence its effect is not transmitted towards the other end. As it moves away from the location of occurrence (of cavitation), the adverse effect of cavitation goes on decreasing which is evident from the measurements obtained from the transducer kept at 20 m from the outlet (Fig 4.20).

4.5.2. Effect of anchors-UPVC pipes

As explained in the experimental setup, the experiments were conducted in UPVC pipe installation, for different flow velocities (Table 3.5) and the results are tabulated (Table 4.7) and plotted. The results were analysed for studying the effect of different anchoring conditions, and curves are prepared accordingly. Experiments were conducted with the four different anchoring conditions as explained in the experimental setup (section 3.5.5). The variation of water hammer pressure at the outlet is plotted in Fig. 4.21 for the closure time of 40 ms, and the flow velocity as 0.4 m/s. From Fig. 4.21, it is clear that the water hammer pressure is

independent of the number of fixed anchors attached to the system even in the case of UPVC pipe.

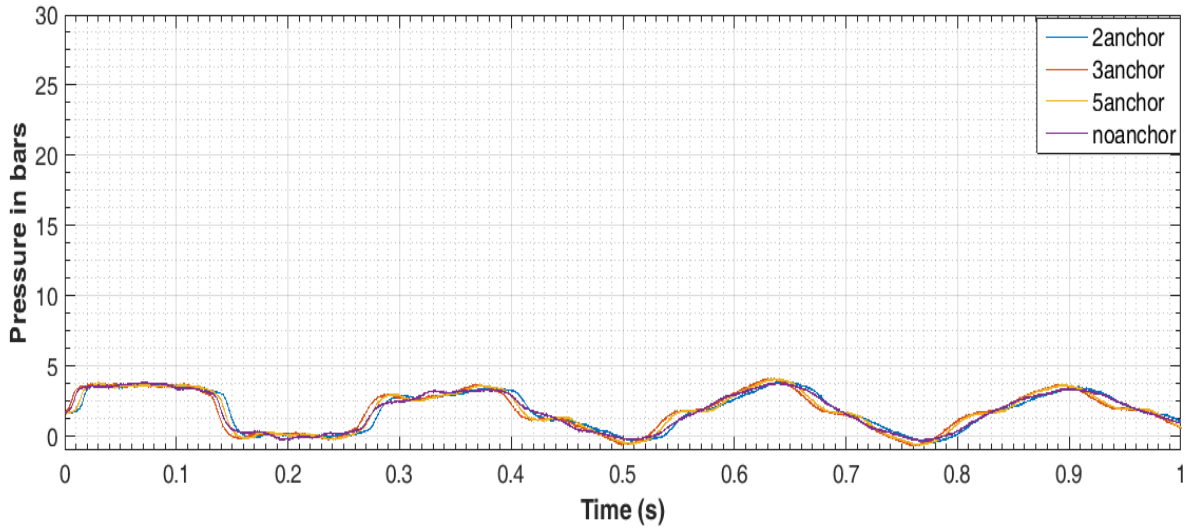

Fig. 4.21 Effect of anchors on the pressure variation at the outlet for a velocity of 0.4 m/s and closure time 40 ms (UPVC pipe)

The pressure variations at the outlet for all the four anchoring conditions and with a flow velocity of 0.6 m/s are included as Fig. 4.22. From Fig. 4.22 it can be inferred that the water hammer pressure is independent of the number of fixed anchors attached to the system, whereas the occurrence of cavitation and cavitation pressure depend on the number of fixed anchors attached to the system. Hence, these characteristics reinforce the fact that the number of anchors and hence, the rigidity of the piping system influences the severity of cavitation in the system.

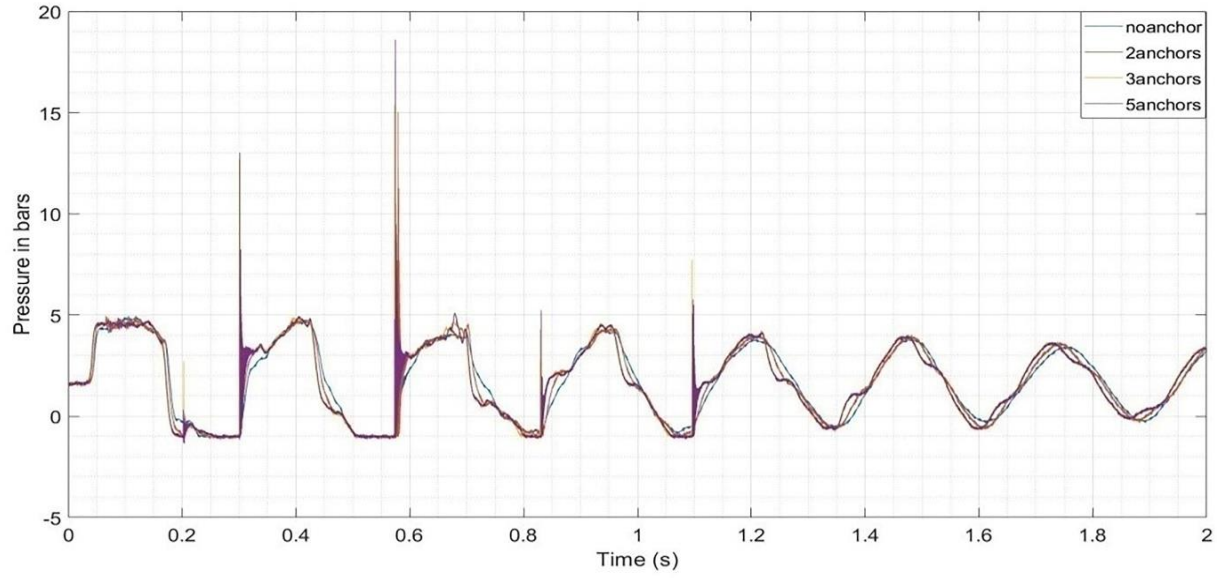

Fig. 4.22 Effect of anchors on the pressure variation at the outlet for a velocity of 0.6 m/s and closure time 40 ms (UPVC pipe)

Table 4.7 tabulates all the water hammer and cavitation pressure values of UPVC pipes with four different anchoring conditions. It can be noted from the table that as the rigidity of the piping system increases (by increasing the number of fixed anchors attached to the system), the water hammer pressure remains unaltered while the cavitation pressure goes on increasing with the increase in the number of fixed anchors. From Table 4.7, it can also be seen that the third pressure peak is more than the second peak in all the cases of UPVC pipes. But the identification of the reason behind this abnormal behaviour needs further investigation.

Table 4.7 Pressure at outlet for UPVC pipe

Velocity (m/s)	Anchoring condition	Water Hammer Pressure (first peak) (Bars)	Cavitation Pressure second peak (Bars)	Cavitation Pressure third peak (Bars)
0.5	No anchor	4.5	3.8	4.5
	Two anchor	4.5	4	4.8
	Three anchor	4.5	13	15
	Five anchor	4.5	18	21.5
0.6	No anchor	5.0	5.0	11
	Two anchor	5.0	5.0	15
	Three anchor	5.0	12.5	16.5
	Five anchor	5.0	13	19
0.7	No anchor	5.5	5.0	15.0
	Two anchor	5.5	14	22
	Three anchor	5.5	>30	>30
	Five anchor	5.5	>30	>30
0.8	No anchor	6.0	14	22
	Two anchor	6.0	>30	>30
	Three anchor	6.0	>30	>30
	Five anchor	6.0	>30	>30

4.5.3. Effect of anchors-HDPE pipes

In a similar way, experiments were conducted in the HDPE pipe installation for different flow velocities, and the results are tabulated and plotted. Experiments were conducted for the three different anchoring conditions as explained in experimental setup (Table 3.5) i.e. two anchors, three anchors and five anchors. The variation of water hammer pressure for a flow velocity of 0.6 m/s with respect to time was plotted at the outlet and is given in Fig. 4.23. The figure indicates that the water hammer pressure is independent of the number of anchors attached to the system also in the case of HDPE pipe.

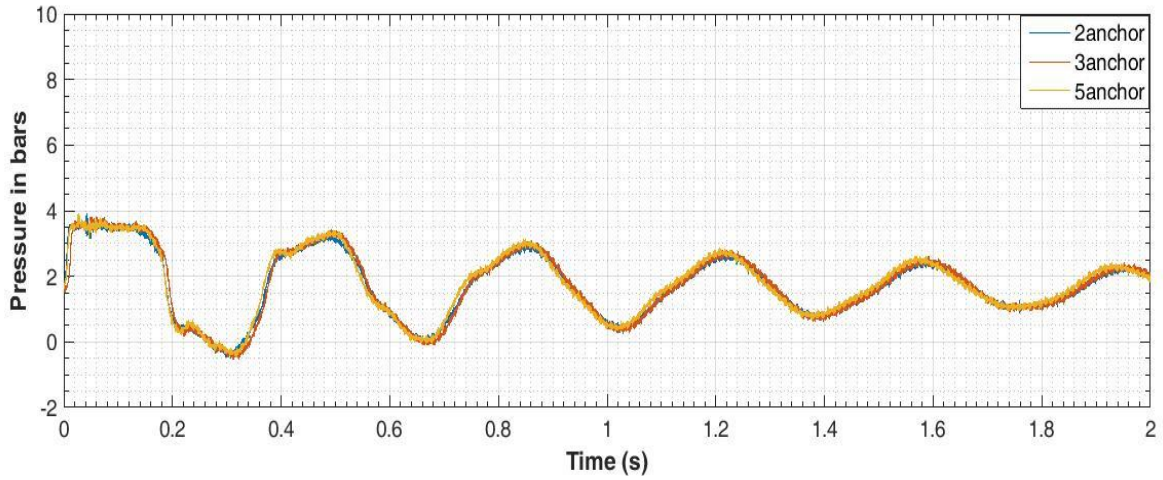

Fig. 4.23 Effect of anchors on the pressure variation at the outlet for a velocity of 0.6 m/s (HDPE pipe)

The pressure variation at the outlet for another flow velocity of 1.2 m/s is included as Fig. 4.24. From Fig. 4.24 it can be concluded that the water hammer pressure is independent of the number of fixed anchors attached to the system, whereas the occurrence of cavitation and the pressure peaks consequent to cavitation depend on the number of fixed anchors attached to the system. The behaviour of HDPE pipe is similar as in the case of other two materials included in the experimental investigation. As these characteristics prevail for all the three types of material tested and all the trails with various velocities, it can be categorically stated that the characteristics of cavitation in a piping system is very much influenced by the rigidity of the piping system. Presence of a greater number of fixed anchors to the system results in reduction of unsupported length and the effective length of the piping system; and makes the system more rigid. This can be the reason for the increase in the cavitation pressure in the system during transient flow. Now, why does the number of anchors affect only the pressure because of cavitation, but not the pressure due to water hammer? The answer to the

question lies with the different nature of the water hammer pressure and the pressure due to cavitation. Water hammer pressure has fixed frequency depending on the length and the velocity of sound in water whereas the cavitation pressure has variable high frequency, resulting from the local nature of reflection as explained in earlier section (section 4.2). The cavitation pressure wave is of local nature, and it oscillates within small stretches. Very high frequency of pressure wave is observed in the case of cavitation compared to that of water hammer pressure wave. The water boundary/pipe boundary near bubble collapse area might be acting as reflection points and hence, the pressure waves oscillate with high frequency. When the rigidity of the pipe wall increases (by providing greater number of fixed anchors), the boundary on which the pressure wave reflects becomes more rigid and absorbs only less energy or undergoes less deformation during the impact of pressure wave. This nature leads to increase in the cavitation frequency and the cavitation pressure with the increase in the number of fixed anchors attached to the system.

Table 4.8 tabulates all the water hammer and the cavitation pressure values of HDPE pipes with the three different anchoring conditions. It can be noted from the table that as the rigidity of the piping system increases (by increasing the number of fixed anchors attached to the system), the water hammer pressure remains unaltered while the cavitation pressure goes on increasing with the number of fixed anchors.

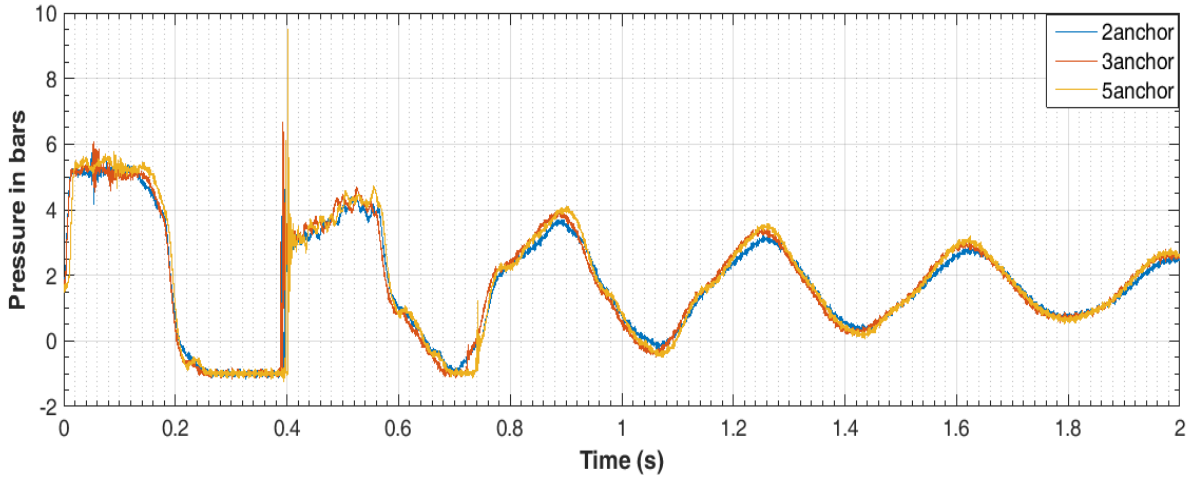

Fig. 4.24 Effect of anchors on the pressure variation at the outlet for a velocity of 1.2 m/s (HDPE pipe)

Table 4.8 Pressure at outlet for HDPE pipe

Velocity (m/s)	Anchoring condition	Water Hammer Pressure (Bars)	Cavitation/ second Pressure peak (Bars)
0.6	Two anchor	3.9	3.3
	Three anchor	3.9	3.3
	Five anchor	3.9	3.3
0.8	Two anchor	4.5	4.0
	Three anchor	4.5	4.0
	Five anchor	4.5	4.0
1.0	Two anchor	5.2	4.0
	Three anchor	5.2	**5.8**
	Five anchor	5.2	**6.3**
1.2	Two anchor	6.0	4.5
	Three anchor	6.0	**6.7**
	Five anchor	6.0	**9.5**

Hence it can be concluded that, for all the three materials included in the present experimental study, the water hammer pressure remains unaltered by the increase in the number of fixed anchors attached to the piping system. But the cavitation pressure increases with the increase in the number of fixed anchors attached to the piping system.

4.6. Pipe Acceleration

Along with the measurement of fluid pressure, the accelerations in y and z directions of the MS pipe were also measured during the experimental study. The variation of acceleration with time was recorded at the centre of span in two-anchor condition and at the quarter span in three-anchor condition. The variation of acceleration with time is plotted for two-anchor and three-anchor conditions.

4.6.1. Two-anchor condition

During the experiment, acceleration was measured at the centre of the pipe for two anchor condition and for all the flow velocities. Fig. 4.25 shows the acceleration in y direction for the flow velocity of 0.181 m/s.

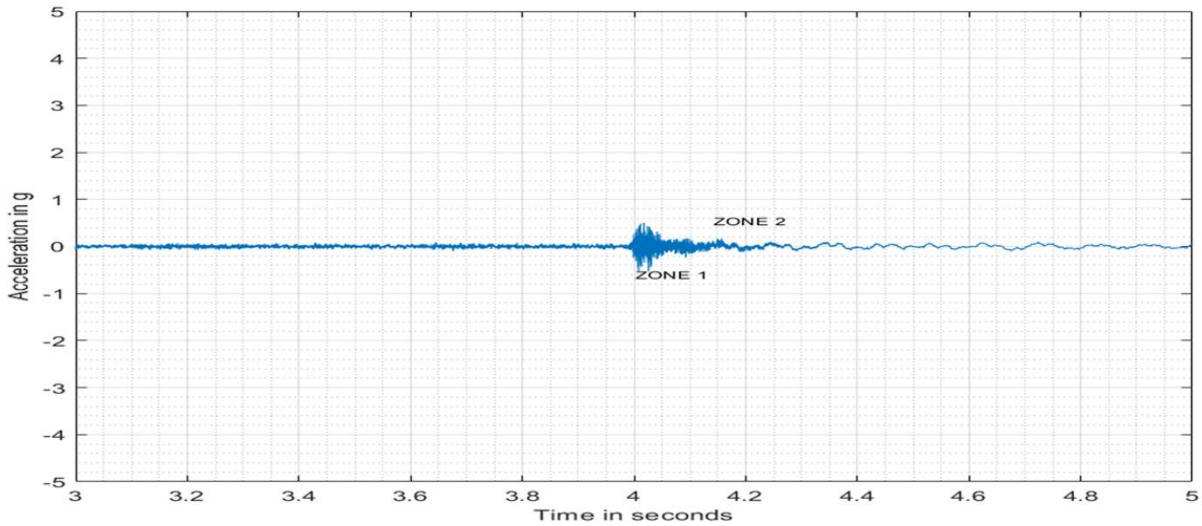

Fig. 4.25 Acceleration in y direction at the centre of pipe – velocity 0.181m/s

The x axis represents time in seconds; and y axis represents acceleration in terms of acceleration due to gravity 'g'. For 0.181 m/s velocity, the maximum acceleration in y direction at the centre of the pipe was only 0.46g, which is 4.5 m/s^2. The acceleration time curve corresponding to the initial velocity 0.181 m/s has two main zones. The first zone was developed during the sudden closure of the QAV and was critical. The acceleration in this zone corresponds to the water hammer pressure and it exists only for a small duration. The zone 2 of acceleration corresponds to the damping zone, and finally, the acceleration approaches zero.

When the velocity was increased to 0.273 m/s, the pattern of acceleration also changed as a result of the occurrence of cavitation, as given in Fig. 4.26. The acceleration-time curve corresponding to 0.273 m/s has three zones. The first zone is similar to that of 0.181 m/s velocity. But, the magnitude of acceleration is 6.5g which is much higher than the acceleration corresponding to the velocity 0.181 m/s. The increase in velocity is only 50 %, but the equivalent increase in acceleration is about 13 times (1300%) the previous acceleration due to water hammer for the velocity of 0.181 m/s. Fig. 4.26 indicates an additional zone, which is related to the pressure rise due to cavitation. The magnitude of that acceleration corresponding to cavitation pressure is 19g, which is 192 % more than the acceleration due to the water

hammer. The increase in pressure because of cavitation is only 55% more than the water hammer pressure for the same velocity 0.273 m/s (Table 4.9).

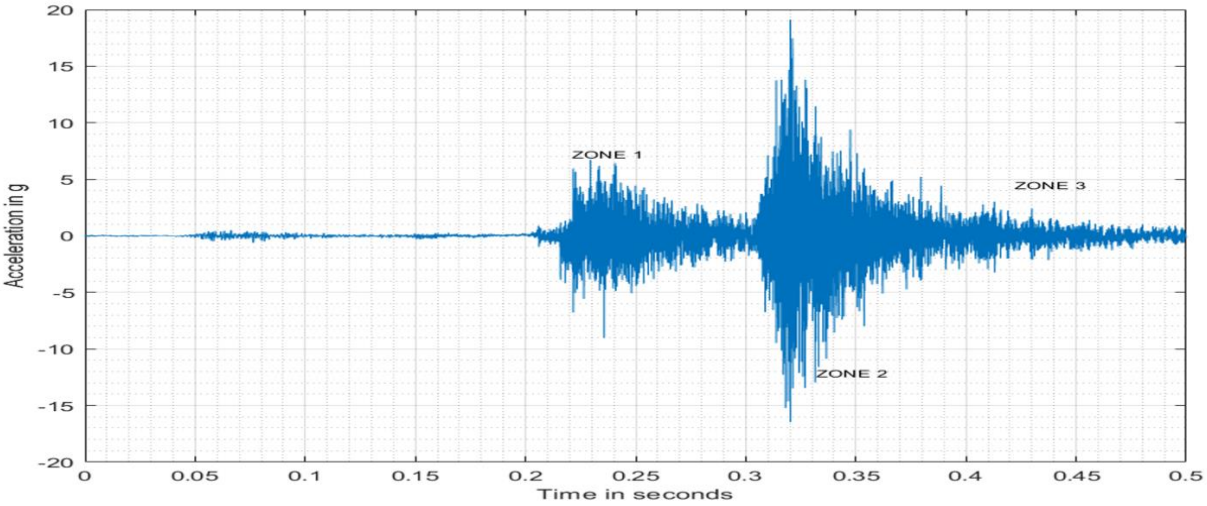

Fig. 4.26 Acceleration in y direction at the centre of pipe – velocity 0.273m/s

In brief, for the flow velocity of 0.273 m/s, the maximum acceleration due to water hammer is around 6.5g which significantly increases to 19g when vapour bubble collapse (cavitation). After that, the acceleration gradually reduces and approaches zero in zone 3 (Fig.4.26).

The acceleration in z direction also shows the same pattern with three zones (Fig. 4.27). For the first zone, the magnitude of acceleration is only 2 g (for velocity 0.273 m/s) which is less than the acceleration in y direction (6.5 g). For the second zone, the acceleration is 8 g which is also less than the respective acceleration in the y direction (19 g). Similar pattern is observed for the other flow velocities (Table 4.9).

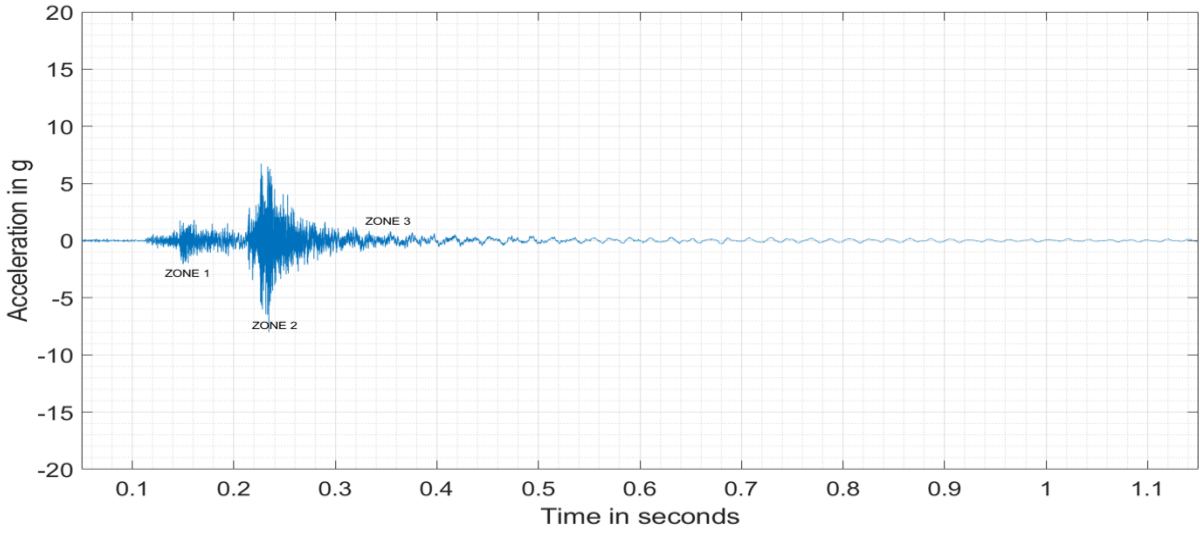

Fig. 4.27 Acceleration time graph in z direction, flow velocity 0.273 m/s

Table 4.9 Pressure and Acceleration at the centre of pipe with 2 anchors

Velocity m/s	WH pressure (Bars)	Cavitation pressure (Bars)	% Increase in pressure due to cavitation	Acceleration Zone 1 (g)	Acceleration Zone 2 (g)	% Increase in acceleration due to cavitation
0.181	4.1	-	-	0.5	-	-
0.273	5.5	8.5	54.55	6.5	19	192.3
0.362	6.5	12	84.62	20	45	125.0

From Table 4.9 it is observed that drastic increase in acceleration and vibration is observed at the centre of pipe with increase in flow velocity when the number of anchors is limited to two.

4.6.2. Three anchor condition

In two anchor condition, the acceleration was maximum at centre. But for three anchor and five anchor conditions, a fixed anchort is introduced at this position of maximum acceleration. As a result, the acceleration is reduced to zero at that position. Hence, the acceleration was measured in the pipe with three anchors at 7.5 m from both upstream and downstream ends. The acceleration at 7.5 m from the outlet for the flow velocity 0.273 m/s is given in Fig. 4.28.

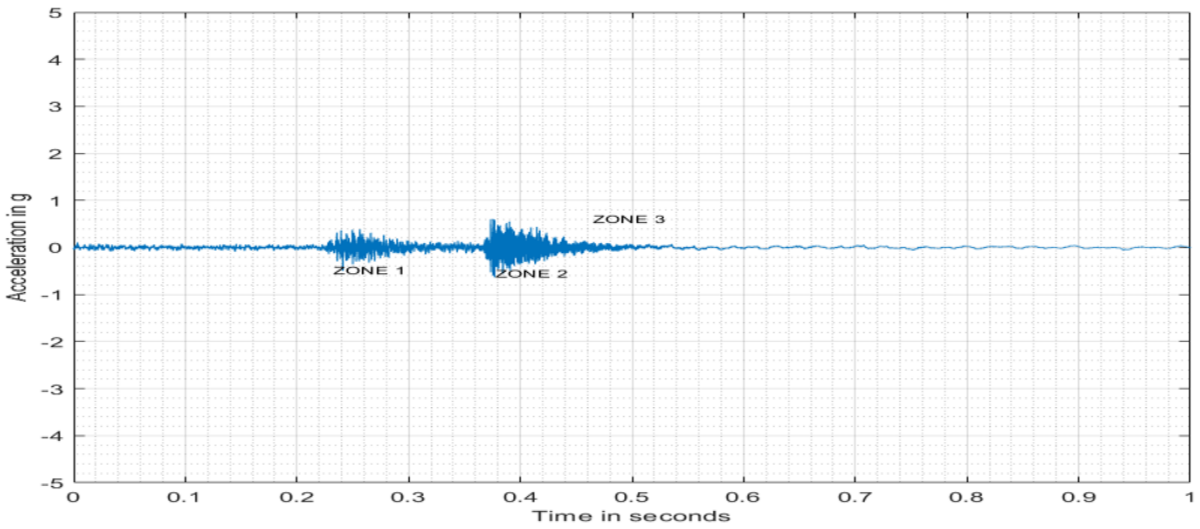

Fig. 4.28 Acceleration in y direction at 7.5 m from outlet – velocity 0.273 m/s

In Fig. 4.28 also, three zones corresponding to the water hammer, the cavitation and the damping states are visible, but the magnitude reduced to a great extent. Acceleration corresponding to the water hammer is 0.5 g and that corresponding to the cavitation is 0.7 g. Thus, it can be concluded that the introduction of more anchors reduces the lateral accelerations and consequent vibration considerably in any piping system.

Vibration of a piping system during a transient flow is a dangerous condition in most of the circumstances, especially in chemical industries, hydro power plants, and nuclear power plants. Vibration sometimes damages the equipment attached to the piping system, particularly measuring equipment. Vibration is also disastrous to the bends and joints in any piping system. This vibration can be controlled to a certain extent by providing a greater number of anchors to make the system rigid. But, the experiments conducted by increasing the number of fixed anchors reveal that it has adverse effect on the flow characteristics, viz., the chance of occurrence of cavitation and the consequent increase in the pressure. For industries where vibration has to be limited, anchors can be provided closely, by taking precautionary measures to avoid the failure as a result of excess pressure due to cavitation. Hence, the spacing of anchors in a piping system should be decided by balancing the vibration of piping system and the pressure as a result of cavitation, according to the type and requirement of the piping system.

4.7 Summary

The influence of various parameters on the characteristics of transient cavitating flow was studied by using experimental observations. From the study, it has been found that all the four parameters considered in the study viz., valve-closure time, initial flow velocity, material property and number of fixed anchors, significantly affect the transient flow characteristics. It is also found that the water hammer pressure is less affected by the change in the above parameters, but the occurrence of cavitation and the cavitation pressure are greatly influenced by these parameters.

CHAPTER 5
RESULTS AND DISCUSSIONS
NUMERICAL INVESTIGATION

5.1. General

Previous studies on transient flow reveal the fact that one-dimensional classical water hammer equations predict the first pressure rise accurately, but fail to model the damping effect of pressure waves. The interaction between pipe material and fluid is a physical phenomenon which does not have full representation in the classical water hammer theory. This lack of representation of fluid-structure interaction in the classical water hammer theory could be one of the possible reasons for having the deviation in the damping of pressure wave. In FSI, there is an interface which is common for both fluid and solid domain. Fluid governing equations and solid governing equations must be satisfied at this interface. Similarly, the fluid and the solid boundary conditions must also be satisfied at this interface. A set of coupling conditions, which initiates the transfer of data between the fluid and solid domains, accomplishes this compatibility. The present study aims to estimate the effect of FSI on the damping of pressure wave during a transient event, by considering three-dimensional governing equations for both the fluid and the solid. The study aims to customise a 3-D model considering the effect of the axial, flexural, rotational, radial and torsion actions in the model, with proper interaction between the equations, at all nodes, at every time step. As explained in sections 3.3 and 3.4 the CFD software, the ANSYS Fluent was used for the fluid equations, the ANSYS Structural for the structural equations, and the system coupling by the ALE method, for the interaction between fluid and structural modules. In addition, it is proposed to assess the effect of fixed supports on the transient flow characteristics. The structural response and the dynamic behaviour of the piping system were also monitored as the part of this study. The study also addresses the numerical modelling of two-dimensional transient cavitation flow by using the ANSYS Fluent.

5.2. Investigation on Water Hammer with FSI - Case1

The experimental results from Mitosek and Szymkiewicz (2012) were initially used for the numerical simulation. For steady flow condition, the water was considered as

incompressible with a density of 998.2 kg/m^3, a viscosity of 0.001003 kg/msand a reference temperature of 298 K. For the simulation of transient flow, the fluid (water) was considered as compressible in the modelling of transient flow.

A pressure wave velocity of 1245 m/s was used as in the reference (Mitosek and Szymkiewicz, 2012). The pipe material was mild steel and was with a density of 7850 kg/m^3, a modulus of elasticity of 200 GPa, a Poisson's ratio of 0.3 and a roughness height of 0.0008. The Inlet and outlet boundaries were given as pressure inlet and mass flow outlet respectively (Fig.5.1). A constant pressure of 51 m was applied at the inlet boundary. The closure time of the valve was 0.021 s (Mitosek and Szymkiewicz, 2012). The piping system was anchored at every 2 m and hence, the external boundary conditions of the piping system were assigned as the fixed supports at 2 m interval as indicated in Fig.5.1 (Mitosek and Szymkiewicz, 2012). The Fig.5.1 also shows the upstream and downstream boundary conditions for the fluid flow.

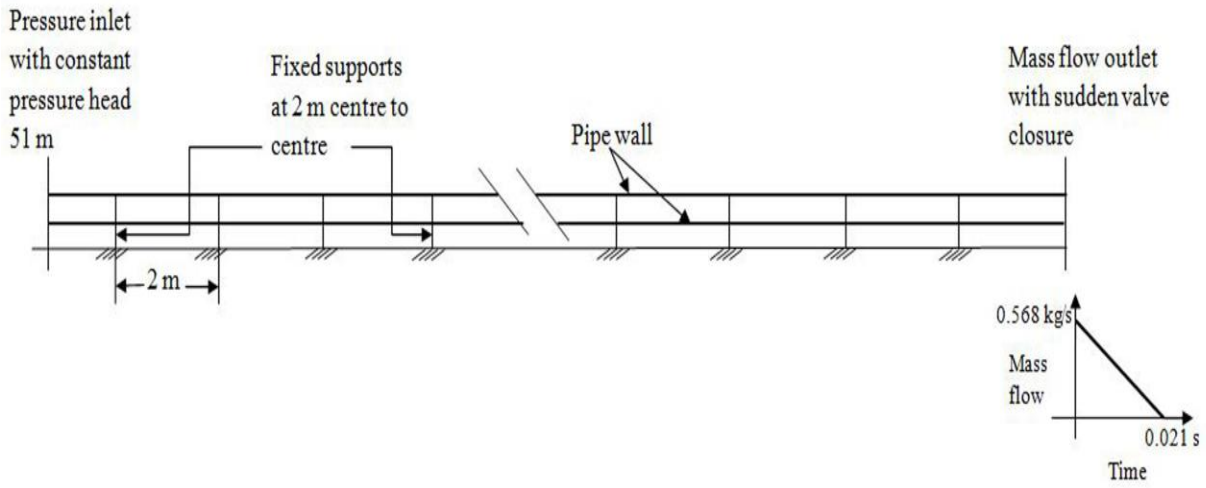

Fig.5.1 Boundary conditions of the experimental set up A (case (1))

In a numerical modelling, the discretisation of the flow domain plays a major role, especially in the modelling of FSI where meshing of the interface is critical. In order to ensure the quality of results, a grid independence study of the model was carried out by considering four different element sizes. Hexahedron elements were used for meshing the fluid. Table 5.1 gives the details of the four different meshes with the maximum element size in the longitudinal direction viz., 5 mm, 10 mm, 22.5 mm and 50 mm. As the element size increases, orthogonal quality and skewness do not change within the element sizes under consideration.

However, the aspect ratio increases and exceeds the maximum value of 10 in case of 50 mm element size. The computed pressure at the outlet for all the four cases are given in Fig. 5.2.

Table 5.1 Details of grid independence study conducted for Case 1

Maximum element size in longitudinal direction	5 mm	10 mm	**22.5 mm**	50 mm
Number of Nodes	17,85,724	8,92,924	**3,96,924**	1,78,684
Number of Elements	16,27,200	8,13,600	**3,61,600**	1,62,720
Aspect Ratio	2.68	6.49	**9.98**	23.43
Orthogonal Quality	0.991	0.991	**0.991**	0.991
Skewness	0.1459	0.1459	**0.1459**	0.1459

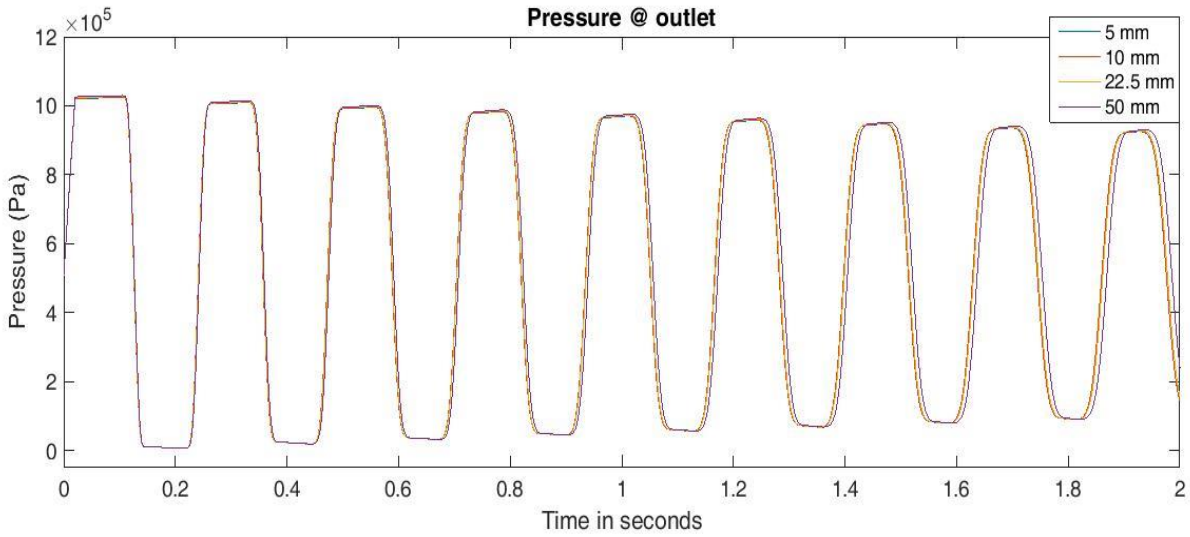

Fig.5.2 Pressure at the outlet - Grid independence study

It shows that there is absolutely no difference in all the results, except a slight variation in the case of element size 50 mm as a result of the aspect ratio deviation from the desired value. Hence, for all the subsequent trials, an element size of 22.5 mm is used (Fig. 5.3) in the longitudinal direction.

The laminar sublayer thickness for this case was worked out to be 0.5 mm. Hence, an element size of 0.5 mm was initially used near the boundary and larger size for the remaining portion, such that the boundary layer thickness is almost equal to the element size used. However, this created exorbitantly large number of elements and an exponential increase in

the computation time. Hence, double the size (1 mm) is used near the surface such that the centre of the control volume of the element is near the thickness of laminar layer. Both the trials (element size 0.5 mm and 1 mm) gave the same results with reference to the first pressure cycle of the pressure wave indicating that the increase in the element size from 0.5 mm to 1 mm near the boundary did not compromise the accuracy of computation, but complement reduction in computation time. Moreover, no separation is expected near the boundary. Hence in all subsequent trials, element size of 1 mm was used near the boundary and was increased gradually in the rest of the fluid domain. The mesh refinement in accordance with the ratios specified by Martins et al. (2014, 2016) were almost impossible as result of the huge computational time required for running the 3-D-CFD-FSI model. Moreover, as indicated earlier, those ratios have limited application in this case. Nonetheless, the present study explores the capability of 3-D-CFD-FSI model by using practically possible mesh sizes. It may be noted that the computed pressure curves exactly follow the measured one through the first cycle of pressure wave (as subsequently shown), which indicate that the flow characteristics were reasonably captured by the current mesh sizes.

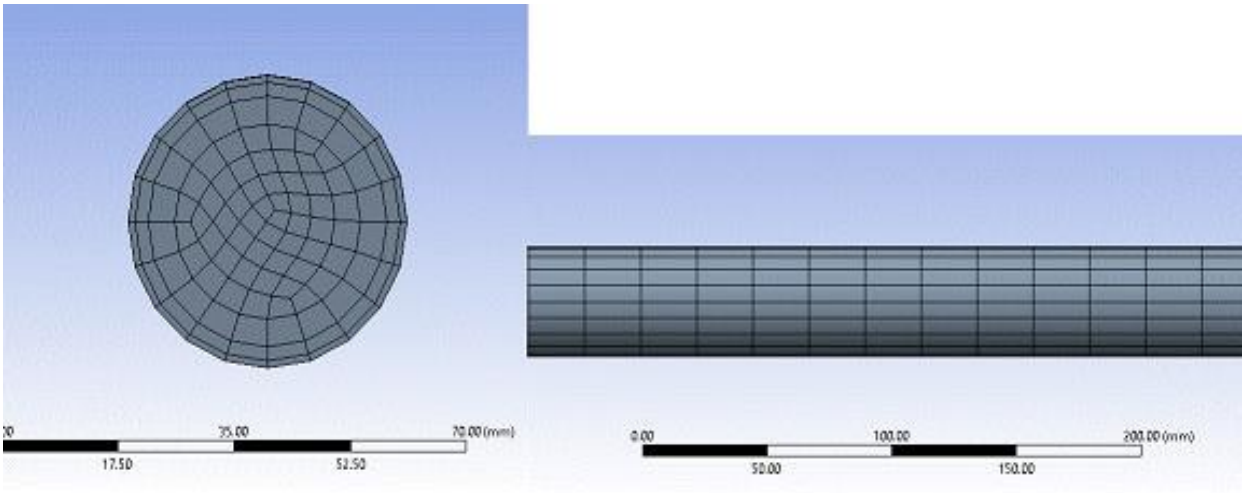

Fig.5.3 Mesh of fluid model (Case 1)

Further, to verify the other characteristics of the flow, the pressure variation and the velocity profiles at the mid-section and at salient instances were plotted as in Fig.5.4 and 5.5. It can be seen that the profile at 0.0273 s (0.118T) (Fig.5.5(a)) has a fully developed steady state velocity profile and it corresponds to an instant just before the pressure wave reaches the mid-section. Fig.5.5(b) and (c) indicate the velocity profiles with a small positive average velocity (0.06 m/s) and a small negative average velocity (0.02 m/s) respectively. The

profiles indicate a steep gradient of negative velocity close to the wall, confirming the presence of an inverse flux. Although the average flow velocities of these profiles are close to zero, there exist flows in both directions, bringing the average velocity near zero. It is also verified that the core of the velocity profile maintains the same shape as that of the steady state velocity profile. Then, the velocity enters a complete negative stage, still keeping the original shape of the profile (Fig.5.5(d) and (e)). The velocity profile 5.5(g) is different from the profile 5.5(a), despite representing almost similar points in the consecutive cycles of the wave. It is in line with the observation made by Martins et al. (2016). Hence, the current level of discretisation was adequate to represent the flow characteristics reasonably, considering the exponential growth of computation time with decrease in the size of element. Hence, the reliability of the model is established.

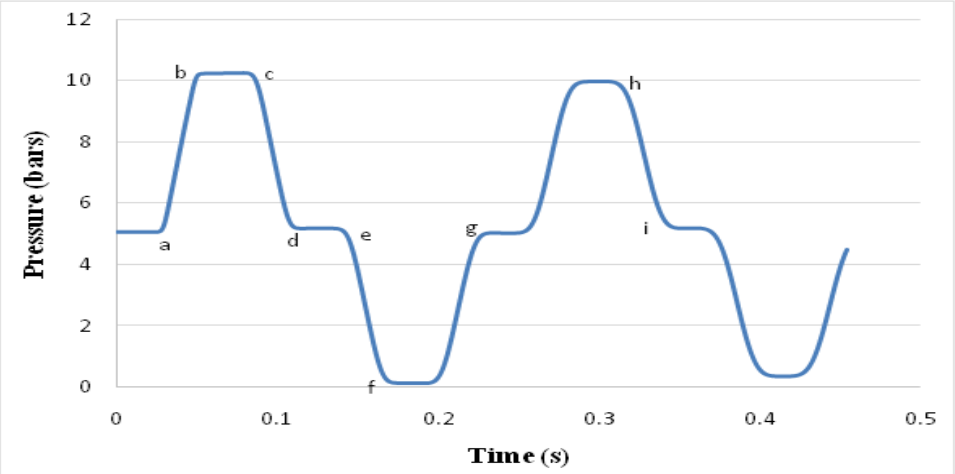

Fig. 5.4 Pressure variation at mid-section (case 1)

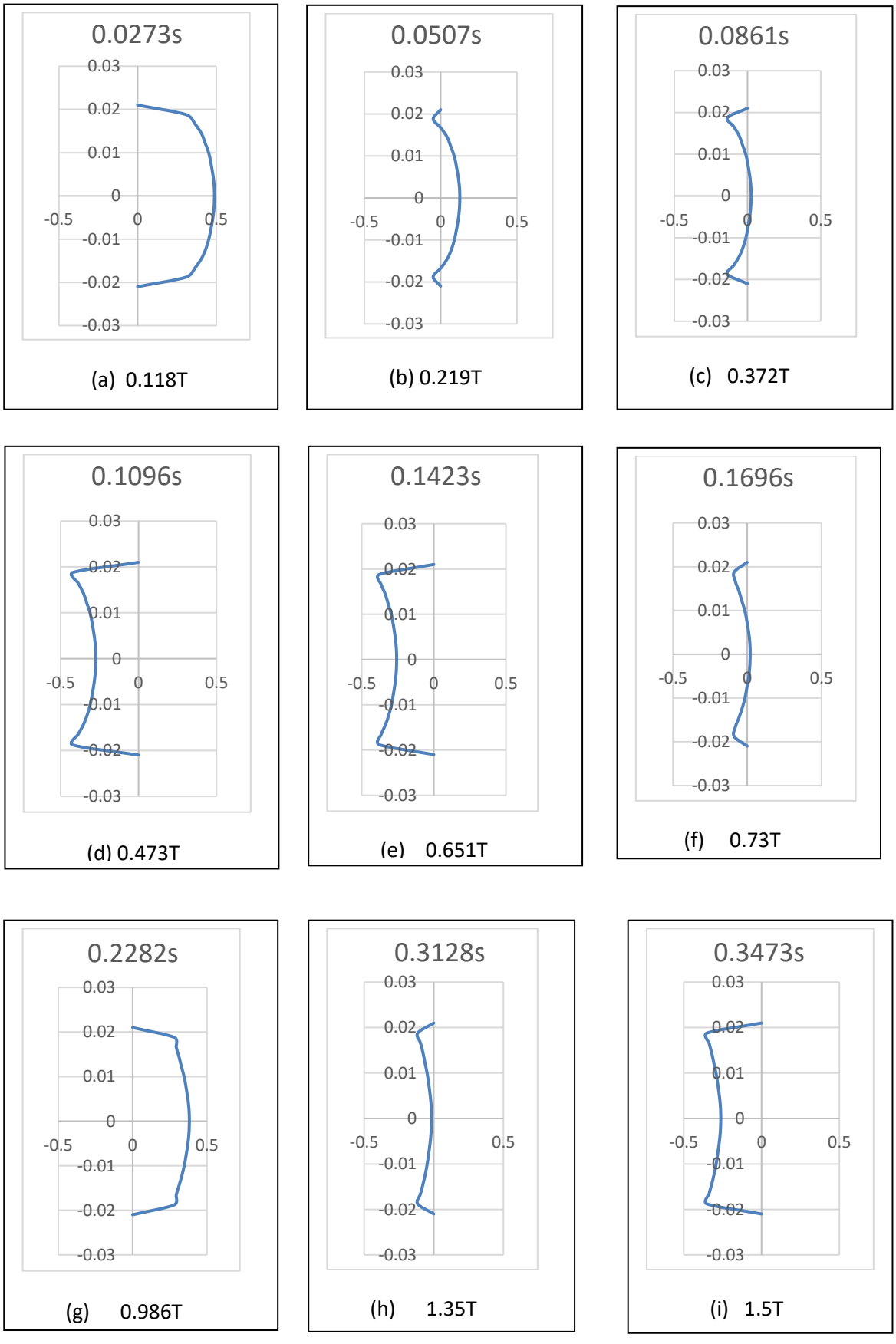

Fig.5 .5 Velocity profiles at midsection (Case 1)

Monajitha et al. (2014) conducted a transient flow analysis for the data from the same experiment setup A by using the classical water hammer theory. The authors of that paper showed that the pressure variation results from the one-dimensional classical water hammer model, deviated from the experimental results, especially in the latter part of the pressure variation even though the model predicted the first water hammer peak correctly. Hence, the current study simulated the flow in the experimental setup A, by using a 3-D-CFD model to verify whether the deviation exists because of the approximation of 1-D model against 3-D model. The model used the same upstream and downstream boundary conditions for the fluid as given in experimental setup A and assigned the pipe as wall boundary to verify whether a 3-D-CFD model (without FSI) can predict the flow characteristics correctly. The pressure variation at the outlet was compared with the corresponding experimental results available from Mitosek and Szymkiewicz (2012) (Fig.5.6).

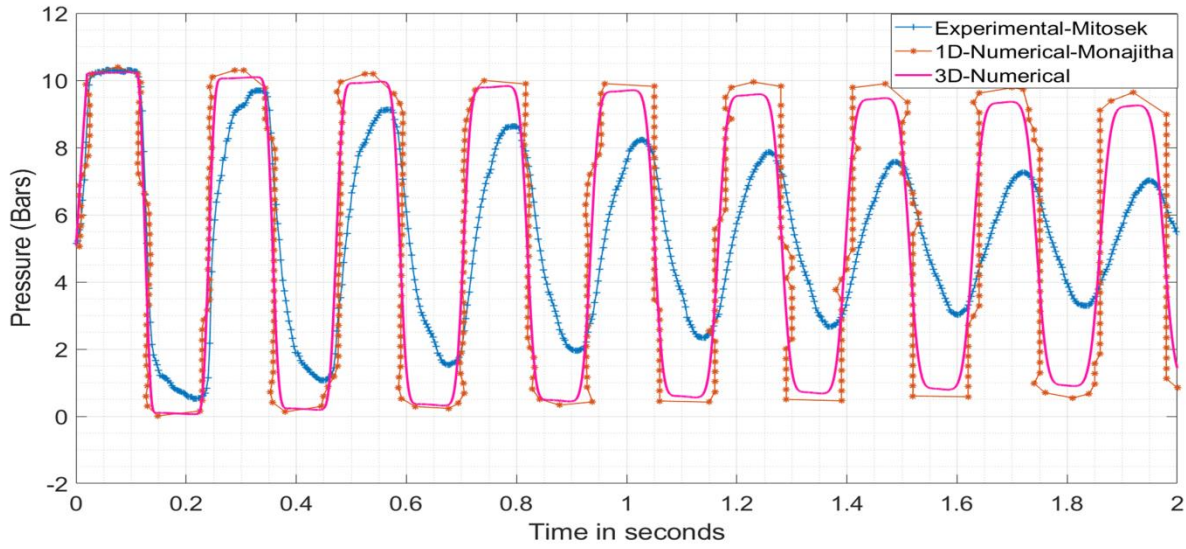

Fig.5.6 Comparison of pressure at outlet-without FSI (Case 1)

Fig 5.6 reveals that the first pressure peaks from the 1-D and 3-D simulation closely match with the experimental results. However, the computed pressure fluctuations do not damp very fast unlike that from the experiments, indicating that the damping rate of pressure wave in the experiment (actual) does not match with that from the 3-D-CFD simulation. The pressure variation of the 3-D-CFD simulation is the same as that of 1-D transient analysis, despite the increase in the complexity of the model. Hence the current study infers that the 3-D-CFD model of the flow situation, despite the increase in the complexity, cannot improve the performance appreciably.

Monajitha et al. (2014) minimised the above deviation in the pressure fluctuations for the same data set, by introducing a variable celerity to the continuity equation and a diffusive term to the momentum equation. The authors of that article reported that the additions to the continuity and momentum equations (1-D) could model the damping of pressure waves to some reasonable level of accuracy. But, the 3-D-CFD model could not. However, these numerical modifications are necessary, may be because of the lack of representation of the actual physical phenomena. Mohan (2016) attempted to model the transient flow incorporating FSI. Normally, a 1-D model is sufficient to predict the first pressure peak accurately (Chaudhry, 1979; Chaudhry and Hussaini, 1985; Hadj and Lili, 2000; Greyvenstein, 2002; Mitosek and Szymkiewicz, 2012; Amara et al., 2013; Shimada and Vardy, 2013; Seck et al., 2017; Martins et al., 2017)). But, the results of Mohan (2016) indicated that the first pressure peak did not match correctly, rather the first pressure peak was overestimated and shape of the first pressure peak distorted. Hence, the model by Mohan (2016) could not capture the basic characteristics; viz., the first peak in water hammer and its shape, and structural responses like support reaction and deformations, the reliability of the model was at stake. However, the model indicated a direction towards the damping of pressure wave. Hence, it is appropriate to study the effect of FSI on the damping of pressure wave along with its ability to predict the characteristics of the flow and structure, viz., the first peak of water hammer pressure, the shape of water hammer pressure, the velocity profiles, support reactions and deformation of the structure such that reliability of model is well established. Hence, the present model accounts for the proper interaction between the fluid and the structure.

The same flow problem was simulated by considering the FSI with the help of the ANSYS Fluent, the Transient structural, and the system coupling with the same initial condition, boundary conditions and support conditions, except for the wall boundary condition. The wall boundary condition became an internal boundary condition which was dynamic, in the sense that the external boundary of the fluid domain moved with the deformed internal boundary of the pipe. The mesh was generated just like the one for modelling the transient flow without FSI, i.e., two layers, one with the fine mesh near the boundary and the coarser mesh for the internal fluid domain. As indicated earlier, the study used a 3-D twenty node hexahedron element for modelling the pipe element and hexahedron element for modelling the fluid. The pipe structure was divided into 76,800 elements with a maximum element size of 22.5 mm in the longitudinal direction (Fig. 5.7).

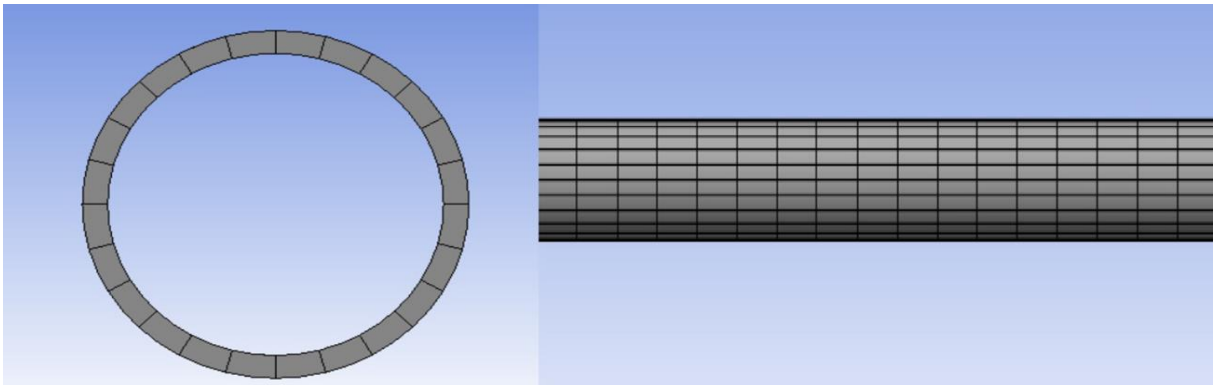

Fig. 5.7 Mesh of pipe model (case 1)

The model set the support conditions of the pipe according to the anchoring conditions (fixed support at every 2 m) in the experimental setup A (Fig.5.1). There are many mechanisms which can be used for providing supports. Feeny et al. (1998) carried out a detailed historical overview of structural and mechanical systems. Ferras et al. (2017) used the Coulomb's dry friction theory for modelling the friction between anchor block and its base. However, the supports that were used by Mitosek and Szymkiewicz, (2012) were fixed supports at every 2 m and hence, the dry friction has limited role to play. Therefore, the fixed supports were created by arresting all the deformations of all the nodes along the circumference of pipe at the support.

The change in the boundary condition owing to FSI was incorporated, by a dynamic mesh option available in Fluent. The model used the dynamic mesh zones as stationary for the inlet and the outlet; deformable for the fluid and system coupling for the solid-fluid interface. The model coupled the Fluid Flow (Fluent) and the Transient Structural by using System Coupling in ANSYS Workbench, to incorporate FSI in the analysis. The standard wall shear function is used in the model. The coupling has been carried out by synchronising each node at the inner surface of the pipe with the respective node of the outer surface of the fluid. i.e., each node in the FEM mesh at the interface had respective node at the interface in FVM. The pressure and shear exerted by the fluid on the face of an element at the interface in FEM generates a deformation and the connected nodes have a nodal displacement. These nodal displacements are transferred to the nodes of the fluid. Hence, the boundary of the fluid domain changes. This is accomplished by the dynamic mesh option in the software. When such a boundary movement occurs, there will be associated forces and stresses created at the boundary. The current study tests the postulate that accounting these additional forces due to internal boundary (interface) movement, at every time step, at every boundary node at the

interface, in both the directions (from structure to fluid and back) along with the standard wall friction model can represent the actual frictional effect leading to damping of the pressure wave. The present study then compared the results obtained from the analyses with and without FSI, with the experimental results, and with the results of 1-D analysis by Monajitha et al. (2014) (Fig. 5.8).

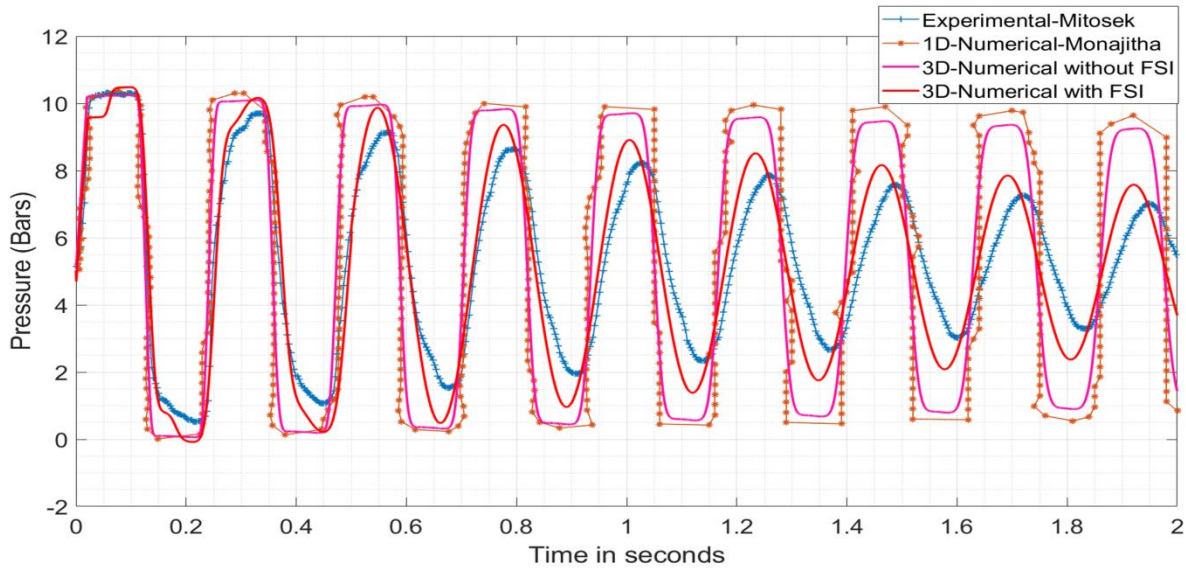

Fig.5.8 Comparison of pressure at the outlet- with FSI (Case 1)

From Fig. 5.8, it is seen that the first peaks from 3-D transient analyses with and without FSI closely match each other unlike the model by Mohan (2016). Moreover, the damping of pressure wave from the numerical simulation incorporating FSI agrees well with the experimental results. The frequency of the pressure wave from the FSI model also matches well with the experimental results. The number of cycles within two seconds in the pressure wave obtained from the 3-D-CFD model without FSI and that from the 1-D model are slightly different from the observed one, indicating that the velocity of the wave is either computed wrongly or the variation of the wave velocity, if any, is not properly represented. But, the number of cycles from the FSI analysis and that from experiments match well and hence, the variation of wave velocity or estimation of it, are represented correctly. The pressure variation curves from the CFD-FSI model and that from experiment match with reasonable level accuracy and hence, the damping in the pressure is very well represented.

5.2.1. Dynamic Response of Pipe during Transient Flow

In addition to the characteristics of pressure wave and their damping, the FSI analysis gives a lot of information about the behaviour of the structure during a transient event. The

principal stress and principal strain in the structure at any point, the absolute maximum principal stress anywhere in the structure, deformations of the structure and support reactions in the structure are available at various locations from the numerical model.

Fig.5.9 shows the variation of major principal stress in the pipe wall at the outlet (at x =72 m), at x= 71 m (1 m from outlet), near the centre (x = 35 m) and the absolute maximum principal stress occurred in the whole body, with respect to time. It indicates that the principal stress in the pipe wall exhibits the same pattern of the pressure variation. The maximum principal stress exerted in the pipe is 8.12 MPa which is much lesser than the allowable stress in steel. The direction of maximum principal stress goes on changing with respect to time. This direction of principal plane does not match with x, y and z directions. However, the hoop stress based on the maximum exerted pressure at the outlet (10.4×10^5 Pa) is 6.62 MPa, the longitudinal stress is 3.31 MPa and the wall shear stress 0.413 MPa. The principal stress computed from these three stresses is 6.67 MPa, indicating that the actual maximum stress can be higher than the computed principal stress by approximate calculation. The Tresca or Von Mises stresses (Timošenko and Goodier, 1951; Boresi et al., 1985; Ameen, 2005) were not considered, as the main purpose of this comparison is to indicate the difference in the value of principal stresses rather than indicating the failure stresses. It may be noted that the FSI analysis takes care of axial, bending and torsional actions, and hence the simple principal stress computation may not give reasonable accuracy. Therefore, the incorporation of FSI between the fluid and the structure not only models the wave damping, but also gives the principal stress which may, sometimes, be higher than the stress computed conventionally from the maximum pressure. This feature indicates the importance of FSI analysis, especially where the factor of safety in the design is small and nearer to one, and where the boundary is curved. Stress anywhere in the pipe or critical points can be obtained and checked against the maximum design capacity of the pipe.

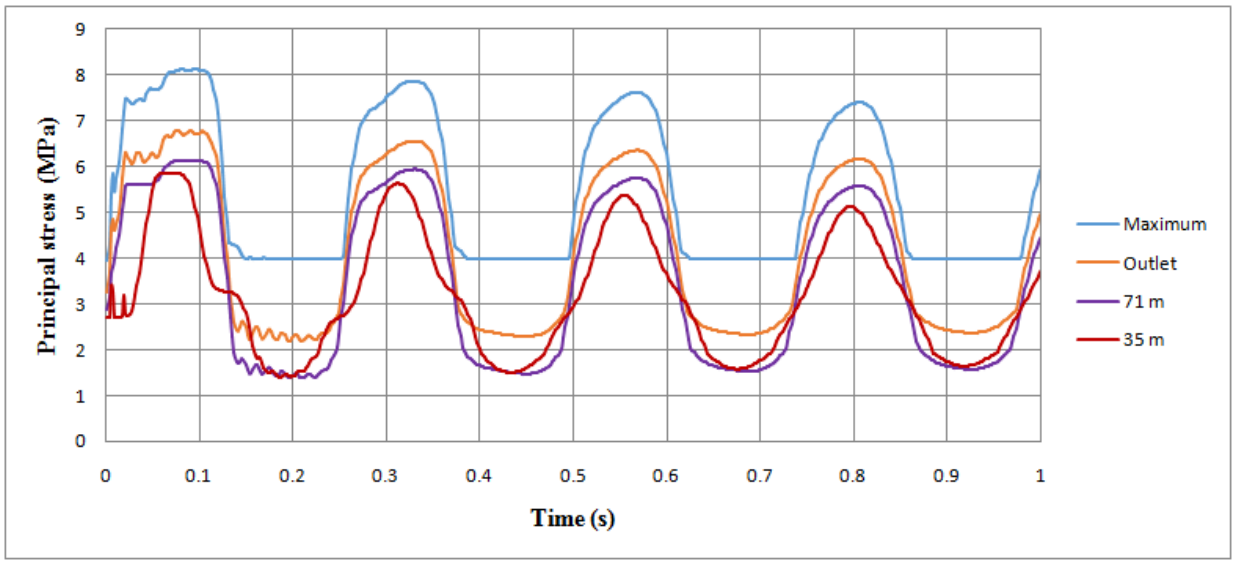

Fig.5.9 Variation of major principal stress with time (case 1)

In addition, the FSI analysis can give the variation in strain with respect to time at any point in the pipe. The Fig. 5.10 gives the variation of principal strain in the pipe wall at the outlet (at x =72 m), at x= 71 m (1 m from outlet), near the centre (x = 35 m) and the absolute maximum principal strain (whole body) with respect to time. Also, this modelling can calculate the deflection of the pipe with respect to time, and Fig.5.11(a) and (b) gives that variation of maximum deflection with respect to time, at a section near the centre (x=35) and at x=71 m. The figure shows that there is an initial fluctuation in the deflection for a short duration of 0.2 s and then the average deflection settles around a non-zero value corresponding to the static component of deflection at that point. In this test setup, the centre to centre distance between the intermediate fixed supports is only 2m, and hence, the deflection is negligibly small (maximum 0.117 mm). But, when the unsupported length increases the deflection also increases. Thus, FSI model can be used for finding out the spacing of supports so that the deflection of the pipeline is within the allowable limit. The analysis can identify the excess deflection leading to plastic state. Moreover, points, where stress concentration is expected, can be examined so that any possibility of failure can be identified. However, this 3-D-CFD-FSI model has a huge computation time which may render the application in a complex practical situation limited.

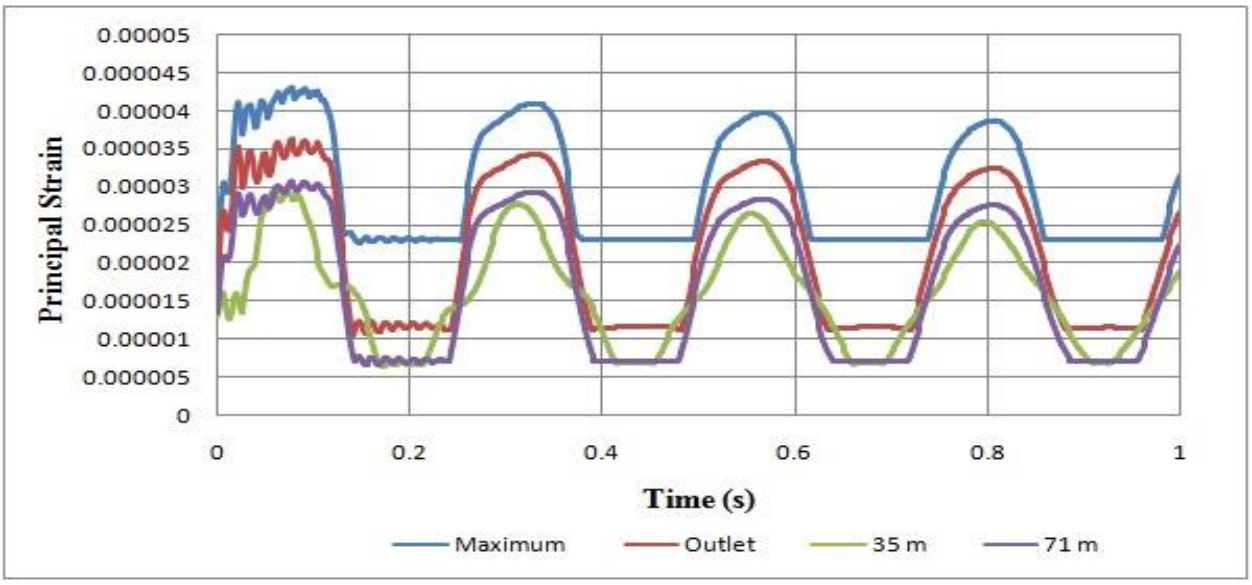

Fig.5.10 Variation of major principal strain with time (case 1)

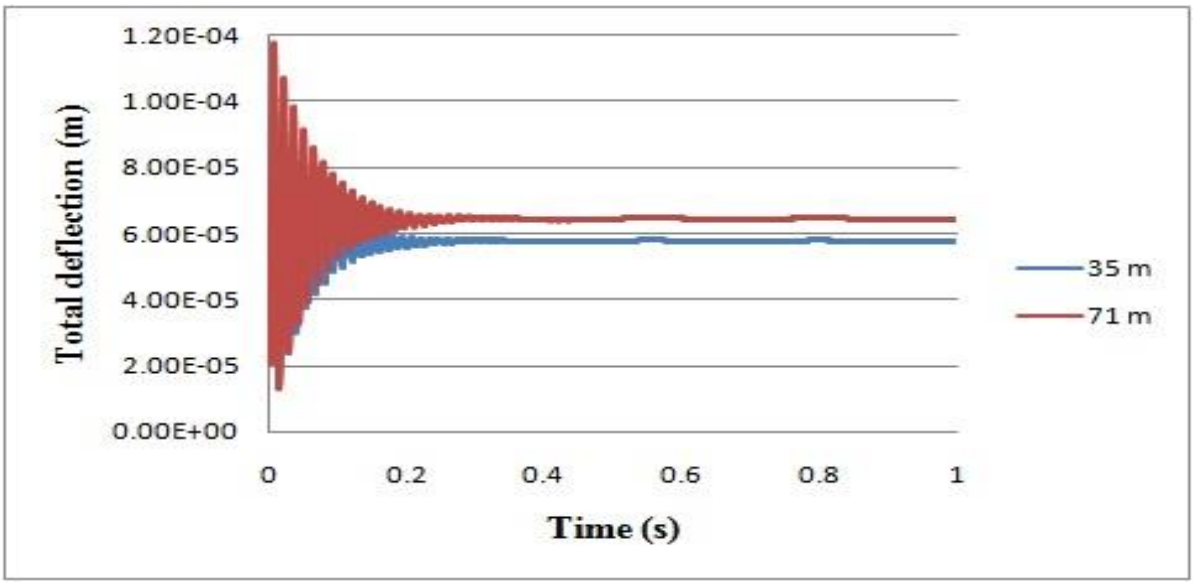

Fig.5.11(a) Variation of total pipe deflection with time

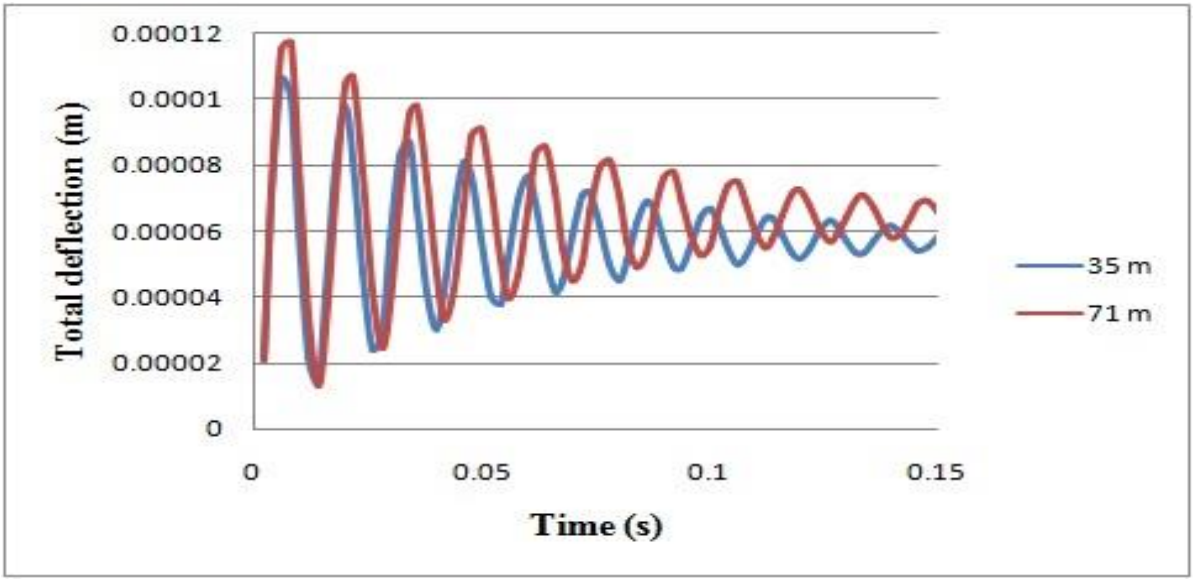

Fig.5.11(b) Initial variation of total pipe deflection with time

5.2.1.1. Support Reactions

The numerical study incorporating the FSI enables us to extract the variation of forces and moments exerted in the anchors in all the directions with respect to time. These results are very much useful for the design of the anchors and anchor bolts. The forces and moments obtained at the outlet and the inlet are given in Fig. 5.12 to 5.15.

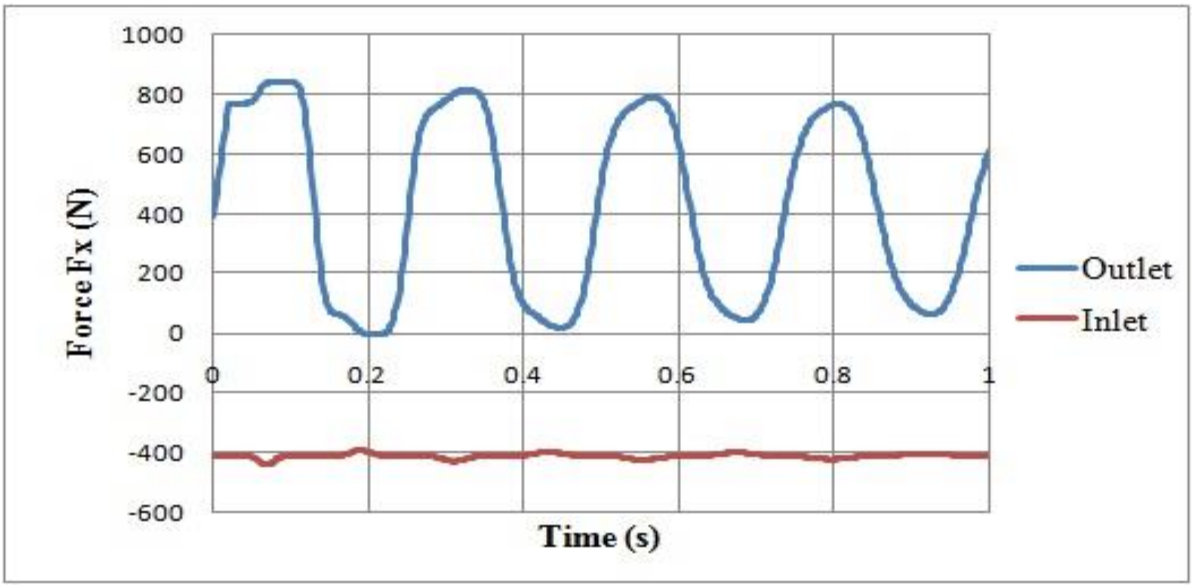

Fig. 5.12 Force in longitudinal direction (Fx) at the outlet and the inlet supports

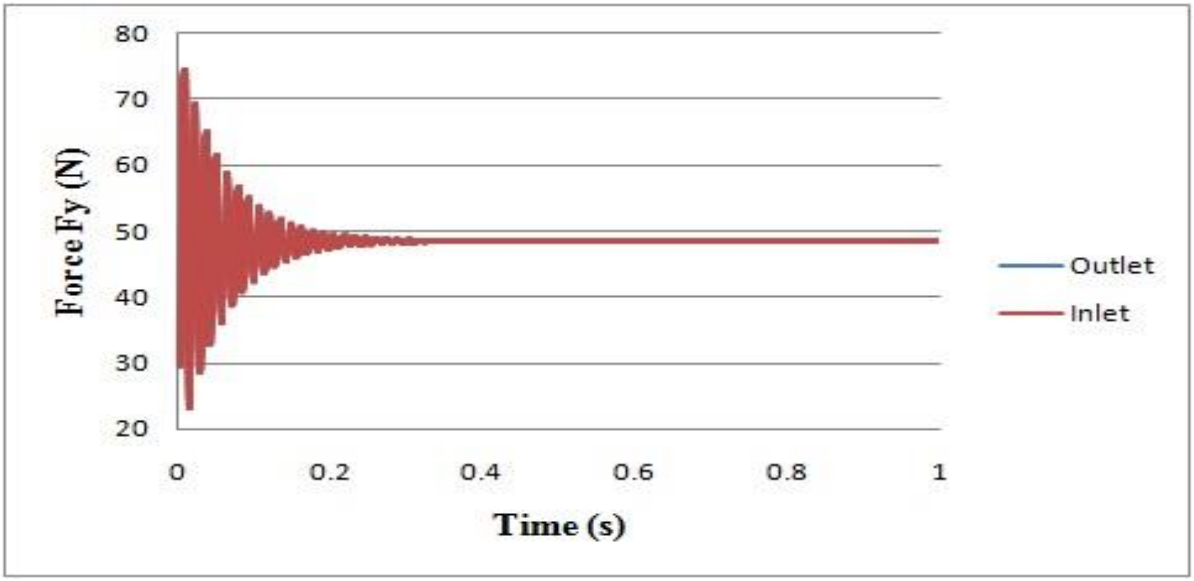

Fig. 5.13 Force in lateral direction (Fy) at the outlet and the inlet supports

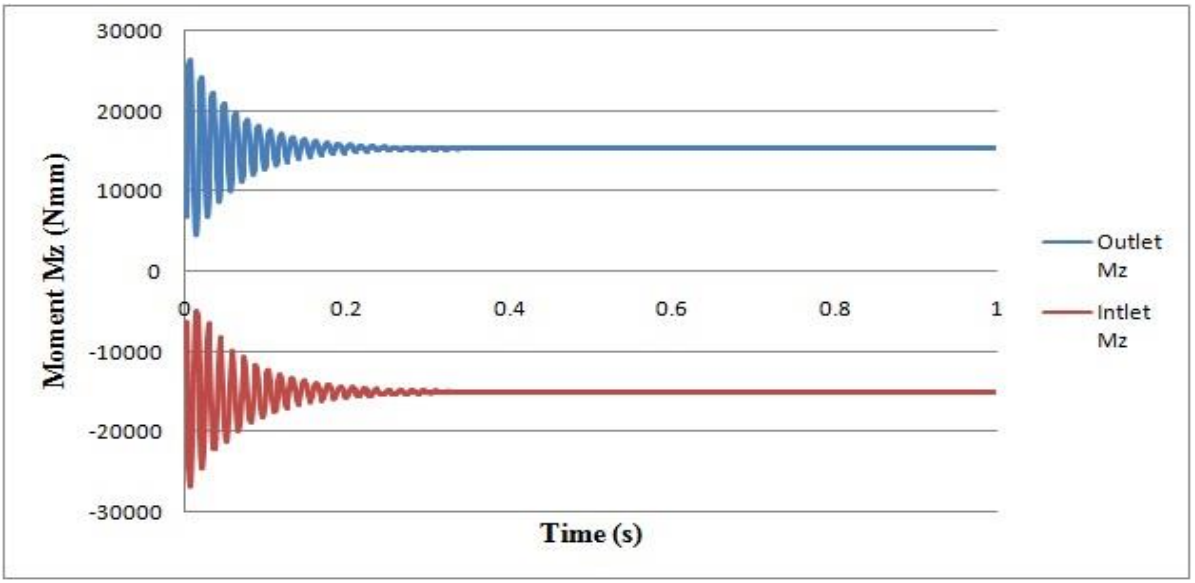

Fig. 5.14 Moment in lateral z direction (Mz) at the outlet and the inlet supports

Among all the responses, the force in longitudinal direction and moment in vertical direction are more predominant. The vertical support reaction fluctuates initially and settles down to a value 48.5 N (for both the inlet and the outlet supports), which is equivalent to the static vertical support reaction. Hence it can be inferred that the FSI modelling gives realistic results.

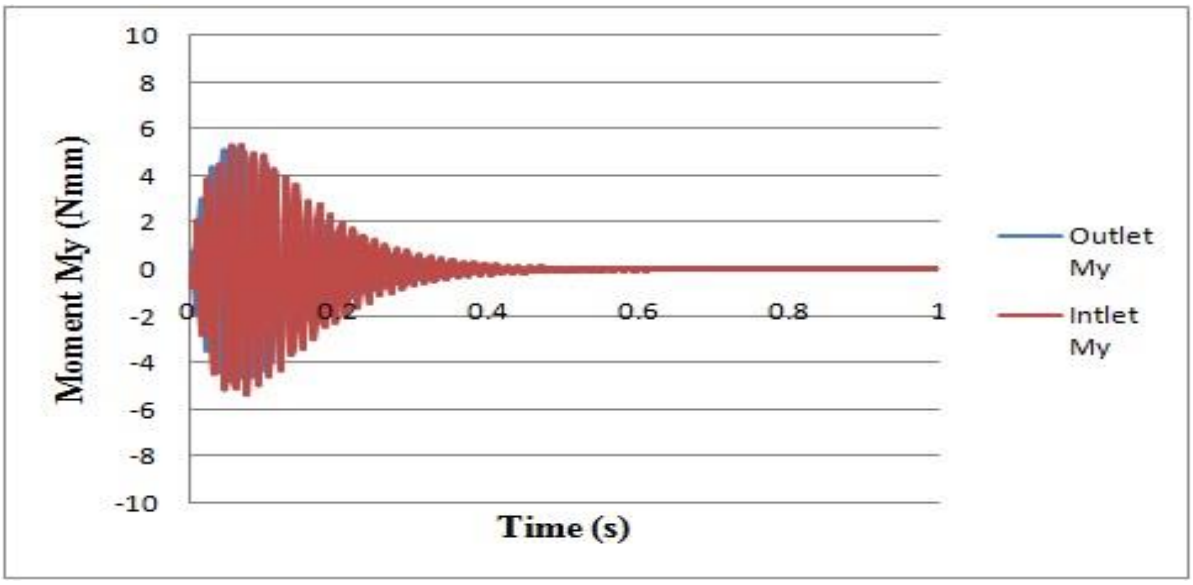

Fig. 5.15 Moment in lateral y direction (My) at the outlet and the inlet supports

From Fig. 5.12, 5.13, 5.14 and 5.15, it is clear that the forces and moments are dynamic in nature. The anchors and anchor bolts are to be designed based on the forces and moments exerted on the supports by the pipe during the transient flow. Some of the stresses consequent to the forces and moments get reversed in their nature (tensile to compressive and vise versa) and can induce fatigue to the system. Hence, this information is very critical in the design of anchors and anchor bolts and also for arriving at an optimum design.

Thus, the incorporation of FSI in the analysis simulates the damping of pressure wave accurately and hence, the model development does not require the incorporation of other factors like variable wave velocity, artificial viscosity, and diffusive terms. Therefore, the deviation in the pressure variation between, that predicted using (1-D or 3-D) fluid model without considering FSI and that measured from the experiment, is due to the lack of representation of the physical phenomena. However, a categorical conclusion requires the reinforcement of this fact with further analysis. Hence, the study used another data set for the modelling with and without FSI. That data set included two data subsets, viz., one for laminar flow and the other for turbulent flow. These data sets satisfied the condition of rigid pipe as the pipe was embedded in concrete and hence selected for the study.

5.3 Investigation on Water Hammer with FSI – Case 2(a)

The details of the experimental setup are given in section 3.5.2. There are two data sets: one for the turbulent flow range and the other for the laminar flow range. As indicated

before in section 3.5, the first one is referred to as case 2(a) and the latter as case 2(b). The geometry of the experimental setup was created in the design modeller and discretised as explained in Case 1. The model set the boundary conditions as given in earlier section. The velocity of flow in the experiment was 0.212 m/s for turbulent flow; and the corresponding mass flow was given as the input. The boundary condition for the closure of valve at the outlet was defined by using the user-defined function which related the variation of the discharge with respect to time. In the experimental setup B, the pipe was buried in the concrete to prevent movement/deformation of the pipe, during the experiment. For the analysis without FSI, the outer fluid boundary was selected as a wall, as explained in Case 1. The anchoring condition for the analysis including FSI, was incorporated in the ANSYS Transient structural, by setting the displacement throughout the boundary as zero in y and z-directions, i.e., two degrees of freedom corresponding to the deformation in the y and z – directions are only arrested.

The numerical analysis of turbulent flow (case 2(a)) was carried out using ANSYS Fluent. The study compared the pressure variation from the three-dimensional transient analysis with and without FSI, to the experimental results from Holmboe and Roleau (1967) (Fig. 5.16 and 5.17).

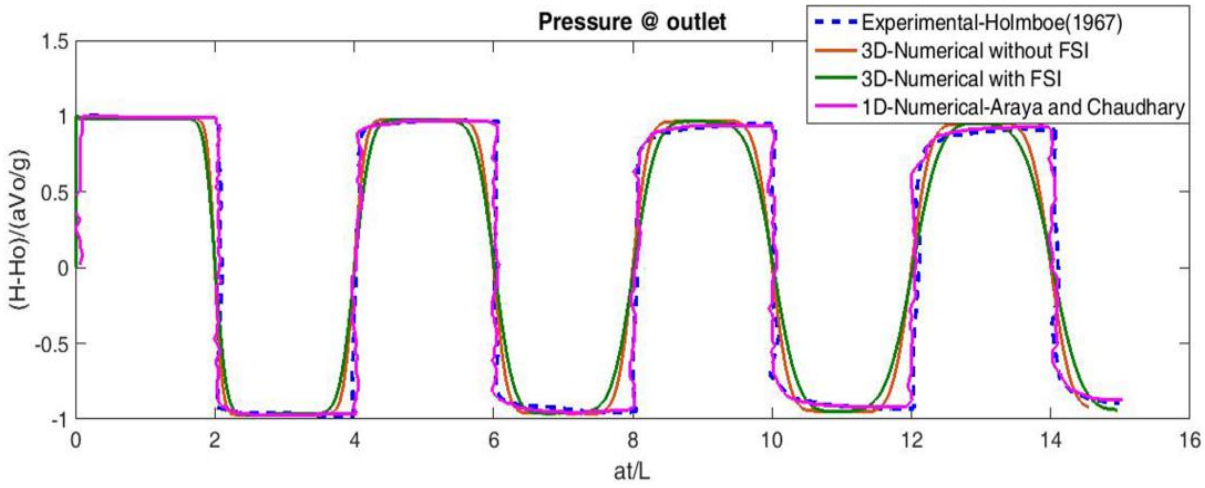

Fig.5.16 Normalised Pressure variation at the outlet-Turbulent flow

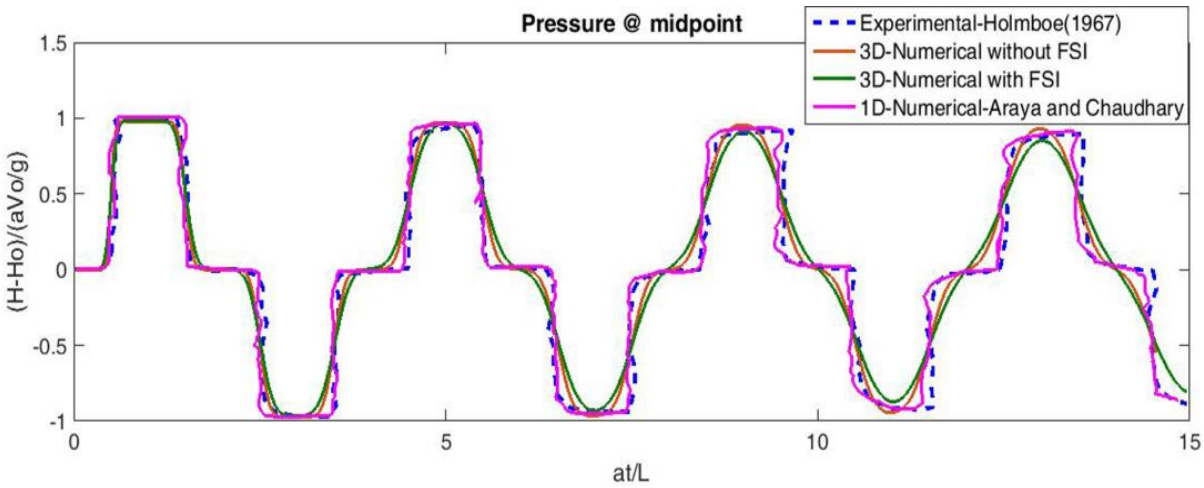

Fig.5.17 Normalised Pressure variation at the midpoint-Turbulent flow

In these figures, the horizontal axis is the time normalised by the wave travel time from the tank to the valve as presented in Holmboe and Roleau (1967) and Araya and Chaudhry (1997). Similarly, the vertical axis is the pressure head divided by Joukowsky head. All the pressure peaks and the period of the pressure wave from the numerical study, match well with the experimental results. The figure compares the obtained results, with the results of the 1-D analysis with unsteady friction conducted by Araya and Chaudhry (1997) (Fig. 5.16). The first and second pressure peaks coincided with each other in all the results.

The pressure variation at the midpoint of the piping system is compared with the available experimental results and that comparison is depicted in Fig 5.17. The pressure peaks and pressure wave at the midpoint of the pipe also exhibit the same behaviour as that at the outlet. In general, the results obtained from the flow analysis of the experimental setup B predict the actual transient flow behaviour satisfactorily. There is no deviation in the pressure variation for all the four cases (1-D analysis with unsteady friction, experimental result, 3-D analysis without FSI and 3-D analysis with FSI) when the pipe is embedded in concrete. In other words, when the assumption of rigid pipe is fully satisfied, all the three methods give the same results. Hence, it verifies the proposition that the deviation mentioned in the earlier case (case 1), among the simulated results, is due to the lack of representation of fluid-structure interaction.

5.4. Investigation on Water Hammer with FSI– Case 2(b)

In the same way, the study simulates the transient flow for the laminar flow condition case 2(b) as well. In this case also, manual closure of the valve at the outlet created the

transient event. The results obtained for the laminar flow at the valve and the midpoint of the pipe length with and without FSI are compared with the corresponding experimental results (Fig. 5.18 and 5.19). The results from the models 3-D with FSI and without FSI are matched closely except for the slight deviation which can be attributed to rounding off error in the computational procedure. The pressure variation curves match satisfactorily for all the methods, especially in case of peak values. The pressure variation at the midsection also depicts the same behaviour (Fig.5.19).

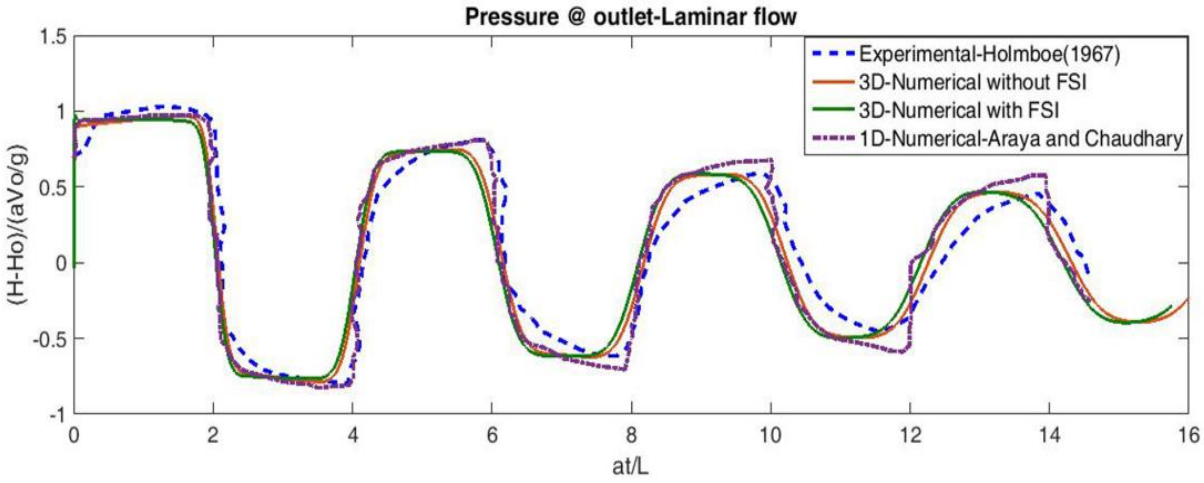

Fig.5.18 Normalised Pressure variation at the outlet-Laminar flow

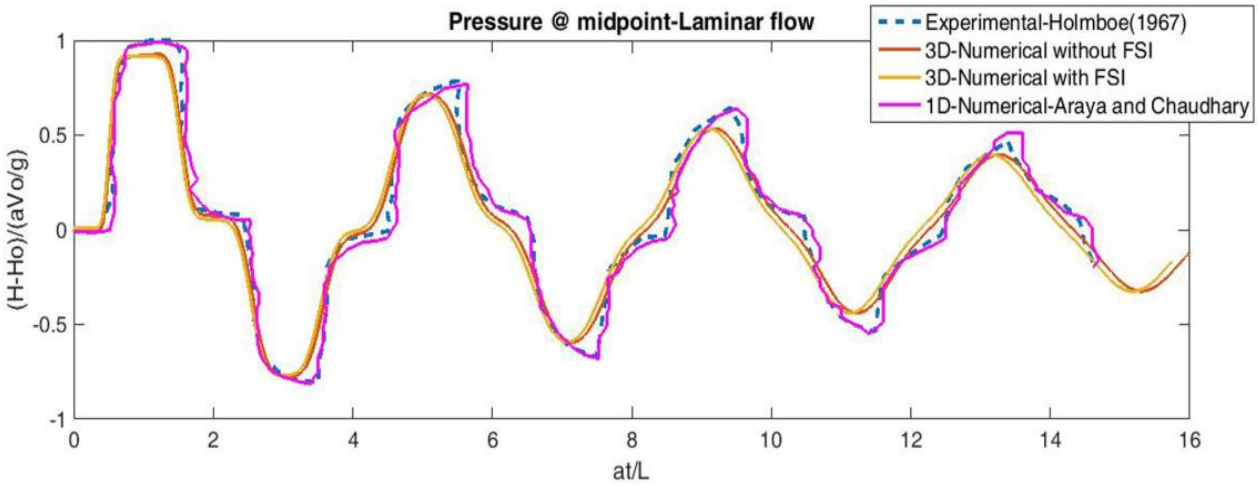

Fig.5.19 Normalised Pressure variation at the midpoint-Laminar flow

Hence, it is concluded that if the piping system is a rigid one, like the pipe buried in concrete as in experimental setup B (Fig.3.2), the incorporation of FSI in the modelling has no significant effects in the transient analysis. Even by using 1-D classical water hammer equations, with unsteady friction, the transient flow can be simulated accurately. But in most of the practical cases, the anchoring condition is not fixed, as given in the experimental setup

B. The piping system is subjected to both axial and radial movement as well as bending and torsion during a transient event and hence, the role of FSI in the transient analysis is significant, for better prediction of pressure rise and wave damping. Also, the analysis with FSI can simulate the duration of actual existence of high / low- intensity pressure/stresses present in the system. This concept can find utilisation in the selection/design of surge protection devices, which mainly depend upon the damping mechanism (Thara et al., 2018).

5.5. Numerical Modelling of Water Hammer with FSI - Case 3

The data corresponding to a flow velocity of 0.181 m/s was used for the numerical modelling of the case 3 because that is the flow velocity which did not cause cavitation. For the experimental setup C, the geometry was created in Design Modeller in ANSYS workbench (Fluent 2012) according to the specifications mentioned in the experimental setup C. The geometry was discretised using meshing tool as explained in setion 5.1. For conducting mesh independence study, the geometry was divided into meshes of different size from fine mesh to coarse mesh.

5.5.1. Effect of FSI on Pressure Wave Damping

The steady state flow was simulated for the given condition and the results were tested with the actual results. Then, the flow was changed to transient flow by suddenly closing the valve at the downstream. The closure time of the valve was 40 ms which was transferred to the model through the boundary condition by using a UDF. Among the available turbulent models, the standard k-ε model is the basic and most widely used model (Fluent 2012) and hence used in this study. Initially, the outlet boundary condition was adopted as mass flow outlet with constant mass flow corresponding to the flow velocity of 0.181 m/s. Then it was changed to zero mass flow by using a UDF that sets a linear variation of mass flow rate from 0.3882 kg/s to zero within 40 ms.

Initially, the model was simulated without considering the FSI. The outer fluid surface was treated as a wall for the simulation without considering the piping system, i.e., without considering the effect of FSI. It means that the pipe wall is considered as rigid and hence, does not undergo any deformation. Internal cell zone was selected as fluid. The boundary condition at the inlet was set as the pressure-inlet, and the inlet-pressure was given. Hybrid Initialization was used for initialising the flow. The flow is simulated with a time step of 10^{-5}

s. The grid independence study was conducted for different element numbers- 551460, 275730, 110292 and 55146. The result of the study is given in Table 5.2 and Fig.5.20. Table 5.2 gives the details of the four different meshes with the element size in the longitudinal direction as, 5 mm, 10 mm, 25 mm and 50 mm. The computed pressure at the outlet for all the four cases are given in Fig. 5.20.

Table 5.2 Grid independence study for case 3

Maximum element size	5 mm	10 mm	**25 mm**	50 mm
Number of Nodes	6,24,283	3,12,193	**1,24,939**	62,521
Number of Elements	5,51,460	2,75,730	**1,10,292**	55,146
Aspect Ratio	1.4072	2.555	**6.3876**	12.775
Orthogonal Quality	0.975	0.975	**0.975**	0.975
Skewness	0.168	0.168	**0.168**	0.168

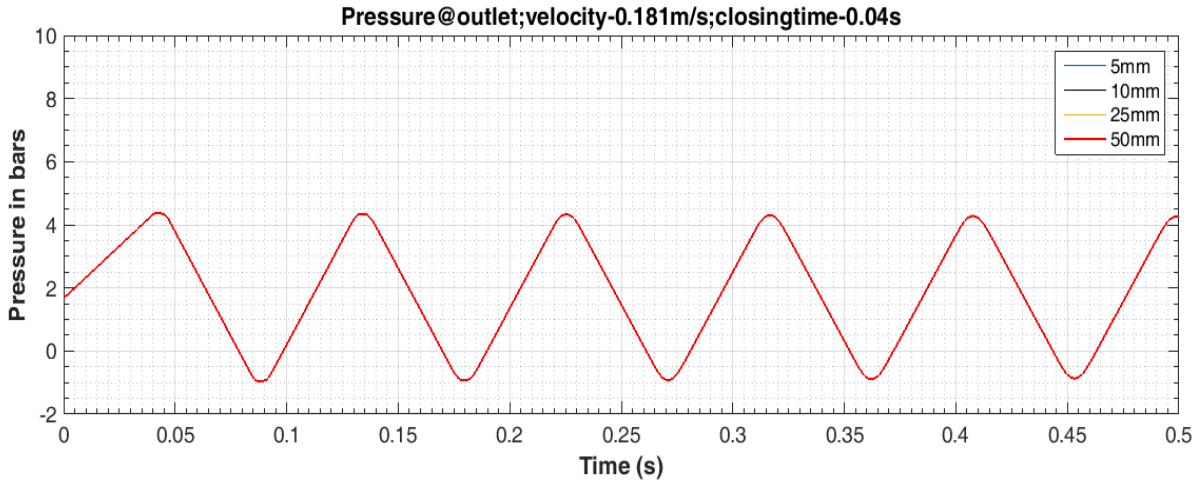

Fig.5.20 Pressure variation at the outlet for different grid size

From Fig. 5.20 it is clear that the change in number of elements from 551460 to 55146 does not make any difference in the pressure variation at outlet. As the element size increases, orthogonal quality and skewness do not change within the element sizes under consideration. However, the aspect ratio of the element increases and exceeds the desired value of 10 in case of element size 50 mm. Hence for further analysis, the number of elements was adopted as 110292, with size as 25mm.

Now, the model (3-D-CFD) was run with the specified setup and the pressure variation obtained from the model was compared with the experimental results (Fig.5.21). From Fig. 5.21, it can be seen that the peak value of water hammer pressure is 4.1 bars from the experiment, which was obtained as 4.3 bars from numerical simulation using 3-D flow equations, using ANSYS FLUENT. The pressure wave frequency was found to get deviated slightly from the experimental results after three cycles.

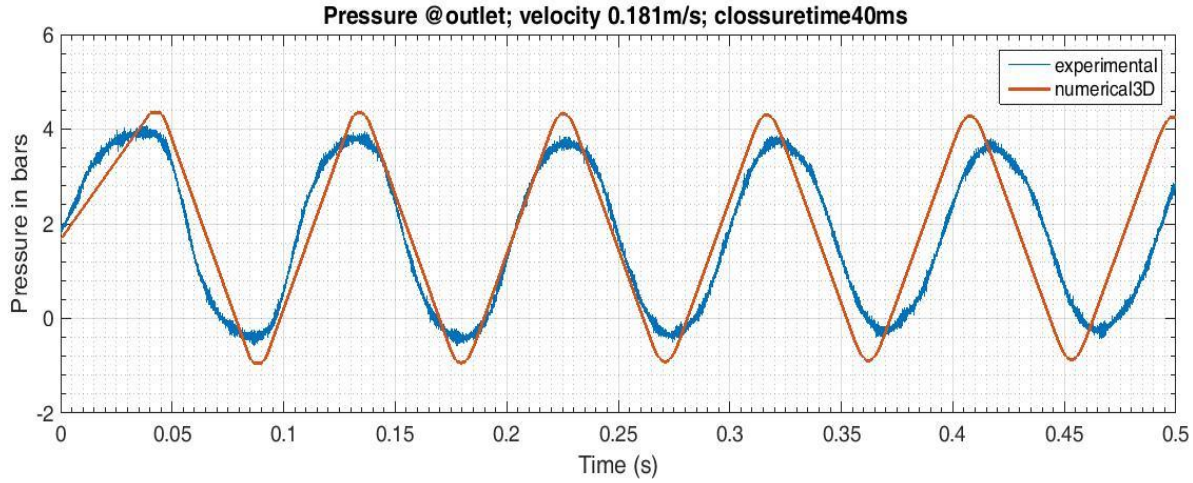

Fig.5.21 Comparison of pressure at the outlet - numerical and experimental results (case 3)

To study the effect of FSI in the transient flow, the same flow problem, considering the FSI was simulated by using the ANSYS Fluent, the Transient structural and the system coupling with the same initial boundary conditions and the support conditions except for the wall boundary. The wall boundary became an internal boundary condition which was dynamic in the sense that the external boundary of the fluid moved with the deformed internal boundary of the pipe. The mesh generation was performed just like the one, which is performed for the modelling without FSI. A 3-D twenty node hexahedron was used for modelling the pipe element as explained in section 5.1. The support conditions of the pipe were provided according to the anchoring conditions in the experimental setup C. The same modelling strategy was used as in section 5.2, for incorporating FSI. But the external boundary condition for the pipe varies as the number of supports changes from case to case. The supports were created with the same dimensions of the physical model and assigned as fixed support for the numerical study. The analysis with FSI was carried out for four different support conditions, mentioned in the experimental details. The results obtained from the analyses with and without FSI for five-anchor support condition were compared with the experimental results and are shown in the Fig. 5.22.

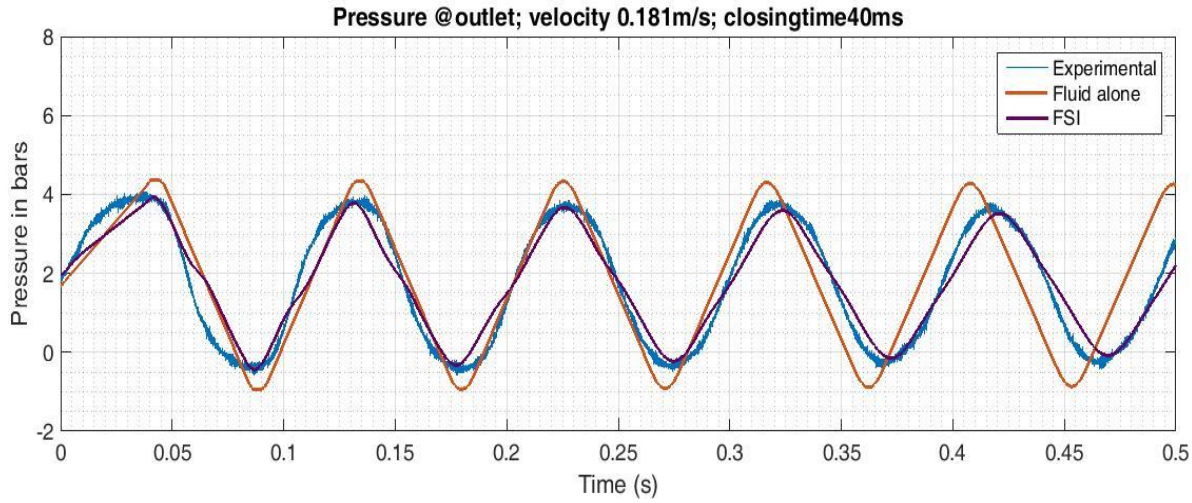

Fig.5.22 Comparison of pressure at the outlet for five anchor support condition

For the sake of easiness in the analysis, the numerical model that does not accounts FSI is called model P and that accounts FSI is called model Q in subsequent discussion in this section. From the Fig.5.22, it is seen that the model P slightly overestimates the water hammer pressure while the model Q gives correct pressure peak when the results from these models are compared with the experimental results. It is also observed that the model Q predicts the damping of pressure wave correctly while the model P does not. The period of pressure wave of the results from the model P does not match with that of experimental results. This is evident from the deviation of curves of pressure waves. On the other hand, the period of experimental pressure wave and that from the model Q match closely with each other, indicated by the coinciding pressure waves. Hence, it reinforces the fact that the damping in the pressure wave and the pressure wave period are very well predicted by incorporating FSI in the numerical model, without adding any additional mechanism which may not be physically present.

5.5.2 Effect of Anchors on Transient Flow

The analysis accounting FSI is repeated for the other three anchoring conditions - no anchor, two anchor and three anchor. In the numerical model, the anchors are created as fixed supports with the same dimension as that of the physical model. The pressure variations at the outlet, for different support conditions are obtained from the model Q by changing the anchoring conditions. The numerical pressure variations at the outlet for different anchoring conditions were then compared with the experimental results. As seen in Fig. 4.17 (experimental results in chapter 4) the experimental pressure variation at the outlet did not

vary with the number of supports. Hence, for the sake of clarity in the figure the numerical results were compared with one of the experimental results. This comparison is given in Fig. 5.23.

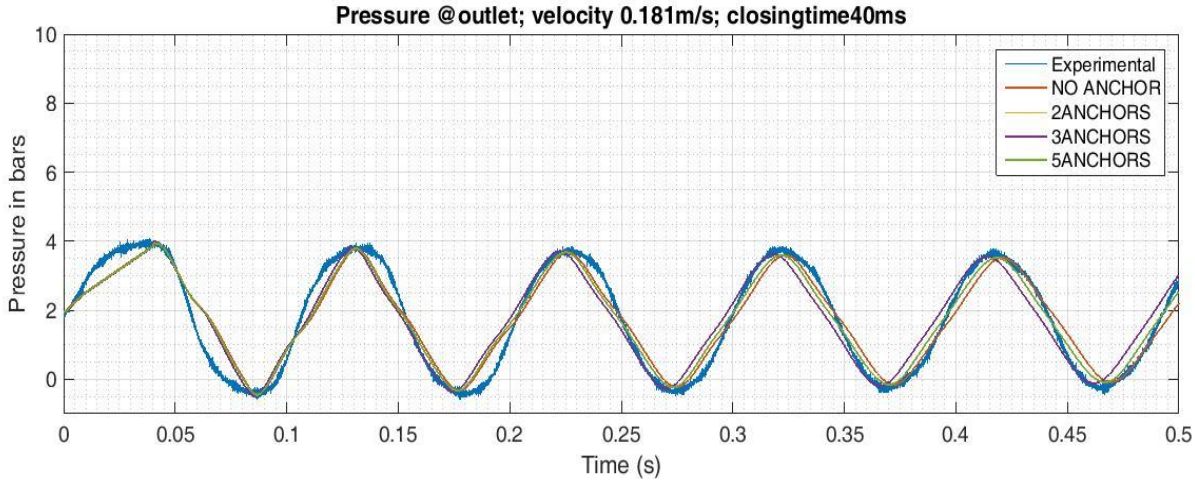

Fig.5.23 Comparison of experimental pressure variation at the outlet for the pipe with numerical results of different anchoring conditions

From Fig. 5.23, it is vivid that there is no change in the water hammer pressure at the outlet for all the four support conditions. The pressure peaks and damping are the same for all the four support conditions. The experimental results also exhibit the same pattern as given in Fig. 4.17.

From Fig. 5.23 and 4.17, it can be observed that the numerical simulation incorporating FSI very well predicts the water hammer pressure and its damping with time. Another important conclusion from this study is that the increase in the number of fixed anchors attached to the piping system does not affect the pressure variation due to water hammer, which agrees well with the conclusion from the experimental results.

5.5.3. Dynamic Response of Pipe during Transient Flow

In addition to the characteristics of pressure wave and their damping, the model Q gives a lot of information about the behaviour of the structure during a transient flow. The stress and strain in the pipe wall in all the three directions, their resultant, deformations of the structure and support reactions in the structure are available at various locations from the numerical simulation. The maximum and minimum values of different structural responses such as the principal stress at various points, the deflection in different directions, the total

deflection, the forces and the moments in all the three directions for support condition with five fixed anchors (a typical example) are tabulated in Table 5.3.

Table. 5.3. Structural response of pipe with five fixed anchors.

Structural Response of pipe	**Max**	**Min**
Maximum Principal stress (MPa)	18.241	1.38
Principal stress at outlet (MPa)	13.87	0.188
Principal stress at inlet (MPa)	12.00	0.180
Deflection in y direction (mm)	-1.375	-0.001
Deflection in x direction (mm)	0.034	-0.034
Total Deflection (mm)	1.375	0.0011
Force Fx- outlet (N)	448.2	-60.9
Force Fx- inlet (N)	-176.7	-182.5
Force Fy –outlet (N)	249.4	27.43
Force Fy –inlet (N)	232.9	27.43
Force Fz- outlet (N)	0.019	-0.017
Force Fz- intlet (N)	0.015	-0.009
Moment Mx- outlet (Nmm)	0.002	-0.004
Moment Mx – inlet (Nmm)	0.003	-0.003
Moment My –outlet (Nmm)	14.1	-11.5
Moment My –inlet (Nmm)	13	-15
Moment Mz – outlet (Nmm)	-383.3	-1.71e5
Moment Mz – intlet (Nmm)	1.49e5	384.5

From the Table 5.3, it is seen that most of the values fluctuate with time. A few of them even changes the direction. This information has importance while considering the design of fatigue-failure-free piping system. Moreover, this information is critical not only in the design of piping system but also in the failure analysis during stress fluctuations. The absolute maximum principal stress occurred anywhere in the pipe structure is obtained as

18.24 MPa which is very less than the allowable stress in steel. However, the hoop stress based on the maximum exerted pressure at the outlet is 2.67 MPa only, indicating that the actual maximum stress can be much higher than the computed stress by approximate calculation. The large difference in these two values occurs because of the bending action.

In the fixed anchor at the outlet, force in longitudinal direction fluctuates between maximum 448.2 N and minimum -60.9 N. Similarly bending moment, in lateral z direction changes between maximum -1.71×10^5 Nmm and minimum -383.3 Nmm. The reactions in the lateral directions are almost same both at the outlet and the inlet. Moments in y direction is almost equal both at the outlet and the inlet supports. It can also be seen that the torsion moment is negligible both at the outlet and the inlet supports for this flow velocity. This is quite obivious in straight pipes. However, this may not be the case for pipes with bends. The anchors and anchor bolts are designed based on the forces and moments exerted on the supports by the pipe during transient flow. If the forces and moments get reversed during the transient flow, the stress acting on the anchors and anchor bolts also reverse the nature (will change to tensile from compressive or vice versa). Hence, this information is very critical in the design of anchors and anchor bolts and for checking the safety of the anchors and anchor bolts under reversal of stresses and also for arriving at an optimum design.

5.6 Water Hammer with Cavitation

A cavitating flow occurs when a liquid is subjected to a pressure below the vapour pressure of the liquid. Then, the liquid starts vaporizing, yielding a two-phase system consisting of a mixture of water and vapour. The vapour formed is generally assumed to be in the shape of a spherical bubble. The modelling of cavitation can be carried out by different conceptual models. Out of the three different cavitation models available in ANSYS Fluent as discussed in Chapter 3, the Schnerr-Sauer cavitation model was selected for the study. The Schnerr-Sauer model is more robust and converges faster, as compared to the Singhal et al. model (Wang et al., 2016; Jansson et al., 2017).

For the analysis of water hammer with cavitation, an initial flow velocity 0.273 m/s was selected for the modelling of flow in MS pipe as the cavitation was occurred for this flow velocity in the experimental study. The experimental setup and other details are as explained in section 3.5.4. The numerical study on water hammer with cavitation was tried with a 3-D model. As explained by Jansson et al. (2017), fine mesh was used in the longitudinal

direction which rendered the number of nodes as 6,24,283 and the number of elements as 5,51,460. The mesh qualities like aspect ratio, skewness, orthogonal quality and element quality were with in the desirable limits and hence, this mesh size was adopted. Among the various multiphase models available in ANSYS Fluent, mixture model with no slip velocity and two Eulerian phases was selected. Water was assigned as phase 1 and vapour was assigned as phase 2. Initially, steady flow was simulated considering water as incompressible fluid with a constant density of 998.2 kg/m^3, a vapour viscosity of 0.001003kg/ms, a thermal conductivity of 0.6 w/m-K, a specific heat of 4182 J/kg-K, a molecular weight of 18.0152 kg/kg- mol and a reference temperature of 298 K. In the multiphase flow, the initial volume fraction of water was taken as 1 and that of vapour was considered as 0 at the inlet. The outlet condition was assigned as the mass flow outlet with a flow of 0.5878 kg/s (flow velocity 0.273 m/s). The mass flow rate of vapour was assumed as zero.

For running the transient simulation, the transient solver was selected. In multiphase flow model, mass-transfer mechanism was created as cavitation. In Schnerr- Sauer cavitation model, the vapour pressure was given as 3540 Pa and the bubble number density as $1x10^{13}$. The water was considered as compressible fluid and the vapour as ideal gas in the analysis. The energy equation was also included in the analysis. The transient event was created as explained in water hammer analysis through an outlet boundary condition (closure of valve). For pressure velocity coupling, SIMPLE algorithm was selected as explained in section 3.3.5.1. For spatial discretisation of continuity equation, PRESTO! (Pressure Staggering Option) method was selected in water hammer simulation with cavitation which was different from the previous cases. The simulation was carried out with time step size 10^{-5}. The model couldn't capture the cavitation pressure, even though the remaining values of pressure are comparable with the experimental results. Such a behaviour was observed in earlier studies also (Sumam et al., 2010; Jansson et al., 2017). This situation was circumvent by reducing the time step to the order of 10^{-6}. However, further reduction of time step was not possible for this model (with the number of nodes as 6,24,283 and number of elements as 5,51,460) because of the huge computation time. Hence, 2-D axi-symmetric simulation was carried out to study the water hammer with cavitation.

The 2D geometry was created by using a fine mesh with the number of elements as 1,33,320. At first, the steady flow was simulated and then transient event was created at the outlet boundary as in the case of 3D model. Then the transient flow was simulated with a time step size 10^{-5}s. The results indicated that the model did not capture the cavitation

pressure as in the previous 3-D analysis. Hence, following the approach indicated in Sumam et al. (2010) and Jansson et al. (2017), the time step was reduced to 10^{-6}s keeping all other parameters as in the previous simulation. However, no improvement was observed in the prediction of cavitation (Fig. 5.24). Nonetheless the simulation with time step size as 10^{-5}s and 10^{-6}s could predict the water hammer pressure and cavitation period accurately, but failed to capture the high pressure generated during the sudden bubble collapse. Therefore, the time step size was further reduced to 10^{-7}s. The axi-symmetric model with a time step size of 10^{-7}s predicted the cavitation pressure during sudden bubble collapse also with reasonable accuracy as shown in Fig.5.25.

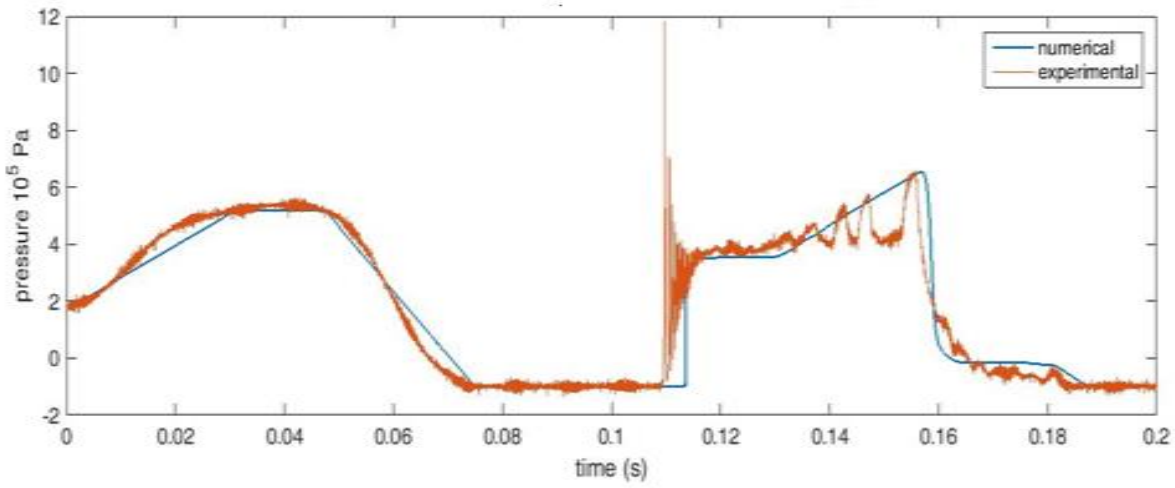

Fig. 5.24 Pressure at the outlet (flow velocity 0.273 m/s) – with time step 10^{-5} and 10^{-6} s

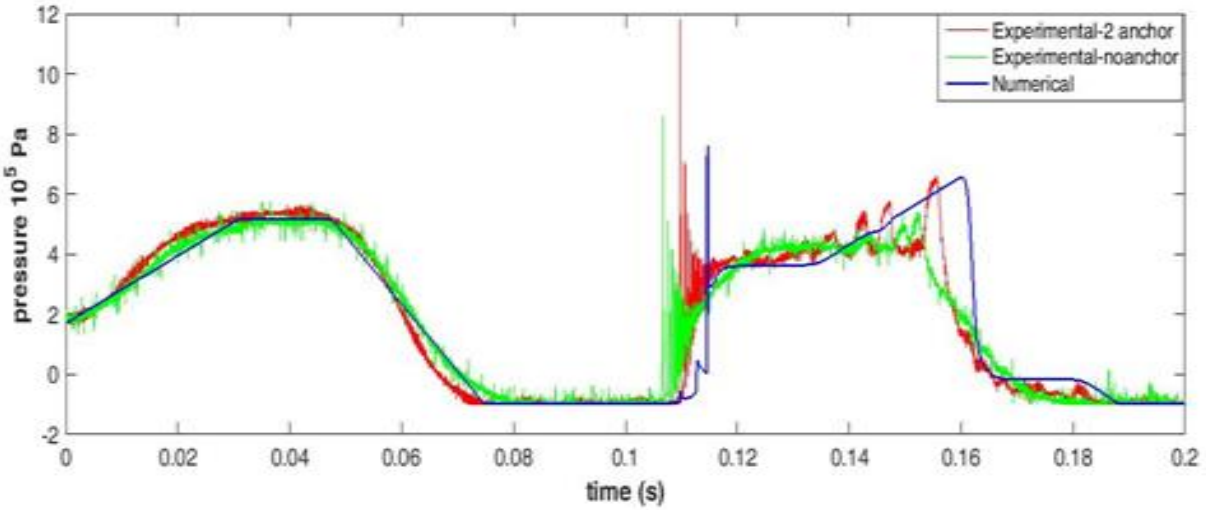

Fig. 5.25 Pressure at the outlet (flow velocity 0.273 m/s) – with time step 10^{-7}s

Huge computation time hinders the modelling process of cavitation. The simulation took huge computation times at the order of several weeks even for the modelling of a 2-D

system. A 3-D model for cavitation took several weeks for running the model with a time step of 10^{-5}s. The FSI analysis in cavitating flow is not an axis symmetric case and hence, the simulation of FSI in a cavitating flow has to be carried out in a 3-D model. Such a modelling with current computational power becomes almost impossible. However, this has to be attempted to verify the effect of anchors on the generation of cavitation as observed in the experiments. The modelling of FSI in a cavitating flow has to be attempted by increasing the computational efficiency, accomplished by using parallel computing or by using super computers. This can be considered as the future scope of the work.

5.7. Summary

This chapter discusses the numerical study of fluid structure interaction in a transient flow. The numerical study was conducted in two parts - the investigation on the role of FSI in the damping of pressure wave by using the available results from the literature and the numerical modelling of the current experimental study. Further, the effect of anchors on water hammer pressure was investigated. The study analysed the structural responses of the pipe at salient points. In addition, the water hammer with cavitation was simulated in a 2-D axi-symmetric model.

CHAPTER 6

SUMMARY AND CONCLUSIONS

6.1. Summary of the Work

Many failures in piping systems were caused by the extreme pressure generated because of water hammer phenomenon. A large number of investigations, both experimental and numerical, were carried out to assess the effect of water hammer on the piping system. Experimental investigations on transient flow in piping systems reported in the literature generally avoid cavitation during the experiments, though the cavitation causes much higher pressure than the water hammer pressure, possibly due to the high frequency oscillations created in the system. It is quite natural that the flow performance including cavitation phenomenon can be influenced by the structural behaviour of the piping system. Limited experiments were reported so far considering water hammer with cavitation and incorporating the impact of fixed anchors. Hence, the influence of fixed anchors attached to the piping system on transient cavitating flow characteristics was selected as the area of the present experimental investigation. Further, the study aimed to evaluate the effect of FSI on the damping of pressure wave and examine the effect of number of fixed supports on transient flow through pipes by numerical modelling.

The present study initially investigated into the effect of valve closure and the spacing of anchors on transient cavitating flow through the pipes of three different materials. Mild steel (MS), unplasticized polyvinyl chloride (UPVC) and high-density polyethylene (HDPE) were the materials used in the study. Experiments were conducted in three different installations in the water flow laboratory of FCRI, Palakkad, Kerala, by varying the four parameters under consideration viz., the closure time of valve, the initial flow velocity, the material properties and the number of fixed anchors attached to the system. The effect of closure time on the water hammer with and without cavitation was initially assessed. Then, the influence of the rigidity of the piping system was examined by conducting experiments with different number of fixed anchors. The present study also included a numerical investigation into the effect of fluid-

structure interaction (FSI) on transient flow characteristics in a piping system and the influence of spacing of anchors, on transient flow. Numerical simulations of four different problems from two different experimental setups, published in literature and the one conducted in the study were used for assessing the effect of FSI on the damping of the pressure wave.

6.2. Conclusions

The overall conclusion from the study is that the FSI has great influence on the damping of pressure waves and also on the magnitude of pressure hike due to cavitation. The following specific conclusions are drawn from the study:

1. The peak value of pressure in a water hammer event, when the closure time is classified as sudden closure, does not depend on the closure time of valve while the occurrence of cavitation and pressure rise due to bubble collapse greatly depend on the closure time. The increase in pressure due to cavitation is more than 200% when there is a 20% reduction in closure time.

2. The severe cavitation pressure waves, generated as a result of the sudden bubble collapse near the outlet, do not travel towards upstream rather they get reflected from the nearby area, resulting into high frequency pressure oscillations. This information has practical importance as localized solution to control the cavitation is enough for safeguarding the pipe from the adverse effect of cavitation.

3. The study proposes a method for identifying the occurrence of cavitation in a piping sytem before installing the piping system or without carrying out the modelling of cavitation process. When the slope of the descending phase of the first water hammer pressure cycle is higher than a value of 200 bars/s, the cavitation can occur and hence, precautionary measures are to be taken for reducing the effect. The utility of this information can be increased by the use of readily available simple 1-D numerical water hammer model. 1-D model can be easily employed for the estimation of the water hammer cycle with great accuracy, thereby finding the slope of the descending phase, and hence identifying the possibility of occurrence of the cavitation without executing a complex cavitation model.

4. Water hammer pressure under sudden closure condition in pipes made of elastic material (MS) is close to the pressure calculated by the Joukowsky formula whereas that in pipe made of visco-elastic materials (UPVC and HDPE) is more than Joukowsky pressure. This finding has practical implication in the design as the Joukowsky formula is generally used for estimating the water hammer pressure in the design calculations.

5. The water hammer pressure in the piping system, for both elastic and visco-elastic materials included in the study (MS, UPVC, HDPE), remains unaltered with the change in the number of fixed anchors attached to the system. But, the chance of occurrence of cavitation and the resulting pressure rise are increased (without any change in the flow conditions) as the rigidity of the piping system is increased by means of more number of fixed anchors. This is valid for both elastic and visco-elastic pipe materials. This fact emphasizes the need for FSI analysis of fluid-filled piping system.

6. As the rigidity of the piping system increases by providing more number of fixed supports, the cavitation pressure increases drastically while all flow parameters remain the same. The lateral acceleration of the piping system decreases significantly with the increase in the number of supports. This information has practical implications, as the spacing of anchors in any piping system should be decided by balancing the lateral acceleration of the piping system and the pressure rise due to cavitation. For industries where the vibration of the piping system has to be limited, anchors can be provided closely, by taking precautionary measures to avoid the failure due to cavitation.

7. The 3-D CFD fluid model with full Navier-Stokes equation and the 1-D model with classic water hammer equation (lumped friction model) for the estimation of maximum water hammer pressure gives similar results in rigid and semi rigid pipes, despite the increase in the complexity in modelling for the former. Hence, the use of the 1-D model is appropriate for the prediction of maximum pressure during water hammer in both semi-rigid and rigid pipes. Where it is possible to justify the assumption of rigid pipes, like in the case of pipes buried in concrete, the 1-D model based on classic water hammer equation is sufficient, even in the modelling of the damping of pressure wave.

8. These models, viz., 1-D model and 3-D CFD model based on the Navier -Stokes equation without incorporating FSI are not able to predict the damping of pressure wave correctly in the case of semi-rigid pipes. A 3-D CFD model incorporating FSI for transient flow can satisfactorily simulate the damping of pressure wave during the transient event in the case of semi-rigid pipes. However, the practical applicability of this model is constrained by the excessive computational load in case large piping system. Nonetheless, the strategy indicates the alternative possibility of theoretical exploration for the mechanisms causing the damping in pressure waves during transient events.

9. The incorporation of FSI between the fluid and the structure in a piping system not only models the wave damping, but also gives the principal stress which may, sometimes, be very much higher than the stress computed conventionally from the maximum pressure. This feature indicates the importance of FSI analysis, especially when the factor of safety in the design is small and nearer to one, or where the boundary is curved. This information is also critical in the optimum design of the anchors and anchor bolts; and also, in checking the safety of the piping system during the reversal of stresses.

10. The modelling of cavitation in three dimensions for a practical piping system becomes almost impossible due to the huge computational loads. Even a two-dimensional cavitation flow model (with very fine mesh size comparable with the boundary layer thickness) for a practical piping system requires a time step as small as 10^{-7}s for the prediction of cavitation pressure with reasonable accuracy and consequently needs huge computation time. This fact emphasises the importance of proposed method of identifying the occurrence of cavitation based on the slope of the descending phase of the first water hammer pressure cycle, calculated by conventional one-dimensional model.

6.3. Research Contributions

1. The study identifies that the peak value of pressure in a water hammer event under sudden closure condition (closure time < the time at which the wave returns to the point of disturbance) does not depend on the closure time of valve while the occurrence of cavitation and pressure rise due to bubble collapse consequent to cavtation greatly depend

on the closure time.

2. The study proposes a method for identifying the occurrence of cavitation in a piping system before installing the piping system or without carrying out the modelling of cavitation process. When the slope of the descending phase of the first water hammer pressure cycle is higher than a value of 200 bars/s, the cavitation can occur and hence, precautionary measures are to be taken for reducing the effect.

3. The study reveals that the Joukowsky formula underestimates the maximum pressure in a water hammer event under sudden closure condition in pipes made of of visco-elastic materials (UPVC and HDPE). This finding has practical implication in the design as the Joukowsky formula is generally used for estimating the water hammer pressure in the design calculations.

4. The study reveals that the increase in the rigidity of the piping system by providing more number of anchors increases the cavitation pressure drastically while it reduces the lateral acceleration of the piping system significantly. This information has practical implications, as the spacing of anchors in any piping system should be decided by balancing the lateral acceleration of the piping system and the pressure rise due to cavitation. For industries where the vibration of the piping system has to be limited, anchors can be provided closely, by taking precautionary measures to avoid the failure due to cavitation.

5. The study unravels that one of the possible reasons for sudden damping of pressure wave consequent to water hammer in a piping system is the effect of fluid structure interaction which is not usually accounted in water hammer analysis.

6.4 Limitations of the Study

The FSI analysis in cavitating flow in practical piping system is not an axi-symmetric case and hence, the simulation of FSI in a cavitating flow has to be carried out in a 3-D model. Such a modelling with current computational power becomes almost impossible as the running time extends to months.

6.5. Scope for Further Study

The modelling of FSI in a cavitating flow shall be attempted by increasing the computational efficiency, accomplished by using parallel computing or by using super computers. This can be considered as the future scope of the work. The influence of visco-elastic material behaviour on transient cavitating flow can be investigated by conducting more experimental and numerical studies.

REFERENCES

1. Adamkowski, A. (2001). Case study: Lapino powerplant penstock failure. *Journal of hydraulic engineering, ASCE*, 127(7), 547-555.
2. Adamkowski, A. and Lewandowski, M. (2009). Improved numerical modelling of hydraulic transients in pipelines with column separation. *In 3rd IAHR International Meeting of the Workgroup on Cavitation and Dynamic Problems in Hydraulic Machinery and Systems*, Brno, Czech Republic, October 14.
3. Adamkowski, A. and Lewandowski, M. (2012). Investigation of hydraulic transients in a pipeline with column separation. *Journal of Hydraulic Engineering, ASCE*, 138(11), 935-944.
4. Ahmadi, A. and Keramat, A. (2008). Investigation of the junction coupling due to various types of the discrete points in a piping system. In *The 12th International Conference of International Association for Computer Methods and Advances in Geomechanics (IACMAG)*, Goa, India, October 1-6.
5. Ahmadi, A. and Keramat, A. (2010). Investigation of fluid–structure interaction with various types of junction coupling. *Journal of fluids and structures*, 26(7-8), 1123-1141.
6. Alnomani, S. N. (2018). Investigation of vibration characteristics for simply supported pipe conveying fluid by mechanical spring. *ARPN Journal of Engineering and Applied Sciences*, 13(11*)*, 3857-3866.
7. Amara, L., Berreksi, A. and Achour, B. (2013). Adapted MacCormack finite-differences scheme for water hammer simulation. *Journal of Civil Engineering and Science*, 2(4), 226-233.
8. Ameen, M. (2005). *Computational elasticity: theory of elasticity and finite and boundary element methods*. New Delhi, Narosa.
9. Anderson, J. D. and Wendt, J. (1995). *Computational fluid dynamics*. New York: McGraw-Hill.
10. ANSYS user's manual (2013). ANSYS Inc. Canonsburg, PA, USA.
11. Araya, W. F. S. and Chaudhry, M. H. (1997). Computation of energy dissipation in transient flow. *Journal of Hydraulic Engineering. ASCE*, 123(2), 108-115.

12. Bakker, A. and Marshall, E. M. (2006). Computational fluid dynamics. *Lecture 4-Classification of Flows, In Encyclopedia of Chemical Processing,* 505-515.

13. Barten, W., Jasiulevicius, A., Manera, A., Macian-Juan, R. and Zerkak, O. (2008). Analysis of the capability of system codes to model cavitation water hammers: Simulation of UMSICHT water hammer experiments with TRACE and RELAP5. *Nuclear Engineering and Design*, 238(4), 1129-1145.

14. Bergant, A. and Simpson, A. R. (1994). Estimating unsteady friction in transient cavitating flow, *In 2nd International Conference on water pipeline system*, Edingburgh, Scotland, May 24-26.

15. Bergant, A. and Simpson, A. R. (1995). *Water hammer and column separation measurements in an experimental apparatus*. Research report, University of Adelaide, Department of Civil and Environmental Engineering.

16. Bergant, A. and Simpson, A. R. (1999). Pipeline column separation flow regimes. *Journal of Hydraulic Engineering, ASCE,* 125(8), 835-848.

17. Bergant, A., Simpson, A. R. and Tijsseling, A. S. (2004). *Water hammer with column separation: a review of research in the twentieth century*. Research report, Eindhoven University of Technology, Department of Mathematics and Computer Science.

18. Bergant, A., Simpson, A. R. and Tijsseling, A. S. (2006). Water hammer with column separation: A historical review. *Journal of fluids and structures*, 22(2), 135-171.

19. Bergant, A., Simpson, A. R. and Vìtkovsk, J. (2001). Developments in unsteady pipe flow friction modelling. *Journal of Hydraulic Research,* 39(3), 249-257.

20. Bhandari, D. and Singh, S. (2012). Analysis of fully developed turbulent flow in a pipe using computational fluid Dynamics. *International Journal of Engineering Research and Technology*, 1(5), 1-8.

21. Bombardieri, C., Traudt, T. and Manfletti, C. (2014). Experimental and numerical analysis of water hammer during the filling process of pipelines. *In Space Propulsion Conference,* Cologne, Germany, May 19.

22. Boresi, A. P., Schmidt, R. J., and Sidebottom, O. M. (1985). *Advanced mechanics of materials*, New York: Wiley.

23. Bourdarias, C. and Gerbi, S. (2002). An implicit finite volumes scheme for unsteady flows in deformable pipe-lines. *In Third International symposium on Finite Volumes for Complex Applications*, Porquerolles, France, June 24-28.
24. Bourdarias, C. and Gerbi, S. (2008). A conservative model for unsteady flows in deformable closed pipes and its implicit second-order finite volume discretisation. *Computers and Fluids*, 37(10), 1225-1237.
25. Brunone, B., Ferrante, M. and Cacciamani, M. (2004). Decay of pressure and energy dissipation in laminar transient flow. *Journal of Fluids Engineering*, 126(6), 928-934.
26. Brunone, B., Golia, U. M. and Greco, M. (1991). Modelling of fast transients by numerical methods. In *International Conference on Hydraulic Transients with Water Column Separation*, Madrid, Spain, September 4.
27. Brunone, B., Karney, B. W., Ferrante, M. and Meniconi, S. (2009). Experimental Investigation of Transients Caused by Rapid Valve Opening. In *33rd IAHR Congress: Water Engineering for a Sustainable Environment.* Vancouver, British Columbia, Canada, August 9-14.
28. Brunone, B., Karney, B. W., Mecarelli, M. and Ferrante, M. (2000). Velocity profiles and unsteady pipe friction in transient flow. *Journal of water resources planning and management*, 126(4), 236-244.
29. Chaudhry M. H. and Hussaini M. Y. (1985). Second-Order Accurate Explicit Finite-Difference Schemes for Water hammer Analysis. *Journal of Fluids Engineering, ASME*, 107(4), 523-529.
30. Chaudhry, M. H. (1979). *Applied hydraulic transients* (No. 627 C4). New York: Van Nostrand Reinhold.
31. Chaudhry, M. H., Bhallamudi, S. M., Martin, C. S. and Naghash, M. (1990). Analysis of transient pressures in bubbly, homogeneous, gas-liquid mixtures. *Journal of Fluids Engineering, ASME*, 112(2), 225-231.
32. Chopra, A. K. (1995). *Dynamics of structures: Theory and applications to earthquake engineering*. Prentice Hall. Inc., Upper Saddle River, NJ.
33. Cook, R. D. (2007). *Concepts and applications of finite element analysis*. New York: John Wiley and Sons.

34. Cook, R. D., Malkus, D. S., Plesha, M. E. and Witt, R. J. (1974). *Concepts and applications of finite element analysis* (Vol. 4). New York: Wiley.

35. Covas, D., Stoianov, I., Mano, J. F., Ramos, H., Graham, N. and Maksimovic, C. (2005). The dynamic effect of pipe-wall viscoelasticity in hydraulic transients. Part II—Model development, calibration and verification. *Journal of Hydraulic Research*, 43(1), 56-70.

36. Covas, D., Stoianov, I., Ramos, H., Graham, N. and Maksimovic, C. (2004). The dynamic effect of pipe-wall viscoelasticity in hydraulic transients. Part I—Experimental analysis and creep characterization. *Journal of Hydraulic Research*, 42(5), 517-532.

37. Donea, J., Giuliani, S. and Halleux, J. P. (1982). An arbitrary Lagrangian-Eulerian finite element method for transient dynamic fluid-structure interactions. *Computer methods in applied mechanics and engineering*, 33(1-3), 689-723.

38. Etlender, R., Iben, U. and Bischoff, M. (2007). Simulation of wave propagation in flexible hoses. *Fluid Structure Interaction and Moving Boundary Problems IV, WIT Transactions on the Built Environment,* 92, 131-141.

39. Feeny, B., Guran, A., Hinrichs, N. and Popp, K. (1998). A Historical Review on Dry Friction and Stick-Slip Phenomena. *Applied Mechanics Rev*iews, *ASME,* 51(5), 321–341.

40. Ferràs, D., Manso, P. A., Schleiss, A. J. and Covas, D. I. (2016a). Fluid-structure interaction in straight pipelines: Friction coupling mechanisms. *Computers and Structures,* 175, 74-90.

41. Ferràs, D., Manso, P. A., Schleiss, A. J. and Covas, D. I. (2016b). Experimental distinction of damping mechanisms during hydraulic transients in pipe flow. *Journal of Fluids and Structures,* 66, 424-446.

42. Ferras, D., Manso, P. A., Schleiss, A. J. and Covas, D. I. (2017). Fluid-structure interaction in straight pipelines with different anchoring conditions. *Journal of Sound and Vibration*, 394, 348-365.

43. Ferreira, J. P. B., Martins, N. M. C. and Covas, D. I. (2018). Ball valve behavior under steady and unsteady conditions. *Journal of Hydraulic Engineering, ASCE*, 144(4), 04018005-1-12.

44. Fluent, (2012). ANSYS Fluent Theory Guide, ANSYS Inc., Canonsburg, PA, USA.

45. Geng, J., Li, D., and Du, G. S. (2017). Simulation of cavitation induced by water hammer. *Journal of Hydrodynamics,* 29(6), 972-978.

46. Ghidaoui, M. S., Zhao, M., McInnis, D. A. and Axworthy, D. H. (2005). A review of water hammer theory and practice. *Applied Mechanics Review, ASME*, 58(1), 49-76.
47. Ginell, R. (1961). Derivation of the Tait equation and its relation to the structure of liquids. *The Journal of Chemical Physics*, 34(4), 1249-1252.
48. Greyvenstein, G. P. (2002). An implicit method for the analysis of transient flows in pipe networks. *International journal for numerical methods in engineering*, 53(5), 1127-1143.
49. Hadj-Taıeb, E. and Lili, T. (2000). Validation of hyperbolic model for water-hammer in deformable pipes. *Journal of Fluids Engineering, ASME*, 122(1), 57-64.
50. Heinsbroek, A. G. T. J. (1997). Fluid-structure interaction in non-rigid pipeline systems. *Nuclear engineering and design*, 172(1-2), 123-135.
51. Heinsbroek, A. G. T. J. and Tijsseling, A. S. (1994). The influence of support rigidity on water hammer pressures and pipe stresses. In *2nd BHR Group International Conference on Water Pipeline Systems*, Edinburgh, UK, May 24-26.
52. Henclik, S. (2010). Mathematical model and numerical computations of transient pipe flows with fluid-structure interaction. *Transactions of the Institute of Fluid-Flow Machinery*, 122, 77-94.
53. Holmboe, E. L. and Rouleau, W. T. (1967). The effect of viscous shear on transients in liquid lines. *Journal of Basic Engineering*, 89(1), 174-180.
54. Hou, G., Wang, J. and Layton, A. (2012). Numerical methods for fluid-structure interaction-a review. *Communications in Computational Physics*, 12(2), 337-377. https://www.eolss.net/Sample-Chapters/C05/E6-165-01-00.pdf
55. Hughes, W. F. (1963). Some aspects of wave propagation in viscous liquids in conduits. *Applied Scientific Research, Section A*, 12(2), 119-133.
56. Hunain, M. B. (2017). The Fundamental Natural Frequency and Critical Flow Velocity Evaluation of a Simply Supported Stepped Pipe Conveying Fluid. *Journal of University of Babylon*, 25(5), 1840-1849.
57. Jansson, M., Andersson, M., Pettersson, M. and Karlsson, M. (2017). Water Hammer Induced Cavitation-A Numerical and Experimental Study. In *15th Scandinavian International Conference on Fluid Power*, Linköping, Sweden, June 7-9.

58. Jiang, B., Tian, M. C., Zhang, G. M., Li, B. X. and Cheng, L. (2009). Influencing parameters of flow-induced structural deformation for a circular tube. *Journal of Hydrodynamics*, 21(4), 520-525.

59. Jinping, L., Peng, W. and Jiandong, Y. (2010). CFD numerical simulation of water hammer in pipeline based on the Navier-Stokes equation. In *the V European Conference on computational fluid dynamics (ECCOMAS CFD 2010)*, Lisbon, Portugal, June 14-17.

60. Jo, J. C. (2004). Pressure Vessels and Piping Systems – Fluid-Structure Interactions. *Encyclopedia of Life Support Systems (EOLSS)*.

61. Karney, B. W. and Filion, Y. R. (2003). Energy Dissipation Mechanisms in Water Distribution Systems**.** *The 4th ASME_JSME Joint Fluids Engineering Conference*, Hawaii, USA, July 6-10.

62. Keramat, A., Tijsseling, A. S. and Ahmadi, A. (2010). Investigation of transient cavitating flow in viscoelastic pipes. In *IOP Conference Series: Earth and Environmental Science,* University of Timişoara, Timişoara, Romania, September 20-24.

63. Keramat, A., Tijsseling, A. S., Hou, Q. and Ahmadi, A. (2012). Fluid–structure interaction with pipe-wall viscoelasticity during water hammer. *Journal of Fluids and Structures*, 28(1), 434-455.

64. Kodura, A. (2016). An analysis of the impact of valve closure time on the course of water hammer. *Archives of Hydro-Engineering and Environmental Mechanics*, 63(1), 35-45.

65. Kono, Y., Sugano, T. and Sugai, Y. (1992). Analysis of penstock fracture by water hammer. In *Pipeline Systems, Fluid Mechanics and Its Applications*, 7, 165-170.

66. Kozubková, M., Rautová, J. and Bojko, M. (2012). Mathematical model of cavitation and modelling of fluid flow in cone. *Procedia Engineering*, *39*, 9-18.

67. Lahane, S., Patil, R., Mahajan, R. and Palve, K. (2015). Analysis of Water Hammering in Pipeline and its CFD Simulation. *International Journal of Engineering Technology, Management and Applied Sciences,* 3(5), 250-255.

68. Lavooij, C. S. W. and Tijsseling, A. S. (1991). Fluid-structure interaction in liquid-filled piping systems. *Journal of fluids and structures*, 5(5), 573-595.

69. Lee, T. S., Low, H. T. and Nguyen, D. T. (2008). Effects of Air Entrainment on Fluid Transients in Pumping Systems. *Journal of Applied Fluid Mechanics*, 1(1), 55-61.

70. Leon, A. S., Ghidaoui, M. S., Schmidt, A. R. and García, M. H. (2008). Efficient second-order accurate shock-capturing scheme for modeling one-and two-phase water hammer flows. *Journal of Hydraulic Engineering, ASCE,* 134(7), 970-983.

71. León, A. S., Ghidaoui, M. S., Schmidt, A. R. and García, M. H. (2007). An efficient finite-volume scheme for modeling water hammer flows. *Journal of Water Management Modelling,* 15(1), 411-430.

72. Li, B., Wang, Z., and Jing, L. (2018). Dynamic response of pipe conveying fluid with lateral moving supports. *Hindawi, Shock and Vibration,* 2018(1), 3295787-1-17.

73. Li, G., Xiao, W., Jiang, G. and Liu, J. (2014). Finite element analysis of fluid conveying pipeline of nonlinear vibration response. *Computer Modelling and New Technologies*, 18(4), 37-41.

74. Li, Q. S., Yang, K. and Zhang, L. (2003). Analytical solution for fluid-structure interaction in liquid-filled pipes subjected to impact-induced water hammer. *Journal of Engineering Mechanics,* 129(12), 1408-1417.

75. Li, Y. H. (1967). Equation of state of water and sea water. *Journal of Geophysical Research,* 72(10), 2665-2678.

76. Liggett, J. A. and Chen, L. C. (1994). Inverse transient analysis in pipe networks. *Journal of Hydraulic Engineering, ASCE,* 120(8), 934-955.

77. Lind, S. J. and Phillips, T. N. (2012). The influence of viscoelasticity on the collapse of cavitation bubbles near a rigid boundary. *Theoretical and Computational Fluid Dynamics*, 26(1-4), 245-277.

78. Löhner, R., Cebral, J. R., Yang, C., Baum, J. D., Mestreau, E. L. and Soto, O. (2006). Extending the range and applicability of the loose coupling approach for FSI simulations. *Fluid-structure interaction*, 53, 82-100.

79. Maajel, B. M., Saleh, F. A. and Habeeb, L. J. (2015). Fluid-Structure Interaction Investigations in Liquid Filled Tube Systems: Recent Literature Review. *AASCIT Journal of Materials*, 1(3), 69-74.

80. Mansuri, B., Salmasi, F. and Bakhshayesh, B. O. (2014). Effects of Pipe's Roughness and Reservoir Head Levels on Pressure Waves in Water Hammer. *Journal of Civil Engineering and Urbanism,* 4(1), 36-40.

81. Martins, N. M. C., Brunone, B., Meniconi, S., Ramos, H. M. and Covas, D. I. (2017). CFD and 1D approaches for the unsteady friction analysis of low Reynolds number turbulent flows. *Journal of Hydraulic Engineering, ASCE,* 143(12), 04017050.

82. Martins, N. M. C., Brunone, B., Meniconi, S., Ramos, H. M. and Covas, D. I. (2018). Efficient computational fluid dynamics model for transient laminar flow modeling: Pressure wave propagation and velocity profile changes. *Journal of Fluids Engineering, ASME*, 140(1), 011102-1-9.

83. Martins, N. M. C., Carrico, N. J., Ramos, H. M. and Covas, D. I. (2014). Velocity-distribution in pressurized pipe flow using CFD: Accuracy and mesh analysis. *Computers and Fluids,* 105, 218-230.

84. Martins, N. M. C., Soares, A. K., Ramos, H. M. and Covas, D. I. (2016). CFD modeling of transient flow in pressurized pipes. *Computers and Fluids*, 126, 129-140.

85. Mitosek, M. (2000). Study of transient vapor cavitation in series pipe systems. *Journal of Hydraulic Engineering, ASCE,* 126(12), 904-911.

86. Mitosek, M. and Szymkiewicz, R. (2012). Wave damping and smoothing in the unsteady pipe flow. *Journal of Hydraulic Engineering, ASCE,* 138(7), 619-628.

87. Mitosek, M. and Szymkiewicz, R. (2016). Reservoir Influence on Pressure Wave Propagation in Steel Pipes. *Journal of Hydraulic Engineering, ASCE,* 142(8), 06016007-1-5.

88. Mittal, S. and Tezduyar, T. E. (1995). Parallel finite element simulation of 3D incompressible flows: Fluid-structure interactions. *International Journal for Numerical Methods in Fluids*, 21(10), 933-953.

89. Modi, P. N. and Seth, S. M. (1985). Fluid mechanics and hydraulics. *New Delhi, India: Dhanpat Rai and Sons*.

90. Mohan, S. (2016) Study on effect of Fluid Structure Interaction on energy dissipation during transients, *M. Tech. Thesis*, Calicut University, Kerala, India.

91. Monajitha, A. S., Sumam, K. S. and Sajikumar, N. (2014). Modelling of Energy Dissipation during Transient Flow. *International Journal of Scientific and Engineering Research*, 5 (7), 368-374.

92. Mostafa, N., Karim, M. M., and Sarker, M. M. A. (2016). Numerical Prediction of Unsteady Behavior of Cavitating Flow on Hydrofoils using Bubble Dynamics Cavitation Model. *Journal of Applied Fluid Mechanics*, 9(4), 1829-1837.

93. Moukalled, F., Mangani, L. and Darwish, M. (2016). The finite volume method in computational fluid dynamics. *An advanced introduction with OpenFoam® and Matlab®. Nueva York: Springer.*

94. Niyogi, P., Chakrabartty, S. K. and Laha, M. K. (2006). *Introduction to computational fluid dynamics*. Pearson Education India. Bengaluru.

95. Patankar, S. (1980). *Numerical heat transfer and fluid flow*. New York: McGraw-Hill.

96. Pezzinga, G. (2002). Unsteady flow in hydraulic networks with polymeric additional pipe. *Journal of Hydraulic Engineering, ASCE*, 128(2), 238-244.

97. Pezzinga, G. and Santoro, V. C. (2017). Unitary framework for hydraulic mathematical models of transient cavitation in pipes: numerical analysis of 1D and 2D flow. *Journal of Hydraulic Engineering, ASCE,* 143(12), 04017053-1-13.

98. Saemi, S., Raisee, M., Cervantes, M. and Nourbakhsh, A. (2014). Computation of laminar and turbulent water hammer flows. In *WCCM-ECCM-ECFD 2014 Congress: 11th World Congress on Computational Mechanics (WCCM XI),* Barcelona, Spain, July 20-25.

99. Sahu, M., Khatua, K. K., Patra, K. C. and Naik, T. (2009). Developed laminar flow in pipe using computational fluid dynamics. *In 7th International R&D Conference on development and management of water and energy resources*, Bhubaneswar, India, February 4-6.

100. Salvador, G., Altozano, P. G. and Arviza-Valverde, J. (2007). Numerical modeling of cavitating flows for simple geometries using FLUENT V6. 1. *Spanish Journal of Agricultural Research*, *5*(4), 460-469.

101. Schnerr, G. H. and Sauer, J. (2001). Physical and numerical modeling of unsteady cavitation dynamics. *In Fourth International Conference on multiphase flow,* ICMF New Orleans, USA, May 27 - June 1.

102. Seck, A., Fuamba, M. and Kahawita, R. (2017). Finite-Volume solutions to the water-hammer equations in conservation form incorporating dynamic friction using the Godunov scheme. *Journal of Hydraulic Engineering, ASCE*, 143(9), 04017029-1-12.

103. Shaik, I., Uddien, S., Krishnaiah, A. and Sutar, S. (2017). Numerical Analysis of Clamped Fluid Conveying Pipe. *Mechanics, Materials Science & Engineering*, 13, 1-14.

104. Shankarachar, S. M., Radhakrishna, M., and Babu, P. R. (2015). An Experimental Study of Flow Induced Vibration of Elastically Restrained Pipe Conveying Fluid. *In the 15th International Mechanical Engineering Congress and Exposition IMECE15*, Houston, Texas, USA, November 13-19.

105. Shen, W., Zhang, J. and Wang, J. (2006). Pipe-entrance flow simulation using multi-grid finite volume. *Technical report TR- 460-06,* University of Kentucky, Lexington, KY.

106. Shimada, M. and Vardy, A. E. (2013). Nonlinear interaction of friction and interpolation errors in unsteady flow analyses. *Journal of Hydraulic Engineering, ASCE*, 139(4), 397-409.

107. Sibetheros, I. A., Holley, E. R. and Branski, J. M. (1991). Spline interpolations for water hammer analysis. *Journal of Hydraulic Engineering, ASCE*, 117(10), 1332-1351.

108. Simão, M., Mora, J. and Ramos, H. M. (2014). Dynamic behaviour of a pipe system under unsteady flow and structure vibration. *In MEFTE 2014*, Porto, Portugal, September 11-12.

109. Simão, M., Mora, J. and Ramos, H. M. (2015). Mechanical interaction in pressurized pipe systems: experiments and numerical models. *Water*, 7(11), 6321-6350.

110. Simpson, A. R. and Bergant, A. (1994a). Developments in pipeline column separation experimentation. *Journal of Hydraulic Research*, 32(2), 183-194.

111. Simpson, A. R. and Bergant, A. (1994b). Numerical comparison of pipe-column-separation models. *Journal of Hydraulic Engineering, ASCE*, 120(3), 361-377.

112. Simpson, A. R., and Wylie, E. B. (1991). Large water-hammer pressures for column separation in pipelines. *Journal of Hydraulic Engineering, ASCE*, 117(10), 1310-1316.

113. Singhal, A. K., Athavale, M. M., Li, H. and Jiang, Y. (2002). Mathematical basis and validation of the full cavitation model. *Journal of Fluids Engineering*, 124(3), 617-624.

114. Skalak, R. (1954). An extension of the theory of water hammer, *PhD Thesis*, Faculty of Pure Science, Columbia University, New York, USA, 1954.

115. Smitha, M. K. and Miji, C. R. (2016). Effect of valve closure time on pressure distribution during transients. *In the National Conference on Emerging Trends in Engineering, Calicut, Kerala*, October 7-8.

116. Soares, A. K., Covas, D. I. and Reis, L. F. (2008). Analysis of PVC pipe-wall viscoelasticity during water hammer. *Journal of Hydraulic Engineering, ASCE*, 134(9), 1389-1394.

117. Soares, A. K., Covas, D. I., Ramos, H. M. and Reis, L. F. R. (2009). Unsteady flow with cavitation in viscoelastic pipes. *International Journal of Fluid Machinery and Systems*, 2(4), 269-277.

118. Stella, F., Giangi, M., Paglia, F., Casata, A., Simone, D. and Gaudenzi, P. (2005). A numerical simulation of fluid–structure interaction in internal flows. *Numerical Heat Transfer, Part B*, 47(5), 403-418.

119. Stephens, M. L., Lambert, M. F., Simpson, A. R. and Vitkovsky, J. P. (2011). Calibrating the water-hammer response of a field pipe network by using a mechanical damping model. *Journal of Hydraulic Engineering, ASCE*, 137(10), 1225-1237.

120. Streeter, V. L. and Wylie, E. B. (1967). *Hydraulic transients*, New York, McGraw-Hill.

121. Sumam, K. S., Thampi, S. G. and Sajikumar, N. (2010). An alternate approach for modelling of transient vaporous cavitation. *International Journal for Numerical Methods in Fluids*, 63(5), 564-583.

122. Tarasevich, V. V. (1980). Maximum pressure during water hammer accompanied by discontinuity of the flow. *Hydrotechnical Construction*, 14(8), 784-790.

123. Thara, S., Sumam, K. S. and Sajikumar, N. (2018). Economic design of a surge tank: An alternative approach. *In the International Conference in Emerging Trends in Engineering, Science and Technology (ICETEST 2018),* Thrissur, Kerala, India, January 18-20.

124. Tijsseling, A. S. (1996). Fluid-structure interaction in liquid-filled pipe systems: a review. *Journal of Fluids and Structures*, 10(2), 109-146.

125. Tijsseling, A. S. (2007). Water hammer with fluid-structure interaction in thick-walled pipes. *Computers and structures*, 85 (11), 844-851.

126. Tijsseling, A. S. and Anderson, A. (2006). The Joukowsky equation for fluids and solids. *Eindhoven University of Technology, Eindhoven*, The Netherlands, CASA-Report.

127. Tijsseling, A. S. and Fan, D. (1991). The response of liquid-filled pipes to vapour collapse. In *Transactions of the 11th international conference on structural mechanics in reactor technology*.

128. Tijsseling, A. S. and Fan, D. (1992). Fluid-structure interaction and column separation in a closed pipe. In *Proceedings of the Second National Mechanics Congress* , Kerkrade , The Netherlands, , November , 205 – 212 .

129. Tijsseling, A. S. and Heinsbroek, A. G. T. J. (1999). The influence of bend motion on water hammer pressures and pipe stresses. *In 3rd ASME/JSME joint Fluids Engineering Conference,* San Francisco, California, July 18-23.

130. Tijsseling, A. S. and Vardy, A. E. (2004). Time scales and FSI in unsteady liquid-filled pipe flow. *In the 9th International Conference on Pressure Surges,* Chester, UK, March 24-26.

131. Tijsseling, A. S., Fan, D. and Vardy, A. E. (1994). Transient fluid-structure interaction and cavitation in a single-elbow pipe system. In *Proceedings First International Conference on Flow Interaction,* Hong Kong, September 5-9, 346-349.

132. Timošenko, S. P. and Goodier, J. N. (1951). *Theory of elasticity*. New York, McGraw-Hill.

133. Urbanowicz, K. and Zarzycki, Z. (2008). Transient cavitating pipe flow: computation models and methods. *Task quarterly*, 12(3), 159-172.

134. Vardy, A. E. and Fan, D. (1986). Water hammer in a closed tube. In *Proceedings 5th International Conference on Pressure Surges,* 123-137.

135. Vardy, A. E. and Fan, D. (1989). Flexural waves in a closed tube. *In the 6th International Conference on pressure surges*, Cambridge, UK, October 4-6.

136. Versteeg, H. K. and Malalasekera, W. (2007). *An introduction to computational fluid dynamics: the finite volume method*. New York, Pearson education.

137. Vítkovský, J. P., Lambert, M. F., Simpson, A. R. and Bergant, A. (2000). Advances in unsteady friction modelling in transient pipe flow. *In the 8th International Conference on pressure surges*, Hague, Netherlands, April 12-14.

138. Wang, H., Zhou, L., Liu, D., Karney, B., Wang, P., Xia, L. and Xu, C. (2016). CFD approach for column separation in water pipelines. *Journal of Hydraulic Engineering, ASCE*, 142(10), 04016036-1-11.

139. Wang, L., Gan, J. and Ni, Q. (2013). Natural frequency analysis of fluid-conveying pipes in the ADINA system. *Journal of Physics: Conference Series,* 448(1), 012014-1-8.

140. Wiggert, D. C. and Tijsseling, A. S. (2001). Fluid transients and fluid-structure interaction in flexible liquid-filled piping. *Applied Mechanics Reviews*, 54(5), 455-481.

141. Wiggert, D. C., Hatfield, F. J. and Stuckenbruck, S. (1987). Analysis of liquid and structural transients in piping by the Method of Characteristics. *Journal of Fluids Engineering, ASME*, 109(2), 161-165.

142. Wilcox, J. and Walters, T. (2012). Evaluating Dynamic Loads in Piping Systems Caused by Water hammer. https://www.aft.com/white-papers/evaluating-dynamic-loads-in-piping-systems-caused-by-waterhammer

143. Wu, D., Yang, S., Wu, P. and Wang, L. (2015). MOC-CFD coupled approach for the analysis of the fluid dynamic interaction between water hammer and pump. *Journal of Hydraulic Engineering, ASCE*, 141(6), 06015003-1-8.

144. Wylie, E. B., Streeter, V. L., and Suo, L. (1993). *Fluid transients in systems* (Vol. 1, p. 464). Englewood Cliffs, NJ: Prentice Hall.

145. Xu, W. W., Wu, D. Z. and Wang, L. Q. (2012). Coupling analysis of fluid-structure interaction in fluid-filled elbow pipe. *In IOP Conference Series: Earth and Environmental Science*, Beijing, China, August 19–23.

146. Zhang, Y. L., Gorman, D. G. and Reese, J. M. (1999). Analysis of the vibration of pipes conveying fluid. *Proceedings of the Institution of Mechanical Engineers, Part C: Journal of Mechanical Engineering Science*, 213(8), 849-859.

147. Zhu, H., Zhao, H., Pan, Q. and Li, X. (2014). Coupling analysis of fluid-structure interaction and flow erosion of gas-solid flow in elbow pipe. *Advances in Mechanical Engineering*, 6, 815945-1-10.

148. Zienkiewicz, O. C., Taylor, R. L., Nithiarasu, P. and Zhu, J. Z. (1977). *The finite element method* (Vol. 3). London: McGraw-hill.

149. Zwart, P. J., Gerber, A. G. and Belamri, T. (2004). A two-phase flow model for predicting cavitation dynamics. In *Fifth International Conference on multiphase flow*, Yokohama, Japan, May 30-June 4.

LIST OF PUBLICATIONS

Papers Published/Communicated in peer reviewed International Journals

Published

1. Miji Cherian R., N. Sajikumar and Sumam K.S. (2020). Effect of valve closure time on transient cavitating flow through piping systems, *ISH Journal of Hydraulic Engineering*, DOI:10.1080/09715010.2020.1729875.
2. Miji Cherian R., N. Sajikumar and Sumam K.S. (2021). Influence of Fluid-Structure Interaction on Pressure Fluctuations in Transient Flow. *Journal of Pipeline Systems Engineering and Practice, ASCE*, 12(2), 04021002-1-15.

Communicated

3. Miji Cherian R., N. Sajikumar and Sumam K.S. Influence of anchors on transient cavitating flow in pipes, communicated to *Journal of Mechanical Science and Technology, Springer* (under review)

Publications in peer reviewed International Conferences

1. Miji Cherian R., Sajikumar, N. and Sumam, K. S. (2018). Fluid structure interaction in transient cavitating flow in pipes—a review. In *Emerging Trends in Engineering, Science and Technology for Society, Energy and Environment: Proceedings of the International Conference in Emerging Trends in Engineering, Science and Technology (ICETEST 2018),* January 18-20, 2018, Thrissur, Kerala, India (p. 101). CRC Press.
2. Miji Cherian R., Sajikumar, N. and Sumam, K. S. (2019). Influence of Material Property of Pipe on Transient Flow through Piping Systems, *Proceedings of the International conference ISH - HYDRO 2019, OSMANIA UNIVERSITY, HYDERABAD, INDIA*, 18-20, December 2019, pp 3234-3240.
3. Miji Cherian R., N. Sajikumar and Sumam K.S. (2021). Modal analysis for a water carrying piping System, *International conference ISH - HYDRO 2020, NIT Rourkela,* March 26-28.